Declassified and Approved For Release 2013/09/14 : CIA-RDP10-02196R000300040005-3

ISSN 0038-531X

Russian Original Vol. 56, No. 5, May, 1984

November, 1984

SATEAZ 56(5) 287-360 (1984)

SOVIET ATOMIC ENERGY

АТОМНАЯ ЭНЕРГИЯ
(ATOMNAYA ÉNERGIYA)

TRANSLATED FROM RUSSIAN

CONSULTANTS BUREAU, NEW YORK

Declassified and Approved For Release 2013/09/14 : CIA-RDP10-02196R000300040005-3

Declassified and Approved For Release 2013/09/14 : CIA-RDP10-02196R000300040005-3

SOVIET ATOMIC ENERGY

Soviet Atomic Energy is abstracted or indexed in *Chemical Abstracts, Chemical Titles, Pollution Abstracts, Science Research Abstracts, Parts A and B, Safety Science Abstracts Journal, Current Contents, Energy Research Abstracts,* and *Engineering Index.*

Mailed in the USA by Publications Expediting, Inc., 200 Meacham Avenue. Elmont, NY 11003.

POSTMASTER: Send address changes to *Soviet Atomic Energy,* Plenum Publishing Corporation, 233 Spring Street, New York, NY 10013.

Soviet Atomic Energy is a translation of *Atomnaya Énergiya,* a publication of the Academy of Sciences of the USSR.

An agreement with the Copyright Agency of the USSR (VAAP) makes available both advance copies of the Russian journal and original glossy photographs and artwork. This serves to decrease the necessary time lag between publication of the original and publication of the translation and helps to improve the quality of the latter. The translation began with the first issue of the Russian journal.

Editorial Board of *Atomnaya Énergiya:*

Editor: O. D. Kazachkovskii

Associate Editors: N. A. Vlasov and N. N. Ponomarev-Stepnoi

Secretary: A. I. Artemov

I. N. Golovin
V. I. Il'ichev
V. F. Kalinin
P. L. Kirillov
Yu. I. Koryakin
E. V. Kulov
B. N. Laskorin
V. V. Matveev
I. D. Morokhov
A. A. Naumov
A. S. Nikiforov
A. S. Shtan'
B. A. Sidorenko
M. F. Troyanov
E. I. Vorob'ev

Copyright © 1984, Plenum Publishing Corporation. *Soviet Atomic Energy* participates in the Copyright Clearance Center (CCC) Transactional Reporting Service. The appearance of a code line at the bottom of the first page of an article in this journal indicates the copyright owner's consent that copies of the article may be made for personal or internal use. However, this consent is given on the condition that the copier pay the flat fee of $8.50 per article (no additional per-page fees) directly to the Copyright Clearance Center, Inc., 21 Congress Street, Salem, Massachusetts 01970, for all copying not explicitly permitted by Sections 107 or 108 of the U.S. Copyright Law. The CCC is a nonprofit clearinghouse for the payment of photocopying fees by libraries and other users registered with the CCC. Therefore, this consent does not extend to other kinds of copying, such as copying for general distribution, for advertising or promotional purposes, for creating new collective works, or for resale, nor to the reprinting of figures, tables, and text excerpts. 0038-531X/84 $8.50

Consultants Bureau journals appear about six months after the publication of the original Russian issue. For bibliographic accuracy, the English issue published by Consultants Bureau carries the same number and date as the original Russian from which it was translated. For example, a Russian issue published in December will appear in a Consultants Bureau English translation about the following June, but the translation issue will carry the December date. When ordering any volume or particular issue of a Consultants Bureau journal, please specify the date and, where applicable, the volume and issue numbers of the original Russian. The material you will receive will be a translation of that Russian volume or issue.

Subscription (2 volumes per year)
Vols. 54 & 55: $500 (domestic); $555 (foreign)
Vols. 56 & 57: $560 (domestic); $621 (foreign)

Single Issue: $100
Single Article: $8.50

CONSULTANTS BUREAU, NEW YORK AND LONDON

c/b
233 Spring Street
New York, New York 10013

Published monthly. Second-class postage paid at Jamaica, New York 11431.

Declassified and Approved For Release 2013/09/14 : CIA-RDP10-02196R000300040005-3

Declassified and Approved For Release 2013/09/14 : CIA-RDP10-02196R000300040005-3

SOVIET ATOMIC ENERGY

A translation of *Atomnaya Énergiya*

November, 1984

Volume 56, Number 5 **May, 1984**

CONTENTS

Declassified and Approved For Release 2013/09/14 : CIA-RDP10-02196R000300040005-3

Declassified and Approved For Release 2013/09/14 : CIA-RDP10-02196R000300040005-3

CONTENTS

(continued)

The Russian press date (podpisano k pechati) of this issue was 4/20/1984. Publication therefore did not occur prior to this date, but must be assumed to have taken place reasonably soon thereafter.

Declassified and Approved For Release 2013/09/14 : CIA-RDP10-02196R000300040005-3

Declassified and Approved For Release 2013/09/14 : CIA-RDP10-02196R000300040005-3

ARTICLES

QUANTITATIVE ESTIMATION OF NUCLEAR SAFETY

B. P. Shishin

UDC 621.039.58

Ensuring nuclear safety of a critical stand or nuclear reactor, i.e., preventing uncontrolled increase in the breeding coefficient of neutrons in a breeder system above unity, presumes the solution of a series of technical problems: the development of special control and protection systems, training of staff, and the production of documentation coordinating and limiting the functional activity of the staff and systems of the equipment. The designers, users, and inspection personnel must evaluate the nuclear-safety level of nuclear-physics equipment in the same way. In such conditions, it is important to formulate and employ objective methods of estimation as an instrument of analysis, as a supplement to the Rules of Nuclear Safety. In the present work, the possibility of quantitative estimation of the nuclear safety of apparatus, primarily critical stands, is demonstrated; it is reduced to the problem of analyzing the reliability of functioning of the systems and elements of the equipment, using the apparatus of mathematical logic and probability theory.

The nuclear installation takes the form of an active region in combination with systems for emergency protection, flooding the active region with water, parameter monitoring, etc. The service personnel are regarded as one of the elements of the systems. Each system consists of elements (sensors, valves, tubes, mechanisms, etc.), which may be in one of several possible states (operative, inoperative, emergency, etc.).

The set of states of the elements determines the set of states of the system, which, in turn, are components of the set of states of the installation. The states if the elements may be taken in accordance with some value of the probability, i.e., the relative proportion of time in which the element is in a particular state. Transition of the system from one state to another in the course of the operating time is also characterized by a probability [1]. Emergency states of the installation correspond to some probability value, which is a measure of the "nuclear hazard," while its inverse is a measure of the "nuclear safety." Estimation of these quantities is an important problem of nuclear safety. Nuclear emergency of the installation may be regarded as the intersection of two events: the nuclear installation is in a supercritical state, and increase in the nuclear flux above a specified limiting value in the active zone does not trigger the emergency-control (EC) devices.

The probability of nuclear emergency $\mathcal{P}$ (NE) is written in the form

$$\mathcal{P}(\mathrm{NE}) = \mathcal{P}(\rho > 0)\, q(\mathrm{EC}), \tag{1}$$

where $\mathcal{P}(\rho > 0)$ is the probability of a supercritical state of the reactor; ρ is the reactivity of the reactor; q(EC) is the probability of EC failure. The probability $\mathcal{P}(\rho > 0)$ consists basically of two components. One $\mathcal{P}_1(\rho > 0)$ is determined by the operating program. In the course of this program, the reactor is sometimes in subcritical, critical, and supercritical states. The probability that the reactor will be in a supercritical state may be estimated if the operating program and the methods of its implementation are known. The second component $\mathcal{P}_2(\rho > 0)$ is determined by random unplanned processes in reactor control, when it becomes supercritical as a result of operator error or by breakdown or loss of functioning in the systems of the installation (systems of moderator and fuel filling, control and safety system, etc.).

The probability of failure of the emergency-control system q(EC) is determined by the specific logic circuit and elements of the installation. If a limiting value of the nuclear-emergency probability is specified, then variation of the values of $\mathcal{P}(\rho > 0)$ and q(EC) is permitted. The nuclear-safety level may be increased by decreasing the probability that the reactor will reach a supercritical state and increasing the reliability of operation of the EC system.

Translated from Atomnaya Énergiya, Vol. 56, No. 5, pp. 275-277, May, 1984. Original article submitted July 6, 1982.

0038-531X/84/5605-0287$08.50 © 1984 Plenum Publishing Corporation

Declassified and Approved For Release 2013/09/14 : CIA-RDP10-02196R000300040005-3

Declassified and Approved For Release 2013/09/14 : CIA-RDP10-02196R000300040005-3

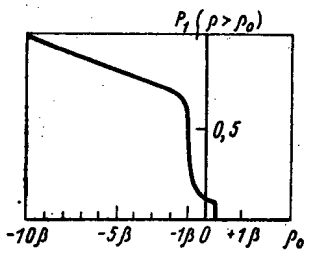

Fig. 1. Dependence of the probability of the reactor state on the reactivity.

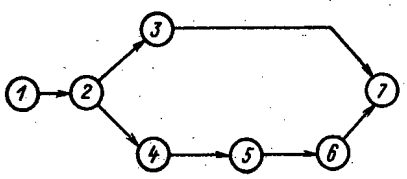

Fig. 2. System for flooding CP with water.

In the present work, an example of estimating the nuclear safety of a critical stand (critical pile with a water moderator, a system for flooding with water, and a control and safety system) is considered, when experimental programs assocated with the attainment of a supercritical state are employed, with possible disruption of the functioning of the water-flooding system and EC failure.

Estimating $\mathcal{P}_1$ ($\rho > 0$).

It is assumed that the critical pile (CP) in the flow of working mixture first moves from a deep subcritical state ($\rho < -10\beta$) to a weakly subcritical state ($\rho \approx -\beta$), and then from this state moves periodically to a supercritical state with a reactivity not exceeding $\rho = \beta/4$. Such experiments are usually conducted with measurements of the differential reactivity. After the experiments, the CP is in a subcritical state. The characteristic dependence of the probability of the reactor state on the reactivity $\rho > \rho_0$ for such experiments is shown in Fig. 1. When $\rho_0 = 0$, which corresponds to a supercritical CP, the probability of this event is ~ 0.1.

Estimating $\mathcal{P}_2$ ($\rho > 0$).

A subcritical reactor may become supercritical as a result of disruption of the normal functioning of the system for flooding the CP with water. The maximum scale of emergency corresponds to instantaneous uncontrollable flooding. The length of the process may be taken into account at the stage of more detailed computations.

In normal conditions, the system (Fig. 2) operates as follows. Water from reservoir 1 is fed by pump 2 to be branch 3-7 or the branch 4-5-6-7, depending on which valves are open (the pump and valves are controlled by the operator). With a deep subcritical state ($\rho < -\beta$), and the need for fast flooding of large volumes, branch 3-7 is used. The other branch is used for the dosed flooding of the CP in near-critical states ($0 > \rho \geqslant -\beta$). The flooding process occurs in two stages here: with valve 4 open and valves 3, 6 closed, volume 5 is flooded; them pump 2 is switched off, valve 4 is closed, and valve 6 is opened, to release the water into CP 7.

Emergency flooding of the CP with water occurs as a result of operator error or technical faults in the following cases:

a) when pump 2 is operating, valve 3 is opened in subcritical conditions $\rho < -\beta$ (in normal use, valve 3 is regarded as closed when $\rho \geqslant -\beta$);

b) when valves 2 is operating, valves 4 and 6 are opened with subcritical conditions $0 > \rho > -\beta$;

Declassified and Approved For Release 2013/09/14 : CIA-RDP10-02196R000300040005-3

Declassified and Approved For Release 2013/09/14 : CIA-RDP10-02196R000300040005-3

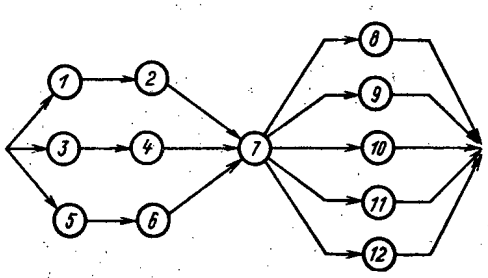

Fig. 3. Emergency-control system

c) with the pump inoperative and intermediate volume 5 filled, valve 6 is opened with subcritical conditions $0 > \rho \geqslant -\beta$.

In all emergencies, control is lost above the valves. In the approximation of "instantaneous flooding," no correction of the operator error or repair of the equipment is assumed.

The given emergency corresponds to the following expressions for the probability of emergency flooding of the critical pile with water

$$P_a(\rho > 0) = p_2^+ p_3^- p_7(\rho < -\beta); \quad (2)$$

$$P_b(\rho > 0) = p_2^+ (p_4^+ + p_4^-)\, p_6^- p_7(0 > \rho \geqslant -\beta); \quad (3)$$

$$P_c(\rho > 0) = p_2^- p_4^0 p_5^+ p_6^- p_7(0 > \rho \geqslant -\beta). \quad (4)$$

Here p_2^+, p_2^- are the partial probabilities of the states of element 2 (the pump): operating or not operating; p_i^0, p_i^+, p_i^- are the same parameters for valves with i = 3, 4, 6: closed, open with normal functioning, and open as result of operator error or fault; p_5^+, p_5^- are the probabilities for element 5 (intermediate volume): filled, not filled; p_7 is the partial probability of the state of the CP (element 7) with respect to the reactivity parameter; $p_7(\rho < -\beta)$ —corresponds to a CP reactivity of less than -β and $p_7(0 > \rho \geqslant -\beta)$ to a CP reactivity in the range $0 > \rho \geqslant -\beta$.

In the given experimental program, the pump may operate for 10% of the operating time in the shift. In this case, $p_2^+ = 0.1$ and $p_2^- = 0.9$. The valves are open in normal use for approximately 5% of the time; thus, $p_3^+ \approx p_4^+ \approx p_6^+ \approx 0{,}05$, and $p_3^0 \approx p_4^0 \approx p_6^0 \approx 0{,}95$. The volume 5 is in the filled state for 90% of the operating time; for 5% of the time, it is empty, and pathway 2-3-7 is used; and for 5% of the time it is filled through valve 4; thus $p_5^+ = 0.90$. The probability of operator error p_o^- may reach 0.02 [2, 3].

The probability of failure of the valves and other components of the hydrosystem in the course of the working shift is approximately 10^{-4}–10^{-5} [4-7].

The probability that a valve opened as a result of operator error remains open is $p_i^+ p_o^- = 0.05 \cdot 0.02 = 10^{-3}$, where i = 3, 4, 6. This quantity may be denoted by p_i^-, the probability of random opening of the valve.

The probability p_7 that the reactor will be in states with $\rho < -\beta$, according to Fig. 1, is ~0.8, while in the range $0 > \rho \geqslant -\beta$, it is approximately 0.1. In such conditions, the probability of random emergency flooding of the CP with water is estimated as

$$\mathcal{F}_2(\rho > 0) = p_a + p_b + p_c = 8 \cdot 10^{-5} + 5 \cdot 10^{-7} + 8 \cdot 10^{-5} = 1{,}6 \cdot 10^{-4}.$$

Estimating q(EC)

In the given example, it is assumed that the EC system (Fig. 3) has two power-measurement channels (1-2 and 3-4), a reactivity-measurement channel (5-6), two groups of EC working components, (8 and 9), elements of manual (10) and automatic (11) regulation, and a compensating unit 12. Sensors 1, 3, 5 send signals to the comparative instruments 2, 4, 6. When the signal exceeds a specified level, it is fed to commutating device 7, resulting in the triggering of all the working elements of the safety and control system (8-12).

Failure of the EC system may occur in the case of failure of the following system elements: 1 or 2, 3 or 4, 5 or 6, or even element 7, or element 8-12. The expression for the

Declassified and Approved For Release 2013/09/14 : CIA-RDP10-02196R000300040005-3

Declassified and Approved For Release 2013/09/14 : CIA-RDP10-02196R000300040005-3

probability of such an event is written in the form

$$q(\mathrm{EC}) = \prod_{i=1,3,5} (q_i + q_{i+1}) + q_7 + \prod_{i=8-12} q_i, \quad (5)$$

where q_i is the probability of failure of the i-th element in the system; Π is the product sign.

The failure rate of the radioelectronic equipment, its components, the relays, drives, electric motors, is 10^{-4}–10^{-6} h^{-1} [5-7]. The failure probability of such equipment in the course of a working shift is 10^{-3}–10^{-5}. According to Eq. (5), the probability of EC-system failure in this case is approximately 10^{-3}–10^{-5}. For nuclear power plants, the approximate failure rate of the control and safety system is a few times 10^{-4} h^{-1} [5, 7].

Probability of Nuclear Emergency

The probability of nuclear emergency in experiments associates with attainment of a supercritical state by the reactor, in the case of possible disruption of the functioning of the flooding system and RC system is calculated from Eq. (1) with

$$\mathcal{P}(\rho > 0) = \mathcal{P}_1(\rho > 0) + \mathcal{P}_2(\rho > 0).$$

With the values of $\mathcal{P}_1(\rho > 0)$, $\mathcal{P}_2(\rho > 0)$, and q(EC) determined above, the probability of such an emergency is $\mathcal{P}$ (NE) = 10^{-4}–10^{-6}.

The maximum contribution comes from AC failure in planned movement of the reactor to a supercritical state in the course of the experiments. The next most probable emergency is associated with erroneous release of water from volume 5 and emergency discharge through channel 3-7 (Fig. 1). If $\mathcal{P}$ (NE) is the probability that there will be an emergency in the course of a single operating shift, the probability of such an emergency in the course of a year (100 operating shifts) is 10^{-2}–10^{-4}. A similar analysis may be conducted with respect to other nuclear-installation systems.

The development of quantitative methods of estimating nuclear safety will facilitate the adoption of more accurate solutions and the reduction in material costs in ensuring the safety of nuclear-physics installations.

LITERATURE CITED

1. V. V. Frolov and V. I. Bulanenko, At. Tekh. Rub., No. 1, 3 (1981).
2. Handbook on Engineering Phychology [in Russian], Mashinostroenie, Moscow (1982).
3. R. Lloyd et al., Nucl. Technol., 42, 13 (1979).
4. S. M. Trunin et al., Reliability of Marine Machines and Mechanisms [in Russian], Sudostroenie, Leningrad (1980).
5. F. Ya. Ovchinnikov et al., At. Énerg., 50, No. 4, 248 (1981).
6. Proceedings of Seventh, Eighth, and Ninth Symposium on Natural Reliability and Quality Control, Washington (1961-1963).
7. Proceedings of a Symposium on the Reliability of Nuclear Power Plants, IAEA, Vienna (1975).

Declassified and Approved For Release 2013/09/14 : CIA-RDP10-02196R000300040005-3

Declassified and Approved For Release 2013/09/14 : CIA-RDP10-02196R000300040005-3

EMISSIONS OF ^{60}Co, ^{110m}Ag, AND ^{54}Mn AT THE ARMENIAN NUCLEAR POWER PLANT, AND THEIR CONTENT IN THE SURROUNDING ATMOSPHERE

E. S. Saakov, A. A. Avetisyan, and K. I. Pyuskyulyan

UDC 551.510.721.614.73

Six years of operation of the Armenian nuclear power plant (NPP) with a VVÉR-440 led to an increase in the contribution of radioactive corrosion products, in particular ^{60}Co, ^{110m}Ag, and ^{54}Mn, to the total activity of the gas–air mixture discharged into the stack (Table 1). According to the data for January-September, 1982, these radionuclides contributed 57% of the total activity of the long-lived aerosols discharged into the atmosphere, neglecting ^{131}I. Consequently, the yearly emission of long-lived radioactive aerosols is due largely to radioactive corrosion products.

The ^{60}Co enters the coolant from abrasion resistant alloys containing this element (pump bushings, control and safety rod actuators, etc.), and from austenitic stainless steels. The ^{54}Mn comes from the same structural materials, and the ^{110}Ag from the silver in alloys used in the thermoelectric heater of the volume compensator and control devices.

Most of the radioactive corrosion products are deposited on the inner walls of the primary loop system. As a result of changes in the coolant velocity and temperature and the water-chemical condition during transient operation there is a change in the relative amounts of corrosion products deposited on the walls of the equipment and in the coolant; during shutdown the amount of ammonia and boric acid in the primary loop is increased. Thus, it was determined that with a drop in power the specific activities of ^{60}Co, ^{110m}Ag, and ^{54}Mn at the Kola NPP increased by factors of 50, 80, and 110 respectively. According to data in [2], about 25% of the corrosion products in the coolant are in the form of large particles, about 75% are colloid, and the ion fraction is less than 1%. The concentrations of the nuclides mentioned reach a maximum in ∿46-48 h after a drop in power. Then the specific activity decreases, and the coefficient of precipitation of radioactive corrosion products becomes an order of magnitude smaller than that obtained under steady reactor operation [1]. In view of this, one should expect that during reactor startup and shutdown the emission of radioactive corrosion products would be appreciably increased. Using the daily measurements of the total activity of the discharge of long-lived aerosols during the period of planned preventive maintenance on the first block of the Armenian NPP, we plotted a graph (Fig. 1) of the time variation of the activity of the discharge. The figure shows that during cooling, hydraulic testing, and reactor startup, the total activity of the discharge increase sharply. The same conclusion can be drawn from spectrometric analysis (Table 2).

TABLE 1. Contribution of Radionuclides to Total Activity of Discharge of Long-Lived Aerosols, %

Period	^{60}Co	^{110m}Ag	^{54}Mn
1978	2,4	1,9	1,7
January-September 1982	12,0	14,0	5,0

Translated from Atomnaya Énergiya, Vol. 56, pp. 278-280, May, 1984. Original article submitted September 20, 1983.

0038-531X/84/5605-0291$08.50 © 1984 Plenum Publishing Corporation

Declassified and Approved For Release 2013/09/14 : CIA-RDP10-02196R000300040005-3

Declassified and Approved For Release 2013/09/14 : CIA-RDP10-02196R000300040005-3

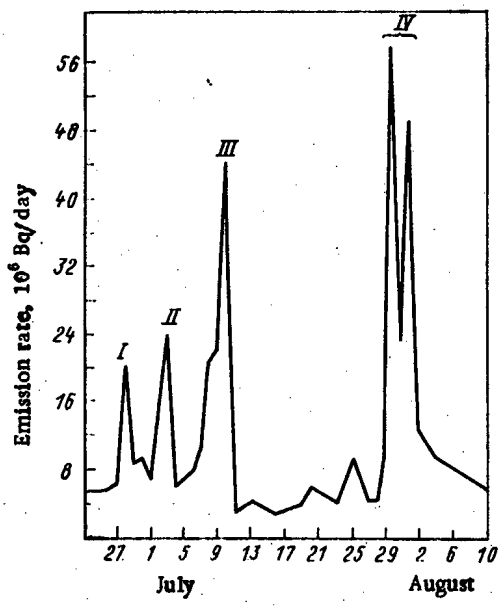

Fig. 1. Total activity of discharge of long-lived aerosols into the stack during: I) cooling; II) unpacking main joint, opening volume compensator; III) refueling; IV) hydraulic testing, output at power.

TABLE 2. Rate of Discharge of Radionuclides in 1982, 10^7 Bq/month

Period	^{60}Co	^{110m}Ag	^{54}Mn
January	1,65	1,30	0,69
February	3,43	3,20	1,30
March	2,60	1,42	0,84
April	20,80	6,75	7,22
May	7,45	7,22	2,37
June	5,21	7,58	1,78
July	4,00	1,85	13,02
August	4,02	2,96	0,91
September	1,66	1,54	0,71

TABLE 3. Concentration of Radionuclides in Air at 1 km from NPP in 1982, 10^{-8} Bq/liter

Period	^{60}Co	^{110m}Ag	^{54}Mn
1st quarter	0,62	0,64	Traces
2nd quarter	1,40	3,00	1,10
July	1,70	4,80	1,00
August	0,80	0,80	Traces
September	Traces	Traces	Traces

The increase in the discharge of ^{60}Co, ^{110m}Ag, and ^{54}Mn coincides with the periods of planned preventive maintenance at the NPP. The time variations of the discharge of ^{60}Co and ^{54}Mn are identical, since they have a common source. The behavior of ^{110m}Ag is somewhat different; in particular there was a sharp increase in the discharge of silver in July due to opening the manhole of the volume compensator and repairing it during planned preventive maintenance on the first block.

Air samples were taken at seven check points in various directions from the Armenian NPP

Declassified and Approved For Release 2013/09/14 : CIA-RDP10-02196R000300040005-3

Declassified and Approved For Release 2013/09/14 : CIA-RDP10-02196R000300040005-3

TABLE 4. Comparison of Calculated and Measured Maximum Concentration of Radionuclides During July, 1982, 10^{-8} Bq/liter

Radionuclide	^{60}Co	^{110m}Ag	^{54}Mn
Calc. values	1,10	3,60	0,51
Meas. values	1,70	4,80	1,00

and at distances of 1, 5, 6, 11, 14, 15, and 50 km from it. The spectrometric analysis was performed by using a DGDK-32A-1 semiconductor detector of AI-4096 and UNO-4096-90 analyzers. The minimum detectable concentration of aerosols estimated by the formula in [3] is 0.4×10^{-8} Bq/liter with an error of 30% (Table 3). Only traces of radionuclides were found in samples taken at 5 and 6 km, and none were found in the samples taken at the remaining points. The results are confirmed by analysis of sedimentation samples. Samples of top soil showed only insignificant amounts of ^{137}Cs and ^{90}Sr due to global fallout.

Evidently the recording of these radionuclides in the air near the Armenian NPP is due to specific climatic conditions in the region. The climate of the Ararat valley is clearly continental, with an arid summer and a short rarely cold winter. The atmospheric precipitation is 250-300 mm. During the long calm summer with an abundance of sunny days, the air is heated up to 40°C. The wind velocity in the industrial region of the Armenian NPP does not exceed 3 m/sec. Under the strong solar heating of the earth's surface, the air temperature decreases with height, so that the vertical temperature gradient is larger than adiabatic. Such conditions lead to intense vertical displacement of the air. The maximum concentration near the ground for the present stack height is relatively large, but it decreases rapidly with distance from the source, depending on the wind direction.

The minimum value of K_d, the average monthly dilution ratio of the contaminant, was calculated from metereological data obtained at stations in the NPP region, and the formula recommended in [4]. The calculated value of K_d was 1.4×10^6 m^3/sec. For comparison we point out that the minimum yearly average dilution ratio for the center of our European territory is 3.4×10^6 m^3/sec [4].

The maximum ground level concentrations of ^{60}Co, ^{110m}Ag, and ^{54}Mn were found form the measured values of their emission and the calculated value of K_d. Within the limits of error, the calculated values agree with the spectrometric analysis of air samples taken at 1 km from the NPP (Table 4).

The data obtained justify the following conclusions and recommendations:

the possibility of recording ^{60}Co, ^{110m}Ag, and ^{54}Mn in the air at 1 km from the Armenian NPP for emission which does not differ from that of other NPP with VVÉR, is due to the specific climatic conditions at its location;

the emission of radioactive corrosion products during reactor shutdown and startup can be reduced by using filters to retain the deposits, after loosening them and scraping them off;

in determining the isotopic composition of the radionuclides in the layer of the atmosphere near the ground, and the radiation doses received by people living near NPP, it is necessary to take account of the contribution of radioactive corrosion products.

LITERATURE CITED

1. V. B. Gall' et al., in: Radiation Safety and Shielding of NPP [in Russian], No. 5, Atomizdat, Moscow (1981), p. 5.
2. I. K. Morozova et al., Removal and Deposition of Corrosion Products of Reactor Materials [in Russian], Atomizdat, Moscow (1975).
3. S. M. Vakulovskii et al., in: Methodological Recommendations for Monitoring the Radioactive Content of Objects in the Environment [in Russian], Moscow (1980), p. 234.
4. N. E. Artemova et al., Admissible Emissions of Radioactive and Harmful Chemicals into the Ground Layer of the Atmosphere [in Russian], Atomizdat, Moscow (1980).

Declassified and Approved For Release 2013/09/14 : CIA-RDP10-02196R000300040005-3

Declassified and Approved For Release 2013/09/14 : CIA-RDP10-02196R000300040005-3

UNLOADING ADDITIONAL ABSORBERS FROM THE RBMK-1000 CORE

N. V. Isaev, V. E. Druzhinin,
and Yu. V. Shmonin

UDC 621.039.539.1

In the initial loading of the RBMK-1000 reactor, the considerable reactivity margin is reduced by loading the channels only incompletely with fuel assemblies (FA), absorbers being inserted in the unfilled channels. The core then contains 234 additional absorbers (AA) and 44 unloaded channels containing water columns (WC).

The RBMK-1000 design envisages a strategy for reloading the channels by dividing them up into periodicity cells (polycells) of size 4×4 cells each [1]. One channel in each polycell is reloaded, and to maintain the loading symmetry and periodicity, one unloads channels identically placed in the polycell. This method has been used in reloading the reactors at Kursk nuclear power station.

Here we examine the effects of AA unloading order on the economic parameters of the second-generation RBMK-1000 reactors in the steady state. As the safety state is attained at 7-8 years after commissioning, the optimum AA unloading strategy in the transition period can be examined only on theoretical models. The unloading of the AA involves about 670-700 effective working days.

Model Description. The REF program [2] is used in calculating the transient state in the RBMK and envisages a specially homogenized core. This program is widely used in determining RBMK characteristics, so the algorithm is not described here.

The OPERA program for optimizing apparatus reloading [3] enables one to perform a detailed full-scale two-group diffusion calculation on the RBMK parameters under conditions of partial and ongoing reloading, including the adjustment of the power production field by varying the insertion lengths of the control and protection rods (CPR). The OPERA program is based on the OPTIMA one [4]. A difference from the OPTIMA algorithm, which is described in [4], is that the OPERA program uses an improved algorithm that instead of using the CPR to compensate the reactivity and equalize the power production (while retaining k_{ef}) enables one to bring the reactor to a given k_{ef} by automatic selection of the necessary rods in the CPR set. In simulating RBMK reloading, the power production field is profiled to a certain set field W_j^{reg}. The following constraints must be met in using the OPERA program:

1. The insertion depth h_i of the CPR is in the range

$$0 \leqslant h_i \leqslant x_{max,\, i}, \tag{1}$$

where $h_{max,\, i}$ — is the maximum permissible insertion depth for CPR rod i.

2. The power W_j in a channel should not exceed the limiting value W_{li}:

$$W_j \leqslant W_{li} \tag{2}$$

3. The values of the coefficients for power production nonuniformity along the radius k_r and over the height k_z should not exceed the corresponding maximum values k_r^{max} and k_z^{max}:

$$k_r \leqslant k_r^{max}; \tag{3}$$

$$k_z \leqslant k_z^{max}. \tag{4}$$

Translated from Atomnaya Énergiya, Vol. 56, No. 5, pp. 280-282, May, 1984. Original article submitted August 10, 1983.

 0038-531X/84/5605-0294$08.50 1984 Plenum Publishing Corporation

Declassified and Approved For Release 2013/09/14 : CIA-RDP10-02196R000300040005-3

Declassified and Approved For Release 2013/09/14 : CIA-RDP10-02196R000300040005-3

4. The relative deviations in the power W_k from W_k^{reg} in channels containing monitoring sensors should not exceed the given value ε:

$$(W_k - W_k^{reg})/W_k^{reg} \leqslant \varepsilon. \quad (5)$$

5. The power W_j in a channel and the water flow rate G_j through it are such that the margin coefficient k_{cr} up to the limiting permissible power is greater than one:

$$k_{cr} > 1. \quad (6)$$

6. During the operation, an operational reactivity margin N(t) not less than the value $N_{op}(t)$ specified by the working rules is to be maintained, which is usually expressed in units of the reactivity introduced by the manual control rod:

$$N(t) \geqslant N_{op}(t). \quad (7)$$

7. A final check is made on obedience to the nuclear safety condition for the final reloading model.

If any of these constraints is violated when the OPERA program is run, and if the violation cannot be eliminated by displacing the CPR, the reloading in that channel is ruled out and the next one is considered.

One primarily considers channels characterized by large deviations of the current W_j from W_j^{reg}, which guarantees maintenance of a pattern close to W_j^{reg}. When the reloading of each channel has been simulated, a check is made on obedience to constraints 2-7. The weights of the reloaded channels are usually known in advance for the RBMK-1000, and therefore the number of these channels per reloading can be determined from the need to produce the required reactivity margin $\Delta N = N - N_{op}$.

Model comparison. As two different models realized in the REF and OPERA programs are used to calculate the RBMK-1000 reloading, the first part of the study involves comparing the results. The comparison was made starting with the instant when the unloading of the AA ends. The following reactor parameters were considered: the time ΔT_1 startup to the end of AA unloading, the reloading rate R(t), the mean burnup in the unloaded fuel $\bar{E}(t)$, the mean burnup in the core $\bar{E}_c(t)$, and the number of FA loaded into the core after startup $n_{FA}(t)$. The values of these parameters calculated from the RED and OPERA programs agreed within about 1%. There was also practically exact coincidence between the values of R, $\bar{E}$, $\bar{E}_c$, ΔT_1, and n_{FA} for various unloading orders, which occurs because these parameters are affected only by the absorbing properties in the plateau in the W_j^{reg} distribution (where most of the AA are). This explains the agreement between the characteristics calculated from REF and OPERA, since the REF program envisages an infinite planar model having the parameters of the plateau zone in the RBMK. By combining these calculations one can economize in computer time. The OPERA program is usually employed to calculate only those characteristics that cannot be obtained from REF (for example, the power distribution in the channel and the FA burnup in the core at various times).

Checking the nuclear safety conditions. This is based on the SAFETY program, which determines the subcriticality when the emergency-protection rods are raised to the upper limit stop, as are the other CPR rods for a given state in the core. To save computer time, the faster SOS program is used to select the most reactive state (calculating the RBMK parameters with an ES-1052 computer on the OPTIMA program requires 4-7 min, while the SAFETY program requires 25-30 min).

Results. The OPERA program has been used to simulate partial reloading the first unit at Smolensk nuclear station. The burnup and channel power calculations were compared with the readings in the centralized SKALA monitoring system. The OPERA program was used to examine various forms of partial and continuous reloading up to complete AA removal from the core and onwards in the transition to the stationary state. Various forms of AA unloading proposed by power station specialists were considered, as well as ones recommended by the OPERA program. To calculate one model for AA unloading with the OPERA program requires about 8 h with the ES-1052. In all the comparative calculations, we used the same typical graph

Declassified and Approved For Release 2013/09/14 : CIA-RDP10-02196R000300040005-3

Declassified and Approved For Release 2013/09/14 : CIA-RDP10-02196R000300040005-3

for the reactor reaching nominal power. Some general regularities on AA unloading were thereby formulated:

1) the most trouble arises over reloading (because of power rise in the surrounding channels) near channels containing shortened CPR, near automatic-protection rods, and near channels containing power-production monitoring sensors;

2) rises in W_j can occur near channels containing WC;

3) it is always possible to unload an AA from a channel whose diagonal environment contains manual-control rods;

4) ΔT_1 is virtually independent of the order of AA unloading;

5) the values of R, $\bar{E}$, $\bar{E}_c$, and n_{FA} obtained with various forms of AA unloading up to the end of ΔT_1 show only very small differences, since the consequences of these make themselves felt only after 6-8 years;

6) the minimal interval in the characteristic instability time on the first azimuthal harmonic τ_{01} is attained only after 900-1100 effective operating days in the absence of local automatic regulators and;

7) it is recommended that OPERA should be used to simulate the operation for about 50 effective days ahead, since the consequences of incorrectly planned realoading can appear within this time.

When the reactor is operating at power, cases can arise where conditions 2-7 are met at the time of channel reloading, but after a certain time there is a power rise in the channel due to accumulation of plutonium in the fuel or to the effects of incorrectly simulated subsequent reloading. The effect from the accumulation of plutonium for the RBMK in the steady state is small. However, allowance must be made for it in the transitional period (especially in the initial stage). During the first 40-50 days of operation, the reactivity hardly falls, and it is therefore impermissible to place several fresh FA together in the core during continuous reloading.

Effects of WC Channels on Core Parameters in the Transitional Period. The calculations show that the RBMK core parameters in the steady state are influenced mainly by the number of water channels, not by their positions within the plateau in the W_j^{reg} distribution. According to the safety conditions, there should not be more than 53 channels containing water columns in the RBMK-1000 core in the transitional period. To estimate the WC effect, we performed two calculations on the transitional periods for the RBMK-1000. In the first, we used a typical initial load with 44 channels containing WC; these WC channels were loaded with fuel after the end of the AA unloading. In the second calculation, the initial reactivity was compensated only by means of AA (for this purpose, the number at the start was increased to 265). In the first case, the transitional period required 25 FA less than in the second (taking account of the total number of FA in the initial load and the number involved in loading during the transitional period). The initial core load in the second model contained 31 FA less than in the first. The presence of the WC channels caused a power redistribution between them (since the total thermal power was taken from a smaller number of FA), and also a slight increase in the reloading rate, as well as neutron capture in the water, and as a result the pure effect at the end of the transitional period was 25 FA.

Recommended AA Unloading Order. These calculations provide a simple procedure for determining the AA unloading order to provide a given W_j^{reg} distribution. The core is split up into polycells of size 4×4 cells as usually employed in RBMK calculations. Each polycell contained two AA in the initial period. We selected four polycell lattices as follows:

1) the first was constituted by polycells arranged in chessboard order with intervals of one from the central polycell;

2) the other three were defined by shifting the first one polycell to the right, downwards, or to the left correspondingly.

We then took the following sequence for unloading the AA from the polycells:

1) unloading applies to one AA out of the two in a polycell (for definiteness we take the AA in the upper row in the polycell);

2) one unloads one AA from each of the polycells in the first lattice, then in the second, etc.;

Declassified and Approved For Release 2013/09/14 : CIA-RDP10-02196R000300040005-3

Declassified and Approved For Release 2013/09/14 : CIA-RDP10-02196R000300040005-3

3) after unloading the first AA from all these lattices, one unloads the second AA using the same order for the polycells as in unloading the first;

4) in partial reloading, one unloads the AA completely from the entire polycell lattice;

5) with continuous reloading, the sequence of AA unloading within a given lattice is determined in accordance with the recommendations from the OPERA program; and

6) when the AA unloading from a given lattice has been completed, one transfers to the next, and so on.

Usually, there are three partial reloads at nuclear stations containing RBMK-1000 reactors, after which continuous reloading begins.

LITERATURE CITED

1. N. A. Dollezhal' and I. Ya. Emel'yanov, The Channel Nuclear Reactor [in Russian], Atomizdat, Moscow (1980).
2. V. S. Romanenko and A. V. Krayushkin, At. Énerg., 53, No. 6, 367 (1982).
3. N. V. Isaev and Yu. V. Shmonin, Nuclear Science and Engineering: Reactor Physics and Engineering Series [in Russian], Issue 8 (37) (1983), p. 35.
4. A. A. Shkurpelov et al., At. Énerg., 54, No. 6, 387 (1983).

Declassified and Approved For Release 2013/09/14 : CIA-RDP10-02196R000300040005-3

Declassified and Approved For Release 2013/09/14 : CIA-RDP10-02196R000300040005-3

DISSOLUTION OF OXIDE FILMS ON CONSTRUCTIONAL STEELS

Yu. G. Bobrov, G. M. Gur'yanov,
A. P. Kovarskii, Yu. P. Kostikov,
and A. V. Motornyi

UDC 621.039.53:537.534

The key problem in the chemical engineering of nuclear power systems is to manage the interaction of contructional materials with the various media (coolants, deactivating solutions, etc.). The specifications are frequently conflcting. For example, to organize proper water treatment for the first circuit in a pressurized water reactor it is desirable for a stable passive film to be formed on the materils, which reduces the corrosion and the accumulation of radioactivity. On the other hand, the performance in decontamininating the circuit after use is directly related to that in removing the surface oxide layers formed during use.

It is necessary to provide relatively uniform dissolution of the oxides of iron (nickel) and chromium in the deactivating solution [1, 2] to provide identically effective removal of the films from the constructional steels 12Kh18N10T, 2Kh13, 48TS, and 22K (a task arising in decontaminating the circuits in the VVÉR-440). Here we consider ways of realizing these conditions.

Methods. As previously [1, 2], model oxide films on these steels were made by keeping polished specimens at about 300°C in a static autoclave containing a solution simulating the coolant in VVÉR-440 reactors (10 mg/liter KOH, 5 mg/liter NH_3, 8 g/liter H_3BO_3, and 200 mg/liter $N_2H_4 \cdot H_2O$). We examined two groups of specimens after oxidation for 1600 and 2200 h.

We analyzed the compositions of the surfaces (layer thickness $\leqslant 100$ Å, 1 Å $= 10^{-10}$ m) by the ÉSCA method (electron spectroscopy for chemical analysis) [3, 4]. The photoelectron spectra were excited with monochromatic K_α aluminum radiation. The spectrum was scanned in the energy range 0-1000 eV.

The contents of an element (relative to Fe) were estimated from the ratio of the heights of the 2p peaks for the element and Fe multiplied by the ratio of the ionization cross sections for the corresponding atomic levels. The error in the estimate is ±20%, and the limit of detection for an element is about 3 at.%.

The NGR ICE method (nuclear γ-resonance spectrometry on internal-conversion electron) [5] was used to examine the chemical form of the iron in the surface layers of the model oxides (thickness $\leqslant 2000$ Å). The γ-ray source was ^{57}Co of activity about 50 mCi in a palladium matrix. The internal-conversion electrons were recorded with a flow counter (helium containing alcohol vapor), with the specimen placed within it. The limit to the detection of a particular form of Fe in the layer was about 10%. In layerwise analysis of the oxides by the SIMS method (secondary ion mass spectrometry) [1, 2], we used a beam of primary O_2^+ ions of energy 5.5 keV and current density 1.7-2.9 A/m^2 on admitting oxygen to the chamber up to a pressure of about 4×10^{-3} Pa. The working layer thickness was several μm.

Results and Discussion. Figure 1 shows the ÉSCA spectra from 12Kh18N10T, 2Kh13, 48TS, and 22K steels oxidized in an autoclave for 1600 h. Table 1 gives the contents of the main components in the metal and the values determined for the surfaces (relatives to Fe) from the ÉSCA spectra.

Table 1 shows that the oxide films are depleted of Cr and enriched in Mn after 1600 h (the value for Ni appears to be an overestimate because of overlap from the Auger lines of Fe). After 2200 h in the autoclave, the surface oxides show only Fe lines. In accordance with the oxidation picture for alloys containing chromium [6], there is a stage in which a layer of Cr oxides is formed, through which Fe cations diffuse to form the outer iron-oxide layer.

Translated from Atomnaya Énergiya, Vol. 56, No. 5, pp. 282-286, May, 1984. Original article submitted August 18, 1983.

0038-531X/84/5605-0298$08.50 © 1984 Plenum Publishing Corporation

Declassified and Approved For Release 2013/09/14 : CIA-RDP10-02196R000300040005-3

Declassified and Approved For Release 2013/09/14 : CIA-RDP10-02196R000300040005-3

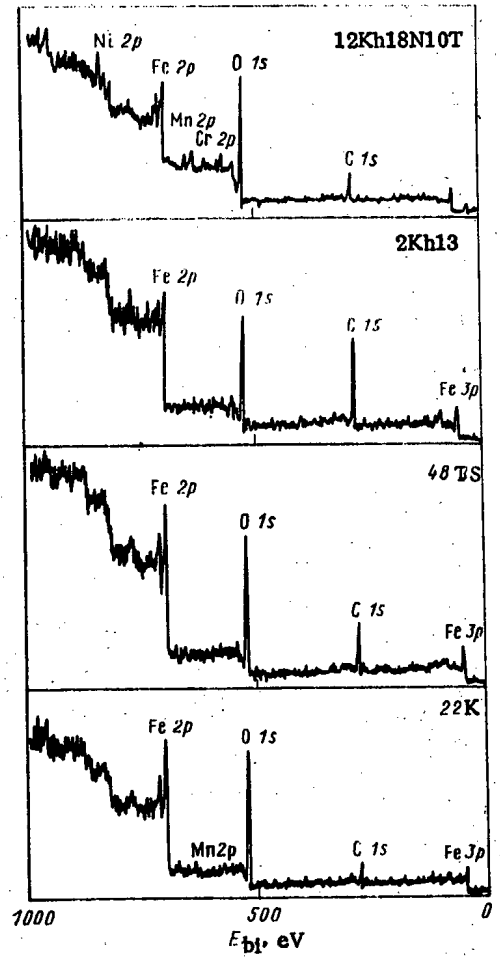

Fig. 1. ESCA spectra from the surface of 12Kh18N10T, 2Kh13, 48TS, and 22K steels oxidized in an autoclave (E_{bi} is the photoelectron binding energy).

TABLE 1. Elemental Compositions of Oxidized Steel Surfaces in Comparison with Alloy Compositions

Steel	Element	Element contents	
		in alloy	in surface oxide
12Kh18N10T	Fe	1	1
	Cr	0,26	0,23
	Ni	0,11	0,31
	Mn	0,03	0,22
48 TS	Fe	1	1
	Cr	0,03	$\leq$ 0,03
	Mn	0,005	$\leq$ 0,03
2Kh13	Fe	1	1
	Cr	0,15	$\leq$ 0,03
	Mn	0,01	$\leq$ 0,03
22 K	Fe	1	1
	Mn	0,01	0,07

Figure 2 shows the NGR spectra of these four steels oxidized in model coolant for 2200 h. The Fe at the surface is present mainly as magnetite Fe_3O_4. The intensity ratio for the two right-hand lines shows that there is not more than 10% γ-Fe_2O_3 (magnetite), which has the spinel structure and forms solid solutions with Fe_3O_4. So far, there is no satisfactory explanation for the spectrum for 12Kh18N10T steel showing the lines of metallic Fe.

SIMS [1, 2] showed that the outer layers are depleted in the alloying elements (apart from Mn), whereas the concentrations are increased at the oxide–metal boundary. The following

Declassified and Approved For Release 2013/09/14 : CIA-RDP10-02196R000300040005-3

Declassified and Approved For Release 2013/09/14 : CIA-RDP10-02196R000300040005-3

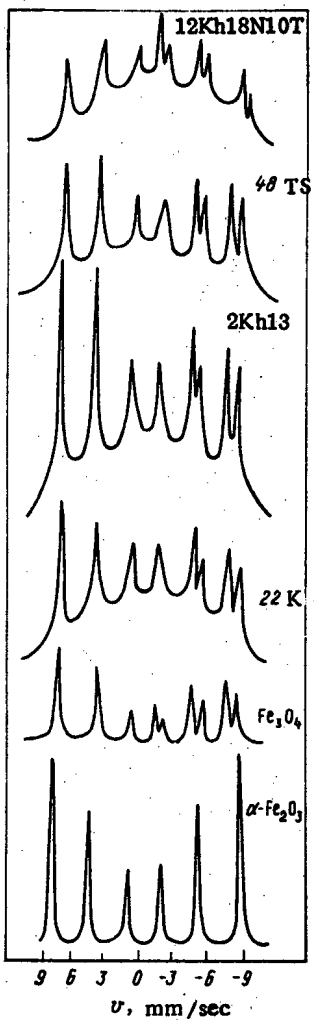

Fig. 2. NGR spectra from the surfaces of 12Kh18N10T, 2Kh13, 48TS, and 22K steels oxidized in an autoclave together with the standard spectra of α-Fe_2O_3 and Fe_3O_4.

TABLE 2. Cr/Fe Ratios at the Surfaces of 12Kh18N10T and 2Kh13 Steels after Various Treatments

Steel	Treatment	Cr/Fe
12Kh18N10T	Autoclave	
	1600 h	0,23—0,63
	2200 h	$<0,03$
	After autoclave	
	I—3 h	1,29—2,38
	I—3 h, II—1,5 h	1,67—3,07
	II—2 h	$<0,03$
2Kh13	Autoclave	
	2200 h	$<0,03$
	After autoclave	
	II—1 h	$<0,03$

structure applies for the films under these model conditions: outer iron—oxide layers of magnetite (sometimes doped with Mn), and inner layers possibly composed of spinels of FeO Me_2O_3, $MeO \cdot Fe_2O_3$ (where Me is Cr, Ni, Mo, etc.).

The outer layers are readily removed [1, 2] in acid decontaminating solutions ($H_2C_2O_4$; $H_2C_2O_4 + HNO_3$, etc.). It is much more difficult to remove the inner layers. The usual

Declassified and Approved For Release 2013/09/14 : CIA-RDP10-02196R000300040005-3

Declassified and Approved For Release 2013/09/14 : CIA-RDP10-02196R000300040005-3

TABLE 3. Treatment Sequence (1 h at 95°C) in Removing Oxide Films from 12Kh18N10T, 2Kh13, 48 TS, and 22K Steels

Treatment	Solution	pH
I	1% $H_2C_2O_4$	~2
II	As in treatment I with the addition of 1-3% OEDP + KOH	~10—12
III	As in treatment II with the addition of $H_2C_2O_4$	2—3
IV	As in treatment III with the addition of KOH	~10
V	As in treatment IV with the addition of $H_2C_2O_4$	2—3

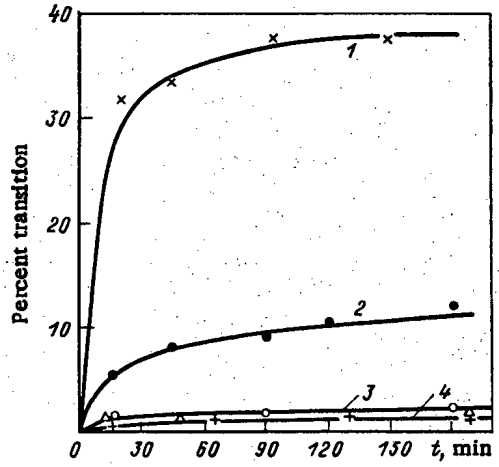

Fig. 3. Dissolution kinetics of model Cr oxide in certain solutions: 1) 0.5% $KMnO_4$ + 1% KOH; 2) 1% OÉDP + KOH (pH 13.0); 3) 9% HNO_3, 1% $H_2C_2O_4$; 4) 3% KOH.

TABLE 4. Specimen Corrosion in Treatments I-V

Steel	Thickness in μm of layer removed in treatment				
	I	II	III	IV	V
12Kh18N10T	0,05	0,10	0,5	0,7	2,6
2Kh 13	1,7	4,2	14,0	15,7	25,3
22 K	3,2	4,6	6,4	7,4	7,8
48 TS	2,6	3,9	5,2	5,8	5,8

method of removing the chromium-bearing layer from stainless or chromium steels is to use a solution of alkaline permanganate, which dissolves [1, 2] the Cr component of the oxide selectively, after which acid treatment removes the chromium-depleted layer. None of the other solutions examines [1, 2] provided substantial dissolution of this layer, which is due to the high stability of the chromium oxides. An exception was represented by OÉDP* citrate solutions examined in [2], which showed some signs of dissolving the Cr components. Therefore, a more detailed study was made of the action of reagents containing OÉDP on the surface oxides on these alloys.

*Oxyethylidene diphosphoric acid.

Declassified and Approved For Release 2013/09/14 : CIA-RDP10-02196R000300040005-3

Declassified and Approved For Release 2013/09/14 : CIA-RDP10-02196R000300040005-3

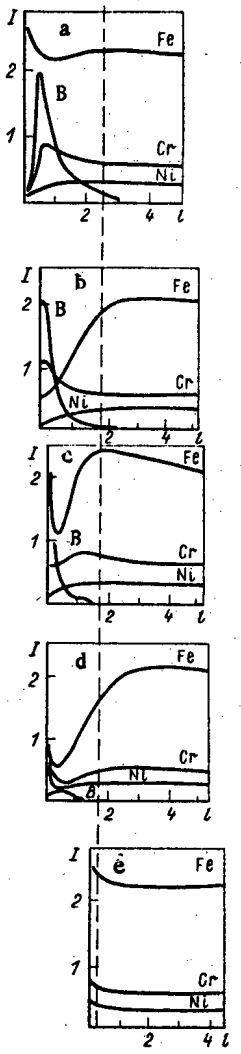

Fig. 4. Layerwise SIME analysis of surface oxide on 12Kh18N10T steel after various treatments: a) initial specimen (220 h in autoclave); b) after treatment I; c) after I and II; d) after I and II; e) the same on a part with the oxide removed (I ion-current intensity in relative units, l depth of etched layer, rel. units).

A standard method [7] was used to synthesize $Cr(OH)_3$ labeled with ^{51}Cr. After exposure to conditions simulating reactor ones (an autoclave at about 300°C) for 96 h, the material was dried. The oxide was identified by x-ray structure analysis as CrOOH, which simulated the Cr component on chromium-bearing steels oxidized under circuit conditions. Figure 3 shows kinetic curves for this oxide dissolving in certain solutions. The relative entry of the model oxide into alkaline OÉDP solution is almost five times higher than those for the acids, being about 30% of the entry into alkaline potassium permanganate solution.

We examined the effects of the following sequence of chemical treatment on oxidized 12Kh18N10T and 2Kh13 chromium-bearing steels: I) 1% $H_2C_2O_4$, 1 h 95°C; II) 1% $H_2C_2O_4$ + 1-3% OÉDP + KOH up to pH 10-12, 1-3 h, 95°C. The purpose of treatment I was to dissolve the iron oxide layer (magnetite) and also to provide selective dissolution of the Fe from the inner layer, which leads to the surface being enriched in Cr before treatment II. The purpose of treatment II was to dissolve the Cr component from the oxide layer enriched in Cr by the previous treatment.

It was assumed that the Cr enrichment by treatment I would tend to equalize the rates of removal for the Cr and Fe components in the inner layer, and would therefore produce more uniform dissolution of the layer as a whole.

Table 2 gives data on the changes in Cr/Fe ratio for these specimens derived from ESCA; it is clear that treatment I removes the magnetic layer and selectively dissolves the Fe from the inner layer, while treatment II does not dissolve the outer iron oxide layer, whereas the inner layer is evidently uniformly attacked as regards the Fe and Cr components, as is evident from the slight increase in the Cr/Fe ratio at the surface in treatment II following I. SIMS provided additional evidence on the mechanisms whereby treatments I and II affect oxidized 12Kh18N10T steel.

Declassified and Approved For Release 2013/09/14 : CIA-RDP10-02196R000300040005-3

Declassified and Approved For Release 2013/09/14 : CIA-RDP10-02196R000300040005-3

Figure 4 shows layerwise analyses for 12Kh18N10T steel. There is selective dissolution of the Fe component in treatments I and IIa (5% $H_2C_2O_4$ solution) and of the Cr component in II. The oxide was partially removed from the steel after treatment IIa.

Complete removal of the oxide layer from 12Kh18N10T steel as formed in about 2200 h required a repeat acid-alkali treatment by successive addition of $H_2C_2O_4$ and KOH to the solution used in treatment II. This was evidently due to the inadequate uniformity in dissolving the Fe and Cr components in treatment II, leading to the surface being enriched in Cr and the dissolution slowing down. Table 3 gives the treatment sequence.

Specimens of 12Kh18N10T, 48TS, 2Kh13, and 22K steels oxidized in an autoclave (2200 h) were given treatments I-V in sequence. The oxide was removed from 22K, 48TS, and 2Kh13 after treatments I and II. To reduce the corrosion of the surfaces of these steels when freed from oxide in treatments III and V, thiourea $[CS(NH_2)_2]$ was added to the solution at the level of 0.1%. The successive treatments removed the model oxide completely from all the steels (a small amount of slime was formed in the removal of the oxide from the stainless steel). Table 4 gives data on the corrosion at the various stages.

The data show that one can attain comparable performance in dissolving the Fe and Cr components of the oxide film on chromium-bearing steels by successively varying the solution compositions. One can use a solution based on oxalic acid and OEDP. The optimum conditions for dissolving the Fe component in this solution are attained at low pH (with the addition of $H_2C_2O_4$), while those for the Cr component are attained at high pH (on the addition of alkali). Treatment in alkaline $H_2C_2O_4$ and OEDP replaces the usual alkaline permanganate treatment, but it enables one to repeatedly adjust the working solution (impossible when using alkaline permanganate) and thus to replace a multibath treatment by a single-bath one. When an inhibitor is introduced, the method is suitable for removing oxides from low-alloy steels. The performance of the successive treatments has been confirmed in removing model oxide films from 12Kh18N10T, 2Kh13, 48TS, and 22K steels.

We are indebted to S. M. Bashilov for assistance experiments.

LITERATURE CITED

1. S. M. Bashilov et al., At. Énerg., 52, No. 2, 122 (1982).
2. Yu. G. Bobrov et al., ibid., 53, No. 3, 171 (1982).
3. A. G. Akimov et al., Usp. Khim., 50, No. 1, 3 (1981).
4. V. I. Nefelov, Surfaces: Physics, Chemistry, and Mechanics [in Russian], No. 1 (1982), p. 3.
5. Yu. V. Baldokhin et al., ibid., No. 8, (1982), p. 48.
6. Metal Oxidation [in Russian], Vol. 2, Metallurgiya, Moscow (1968).
7. Yu. V. Karyakin and I. I. Angelov, Pure Chemical Substances [in Russian], Khimiya, Moscow (1974).

Declassified and Approved For Release 2013/09/14 : CIA-RDP10-02196R000300040005-3

Declassified and Approved For Release 2013/09/14 : CIA-RDP10-02196R000300040005-3

INFLUENCE OF COLD DEFORMATION ON THE BEHAVIOR OF HELIUM IN STEEL OKh16N15M3B

A. G. Zaluzhnyi, M. V. Cherednichenko-Alchevskii, O. M. Storozhuk, V. F. Reutov, and G. T. Zhdan

UDC 621.039.53:539.219.3

It is known that one of the basic factors limiting the working life of materials at large neutron fluxes is high-temperature radiational embrittlement (HTRE), which, according to most hypotheses, is explained by the formation and accumulation of helium in the material as a result of (n, α) reaction. According the current concepts, the basis of HTRE is the helium-induced disruption of the relation between the strength of the body and the grain boundaries [1-4].

In a series of works, it has been shown that reduction in HTRE is facilitated by optimal cold deformation [5, 6], in connection with which there is considerable interest in investigating the behavior of helium in irradiated constructional materials subjected to preliminary cold deformation.

In the present work, the kinetics of helium liberation is studied in the course of heating at constant rate and by isochronous annealing of samples of steel OKh16N15M3B uniformly (over the thickness) saturated with helium [7] to a concentration of $2 \cdot 10^{-3}$ at.%, as a result of α-particle bombardment in a cyclotron. Samples in the austenitic state and after preliminary 15% and 50% cold deformation are considered. The irradiation temperature is no more than 370°K.

The apparatus and method of investigating the kinetics of gas liberation in different conditions of heating were described in [8]. Immediately before the experiment, the samples (of dimensions $5 \times 5 \times 0.1$ mm) are electrically polished with subsequent washing in alcohol to remove any possible oxide film.

Spectra of the rate of gas liberation from samples of steel OKh16N15M3B in different states are shown in Fig. 1. The spectra are plotted by graphical differentiation of kinetic curves of helium accumulation in the experimental volume of the apparatus in the course of heating the samples [8]. A temperature dependence of the helium accumulation in the experimental volume of the apparatus after isochronous annealing of duration 0.5 h is also shown.

It is evident from Fig. 1 that helium is liberated in several stages, with a maximum of gas liberation (a peak) at temperature of 37-400 (A), 500-520 (B), 750-780 (C), and 1160-1190°K (D). In addition, for cold-deformed samples there is an additional peak at ∿900°K (D'), while peak B appears more clearly and peak D is somewhat modified in form. Note that considerable gas liberation from samples of 50% cold-deformed steel is observed even at temperatures above 550°K (Fig. 1d), but the total fraction of gas liberated in the course of isochronous annealing to 1370°K is approximately the same for all the samples. It is also interesting that, in the temperature range corresponding to peak C, there is considerable liberation of nitrogen and a small amount of other chemically active gases.

It is logical to assume that the features of gas liberation from cold-deformed steel observed are associated with the presence of a developed dislocational structure. To explain the results obtained, it is assumed that the activation energy of helium diffusion over dislocational tubes is considerably less than the activation energy of diffusion by the vacancy mechanism. Indirect confirmation of this hypothesis comes, in particular, from the data of [9, 10]. In [9], by means of a transmission electron microscope, the structure of the dislocational walls in a high-nickel alloy saturated with helium was investigated. It was established that, on annealing the experimental samples, helium bubbles appear; for a regular hexagonal lattice, all the bubbles were practically of the same size and positioned at coupled points. In [10], the kinetics of helium liberation from samples of aluminum alloy

Translated from Atomnaya Énergiya, Vol. 56, No. 5, pp. 286-288, May, 1984. Original article submitted May 30, 1983.

 0038-531X/84/5605-0304$08.50 © 1984 Plenum Publishing Corporation

Declassified and Approved For Release 2013/09/14 : CIA-RDP10-02196R000300040005-3

Declassified and Approved For Release 2013/09/14 : CIA-RDP10-02196R000300040005-3

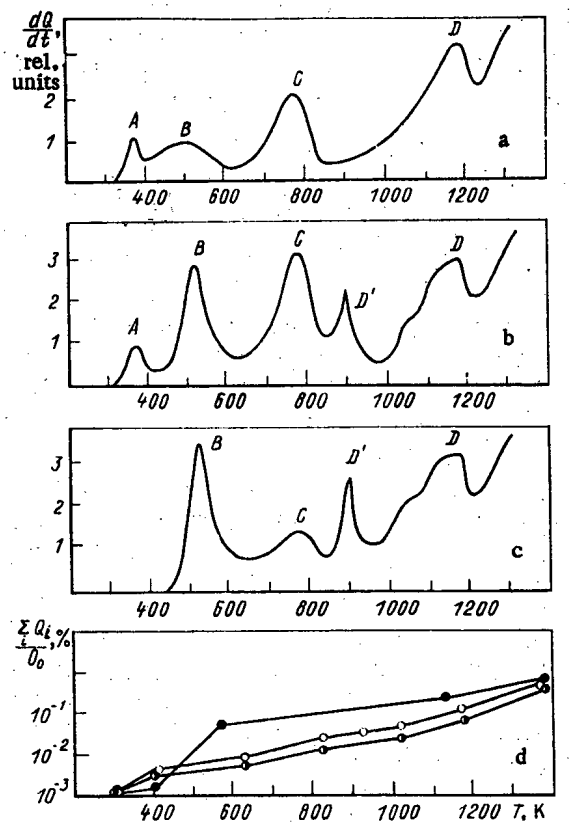

Fig. 1. Temperature dependence of the rate of helium liberation from samples of steel OKh16N15M3B bombarded by α particles in a cyclotron in the austenitic state (a) and after cold deformation by 15% (b) and 50% (c) in the course of linear heating at a rate of 7 K/min; d) helium accumulation in the experimental volume of the apparatus after isochronous annealing; ◐) austenitic state; ○, ●), 15% and 50% cold deformation, respectively.

irradiated in the initial state and subjected to a sign-varying load was studied. With increase in the applied flexural stress, an increase in the amount of helium liberated at the low-temperature stage was observed, together with a corresponding decrease at moderate and high temperatures. The effect observed was explained by more intense capture of helium by flexural dislocations and subsequent easy escape on heating along the channels of the dislocational structure.

The interpretation of the stages observed in the liberation of helium has been confirmed for the example of the spectra of gas liberation from samples of cold-deformed steels (Fig. 1b).

Peak A at 320-400°K may be associated with the migration of helium atoms in interstitial positions. Some of the gas then moves to the surface of the sample and the grain boundary, some is captured by vacancies and moves to substitutional positions, and some is captured by dislocations, forming a Cottrell atmosphere. The absence of this peak for a sample of 50% cold-deformed steel must be associated with the absorption of helium diffusing interstitially by dislocations, the density of which is considerably higher than in the undeformed and 15% deformed samples.

Peak B, covering the range 400-600°K with a maximum at ∿520°K, is most probably associated with migration of helium atoms along dislocations. The amount of helium liberated in this stage (Fig. 1d) depends strongly on the degree of cold deformation, since increase in the dislocation density is associated with increase in the probability of capture of interstitial helium atoms by dislocations, and increase in the proportion of gas liberated at this stage of annealing over channels of the dislocational structure to the grain boundaries, the sample surface, and other sinks.

Declassified and Approved For Release 2013/09/14 : CIA-RDP10-02196R000300040005-3

Declassified and Approved For Release 2013/09/14 : CIA-RDP10-02196R000300040005-3

Peak C appears at 600-850°K; according to the data of [11], it is assumed that gas liberation is associated with growth of the dislocation loops, their escape to the surface, and the liberation of the associated helium over dislocational tubes. The influence of the proposed mechanism should appear more clearly at a smaller dislocation density, as follows from Fig. 1.

Peak D' at 900°K appears only for cold-deformed samples. According to electron-microscope investigations [11], annealing of the dislocational loops occurs at this temperature, and helium porosity begins to form. In addition, it follows from Fig. 1 that in the same temperature range the next stage of gas liberation (peak D) begins, associated with the diffusion of helium atoms by a vacancy mechanism. Therefore, the characteristic peak D' obviously owes its appearance to two competing processes: on the one hand, the presence of a developed dislocational structure facilitates the intense liberation of helium atoms diffusing by the vacancy mechanism and captured by dislocations and, on the other hand, decrease in dislocation density and the appearance of internal sinks (bubbles) leads to decrease in the rate of gas liberation.

As already noted, peak D is associated with the diffusion of helium atoms by a vacancy mechanism. Increase in helium mobility in this temperature range is also indicated by the formation of helium porosity [11]. Broadening of peak D for cold-deformed samples toward lower temperatures is probably also associated with more intense gas liberation on account of migration of helium atoms over the channels of the dislocation structure. Note, however, that the amount of gas liberated in stage D depends only slightly on the degree of deformation, since at the given temperature practically all the helium is evidently in stable complexes or bubbles. Therefore, gas liberation at higher temperatures may only occur on account of the migration of helium complexes to the surface of the sample. A break on the ascending branch of peak D for cold-deformed samples may be associated with polygonization of the structure.

To estimate the activation energy of processes responsible for the liberation of helium on heating, the relation obtained earlier [12] is used; according to this relation, the activation energy of helium diffusion in OKh16N15M3B steel by an interstitial mechanism is E_A = 0.2-0.3 eV, while in the case of diffusion by a vacancy mechanism E_D = 2.0-2.5 eV. With formal use of this method we estimate the activation energy of the migration of helium atoms along dislocational tubes to be E_B = 0.6-0.7 eV.

The activation energy of gas liberation in the temperature range of peak C is determined on the basis of investigations of the rate of growth of the interstitial-atom loop [11, 13]: E_C = 0.7-0.8 eV. As already noted, in this temperature range there is an accompanying liberation of chemically active gases, which may influence the growth of the loop and the liberation of helium.

Thus, on the basis of the experiments, it may be concluded that the dislocational structure of the steel exerts considerable influence on the distribution and liberation of helium in the course of heating.

LITERATURE CITED

1. A. M. Parshin et al., Vopr. At. Nauki Tekh., Ser. Fiz. Rad. Povrezhd. Rad. Mater., No. 2(10), 70 (1979).
2. V. F. Zelenskii et al., in: Some Problems of the Physics of Radiational Damage of Materials [in Russian], Naukova Dumka, Kiev (1979), p. 95.
3. Yu. N. Sokurskii et al., Vopr. At. Nauki Tekh., Ser. Fiz. Rad. Povrezhd. Rad. Mater., No. 2(13), 39 (1980).
4. A. S. Nikiforov, At. Énerg., 53, No. 1, 3 (1982).
5. H. Böhm, A. Hauck, and G. Hess, J. Nucl. Mater., 33, 347 (1969).
6. E. Bloom and F. Wiffen, J. Nucl. Mater., 58, 171 (1975).
7. V. F. Reutov and Sh. Sh. Ibragimov, Inventor's Certificate No. 531433 Byull. Izobret., No. 23, 223 (1978).
8. A. G. Zaluzhnyi et al., At. Énerg., 52, No. 6, 40 (1982).
9. A. M. Parshin, S. A. Fabritsiev, and V. D. Yaroshevich, At. Énerg., 53, No. 1, 418 (1982).
10. A. G. Zaluzhnyi et al., Poverkhn., Fiz., Khim., Mekh., No. 6, 51 (1983).
11. D. M. Skorov et al., At. Énerg., 40, No. 5, 387 (1976).
12. V. S. Karasev et al., At. Énerg., 34, No. 4, 251 (1973).
13. A. C. Damask and G. J. Dienes, Point Defects in Metals, Part 2, Theory of Point Defects, Gordon and Breach (1964).

Declassified and Approved For Release 2013/09/14 : CIA-RDP10-02196R000300040005-3

Declassified and Approved For Release 2013/09/14 : CIA-RDP10-02196R000300040005-3

ISOTOPIC COMPOSITION OF FUEL IN THE BLANKET OF A HYBRID THERMONUCLEAR REACTOR WITH A THORIUM CYCLE

S. V. Marin and G. E. Shatalov

UDC 621.039.516.22

In order to determine and analyze the potential feasibilities of hybrid thermonuclear reactors as sources of energy and generators of secondary nuclear fuel intended for outside users, it will be necessary to study the change of isotopic composition of the initial charge during irradiation [1-3].

The high probability of (n, 2n) and (n, 3n) nuclear reactions in the nuclei of the initial charge leads to nuclear transformations, as a result of which isotopes with a small mass number are formed. Characteristic differences arise in the isotopic composition of the spent fuel of thermonuclear and nuclear reactors. It is particularly interesting to investigate the process of the formation of highly active ^{232}U, the amount of which in the uranium made mainly determines the radiation environment at certain sections of the technological process of the plants of the external fuel cycle [4]. For a hybrid thermonuclear reactor with thorium fuel, the chains by which the formation of ^{232}U takes place are relatively short:

$$^{232}\mathrm{Th}\,(n,\,2n)^{231}\mathrm{Th}\xrightarrow{\beta^-}{}^{231}\mathrm{Pa}\,(n,\,\gamma)^{232}\mathrm{Pa}\xrightarrow{\beta^-}\rightarrow{}^{232}\mathrm{U}\xrightarrow{\alpha}\ldots \quad (1)$$

$$^{232}\mathrm{Th}\,(n,\,\gamma)^{233}\mathrm{Th}\xrightarrow{\beta^-}{}^{233}\mathrm{Pa}\xrightarrow{\beta^-}\rightarrow{}^{233}\mathrm{U}\,(n,\,2n)^{232}\mathrm{U}\xrightarrow{\alpha}\ldots \quad (2)$$

$$^{233}\mathrm{U}\,(n,\,2n)^{232}\mathrm{U}\xrightarrow{\alpha}\ldots \quad (3)$$

They reflect the succession of nuclear reactions taking place with a higher probability than the similar chains in uranium fuel.

With the presence in thorium of ^{230}Th, which is formed in uranium–thorium ore by the decay of ^{234}U, one further chain appears, leading to the formation of ^{232}U:

$$^{230}\mathrm{Th}\,(n,\,\gamma)^{231}\mathrm{Th}\xrightarrow{\beta^-}{}^{231}\mathrm{Pa}\,(n,\,\gamma)^{232}\mathrm{Pa}\xrightarrow{\beta^-}\rightarrow{}^{232}\mathrm{U}\xrightarrow{\alpha}\ldots \quad (4)$$

In addition, the presence of ^{230}Th leads to the formation of ^{228}Th, which is the decay product of $^{232}U\xrightarrow{\alpha}{}^{228}Th\xrightarrow{\alpha}$:

$$^{230}\mathrm{Th}\,(n,\,3n)^{228}\mathrm{Th}\xrightarrow{\alpha}\ldots \quad (5)$$

$$^{230}\mathrm{Th}\,(n,\,2n)^{229}\mathrm{Th}\,(n,\,2n)^{228}\mathrm{Th}\xrightarrow{\alpha}\ldots \quad (6)$$

As the formation of ^{232}U in thorium fuel proceeds via threshold nuclear reactions, in order to analyze the change of isotopic composition of irradiated fuel, a version of the hybrid thermonuclear reactor blanket was chosen [1], characterizing the high-energy spectrum of the neutron field. The neutron-physics calculation of the blanket and the solution of the equations for the change of isotopic composition were performed by using the BURNEL program [5], taking account of the nuclear transformations of the thorium fuel (Fig. 1). Such principal neutron-physical parameters of the blanket as the tritium breeding factor, power multiplication in the blanket, the coefficient of production of secondary nuclear fuel, and a number of other parameters are calculated for discrete instants of time in the interval up

Translated from Atomnaya Énergiya, Vol. 56, No. 5, pp. 289-291, May, 1984. Original article submitted September 18, 1983.

0038-531X/84/5605-0307$08.50 © 1984 Plenum Publishing Corporation

Declassified and Approved For Release 2013/09/14 : CIA-RDP10-02196R000300040005-3

Declassified and Approved For Release 2013/09/14 : CIA-RDP10-02196R000300040005-3

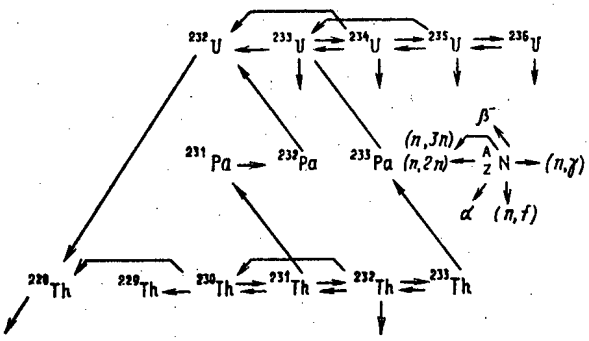

Fig. 1. Scheme of nuclear transformations.

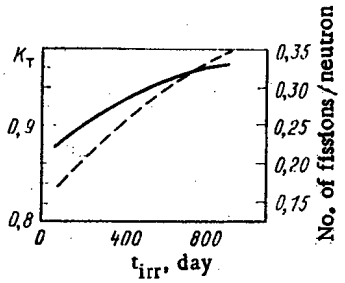

Fig. 2. Dependence of K_T (——) and number of fissions (- - -) on the time.

up to 1000 days. The neutron loading on the primary wall of the reactor was assumed to be equal to 1 MW/m^2. The calculations were performed with consideration of the spatial change of isotopic composition during irradiation at each interval of time.

At the start of irradiation, when the charge consists only of thorium and uranium has not yet been formed, fission takes place predominantly in the range of neutron energies from 13 to 14.1 MeV. The fraction of fissions in this range of neutron energies amounts to ∿80% of the total number of fissions in the fuel zone of the blanket in a given isotope. Approximately 15% of the fissions take place in the range of neutron energies from 3.0 to 13.0 MeV. According to the buildup of uranium, the contribution of uranium fission neutrons in the total source of neutrons increases. The number of fissions with normalizing to a single fusion neutron, incident on the surface of the primary wall of the reactor, is increased twofold from 0.17 at the start of irradiation during 1000 days. If, in the initial period, the energy release in the blanket is due exclusively to fission of thorium, then at the end of the run the contribution from fission of ^{232}Th and ^{233}U is approximately identical. The whole system is found to be in the subcritical state (k_{eff} = 0.16). The velocity of the nuclear reaction $^{232}Th(n, \gamma)$ also increases due to the increase of the internal source of fission neutrons (from 0.79 to 0.92). In view of the increase of the fraction of fission neutrons in the spectrum of the neutron field of the blanket, due to fission of heavy element nuclei formed, the velocity of the threshold nuclear reactions (n, 2n) and (n, 3n) is essentially unchanged with time. The number of (n, 2n) nuclear reactions w-ith normalizing to a single fusion neutron incident on the primary wall of the reactor amounts to 0.28 and 0.27, respectively, at the beginning and end of irradiation, and for (n, 3n) reactions — 0.11 and 0.10. The production of tritium in this model of the blanket is achieved in ^{6}Li; the contribution of the $^{7}Li(n, n'\alpha)T$ threshold reaction to the formation of tritium is less than 2%. The change of the tritium breeding coefficient and the number of fissions in the blanket with time is shown in Fig. 2.

The rate of production of uranium in the blanket being studied amounts to ∿4 kg ^{233}U/t fuel·yr. During 1000 days ∿1.8% of the thorium is burned and ∿10.3 kg ^{233}U/ton fuel is accumulated. After cooling the fuel until total decay of ^{233}Pa ($T_{\frac{1}{2}}$ = 27 days) the uranium content increases to approximately 11 kg ^{233}U/ton of fuel. On the average, during the time of irradiation of the fuel, ∿5% of the accumulated uranium is burned, and burnup of the uranium takes place predominantly as a result of its fission.

Declassified and Approved For Release 2013/09/14 : CIA-RDP10-02196R000300040005-3

Declassified and Approved For Release 2013/09/14 : CIA-RDP10-02196R000300040005-3

TABLE 1. Isotopic Composition of Fuel (average over the fuel zone), kg Isotope/ton Fuel

Isotope	Irradiation time, days				
	200	400	600	800	1000
^{228}Th	$6{,}0\cdot10^{-5}$	$2{,}9\cdot10^{-4}$	$1{,}6\cdot10^{-3}$	$3{,}7\cdot10^{-3}$	$7{,}1\cdot10^{-3}$
^{230}Th	0,29	0,58	0,87	1,15	1,43
^{232}Th	996,51	992,98	989,44	985,85	982,24
^{231}Pa	0,68	1,30	1,85	2,33	2,75
^{233}Pa	0,45	0,46	0,46	0,47	0,47
^{231}U	$1{,}8\cdot10^{-5}$	$8{,}9\cdot10^{-5}$	$2{,}1\cdot10^{-4}$	$3{,}9\cdot10^{-4}$	$6{,}2\cdot10^{-4}$
^{232}U	$3{,}4\cdot10^{-2}$	0,13	0,29	0,51	0,78
^{233}U	1,77	3,94	6,09	8,23	10,3
^{234}U	$3{,}4\cdot10^{-3}$	$1{,}4\cdot10^{-2}$	$3{,}3\cdot10^{-2}$	$5{,}8\cdot10^{-2}$	$9{,}0\cdot10^{-2}$
^{235}U	$4{,}4\cdot10^{-6}$	$4{,}1\cdot10^{-5}$	$1{,}4\cdot10^{-4}$	$3{,}3\cdot10^{-4}$	$6{,}5\cdot10^{-4}$
^{236}U	$6{,}0\cdot10^{-9}$	$1{,}2\cdot10^{-7}$	$6{,}2\cdot10^{-7}$	$2{,}0\cdot10^{-6}$	$4{,}9\cdot10^{-6}$
Fission products	0,51	1,17	1,93	2,71	3,83
$(\sum_i^i U + {}^{233}Pa)$	2,26	4,54	6,87	9,27	11,64

TABLE 2. Isotopic Composition of Uranium Produced (average over the fuel zone of the blanket), kg Isotope/ton Fuel

Isotope	Irradiation time, days				
	200	400	600	800	1000
^{232}U	1,5	2,86	4,22	5,50	6,70
^{233}U	98,2	96,9	95,3	93,9	92,5
^{234}U	$1{,}5\cdot10^{-3}$	$3{,}1\cdot10^{-3}$	$4{,}8\cdot10^{-3}$	$6{,}3\cdot10^{-3}$	$7{,}7\cdot10^{-3}$
^{235}U	$0{,}2\cdot10^{-5}$	$0{,}9\cdot10^{-5}$	$2{,}0\cdot10^{-5}$	$3{,}6\cdot10^{-5}$	$5{,}6\cdot10^{-5}$

The high probability of (n, 2n) and (n, 3n) nuclear reactions has a significant effect on the ratio of the nuclides produced in the blanket of the thorium thermonuclear reactor with a high-energy neutron field with respect to the same isotopes formed during the irradiation of thorium in the spectrum of nuclear reactor neutrons. The results of a calculation of the isotopic composition of thorium fuel, irradiated during 1000 days in the blanket of a hybrid thermonuclear reactor, are given in Table 1. Data about the content of uranium isotopes in the uranium produced, taking account of the total decay of ^{233}Pa, are given in Table 2.

The content of ^{233}U in the uranium produced is relatively high ($\sim$92%). For comparison, it can be pointed out that for HTGR reactors it amounts to 70% [1]. As can be seen from the data presented in Table 1, the production of uranium in the thorium blanket with a high-energy neutron field is accompanied by a high rate of formation of ^{232}U. Its content in the spent fuel is $\sim$0.8 kg/ton of fuel or $\sim$7% in the uranium produced. This value is a factor of many higher than the maximum permissible ^{232}U content in the fuel, allowing safe operating conditions with it in the technological processes with the presence of manual operations. According to the data of [1, 4], this value, determined by the level of γ radiation and the content of gaseous isotopes in the ^{232}U decay chain, amounts to $\sim(0.1\text{-}1.0)\cdot10^{-6}$.

The formation of ^{232}U takes place predominantly as a result of nuclear transformations, described by chains (1) and (3). Their total contribution amounts to $\sim$90%. With increase of the ^{233}U content in the fuel, the effect of nuclear reaction (3) increases. The presence in the original fuel of ^{230}Th leads to an additional increase of the ^{232}U content (up to 10-15%). The fundamental differences should be noted of the effect of the ^{230}Th content on the rate of formation of ^{208}Tl, depending on the spectrum of the neutron field. In a low-energy neutron field, ^{228}Th is formed predominantly as the result of the natural radioactive decay of ^{232}U (half-life 72 yr), which is formed by chain (4). For the high-energy field, through

Declassified and Approved For Release 2013/09/14 : CIA-RDP10-02196R000300040005-3

Declassified and Approved For Release 2013/09/14 : CIA-RDP10-02196R000300040005-3

TABLE 3. ^{232}U content in Uranium (per 10^6 parts uranium)

Reactor	Maximum	Average	Minimum
Hybrid thermonuclear reactor (present paper), 1000 days	25 600	15 600	7 000
Hybrid thermonuclear reactor [1], 200 days	—	3 600	—
LMFBR [6] (100% Th), blanket	443	127	30
LMFBR [6], (10% U + 90% Th), zone	96	20	1,8

chains (5) and (6) from ^{230}Th as a result of (n, 3n) threshold reactions, and two successive (n, 2n) reactions, ^{228}Th is formed directly. In this case, in the chain of formation of ^{228}Th, there is no time delay due to the natural radioactive decay of ^{232}U, which leads to an earlier increase of activity of the spent fuel after its discharge.

From the point of view of the organization of radiation safety operations at the stage of repeated use of the secondary nuclear fuel bred in the hybrid thermonuclear reactor, the high content of ^{232}U in the uranium imposes more rigid demands on shielding from radiation than in the case of uranium–plutonium fuel reprocessing. Moreover, in the uranium–plutonium fuel cycle a shift in time of the instant of attaining the maximum permissible content of ^{208}Tl is possible, by the additional purification of the plutonium from uranium and thorium nuclides. If the purification of uranium from thorium is really feasible, then the separation of ^{232}U and ^{233}U to all appearances, is a complex and expensive technological process.

Data about the content of ^{232}U in spent thorium fuel are compared in Table 3, whence it can be seen that the content of ^{232}U in spent uranium fuel, or fuel irradiated over 200 days from hybrid thermonuclear reactors, is a factor of 10^2–10^3 higher than its content in the uranium of nuclear reactors with a thorium charge.

Thus, when investigating the isotopic composition of the spent fuel of a hybrid thermonuclear reactor with a high-energy neutron field in the blanket, high content of ^{233}U and ^{232}U in the uranium is established (∿92 and ∿7%, respectively).

LITERATURE CITED

1. B. Leonard and U. Jenquin, BNWL-SA5750, Washington, (1976), p. 12.
2. Yu. G. Bobkov et al., At. Énerg., 48, No. 6, 395 (1980).
3. S. V. Marin and G. E. Shatalov, At. Énerg., 52, No. 5, 301 (1982).
4. L. V. Matveev and É. M. Tsenter, At. Tekh. Rubezhom, No. 4, 10 (1980).
5. S. V. Marin, Preprint IAE-3111 [in Russian], Moscow (1979).
6. F. Mann and R. Schender, Nucl. Sci. Eng., 65, No. 3, 544 (1978).

Declassified and Approved For Release 2013/09/14 : CIA-RDP10-02196R000300040005-3

Declassified and Approved For Release 2013/09/14 : CIA-RDP10-02196R000300040005-3

RECUPERATOR WITH INHOMOGENEOUS ELECTRIC AND MAGNETIC FIELDS

S. K. Dimitrov and Ya. A. Mel'nik

UDC 621.3.032.266.001.5

In order to increase the energy efficiency of injectors of neutral particles in thermonuclear machines as well as in some electron devices (klystrons, traveling-wave tubes, electron-beam valves, etc.) direct convertors of the energy of charged particles, i.e., recuperators, are used. In this paper we present one recuperation scheme.

In [1] Timofeev described a recuperation scheme with a homogeneous electric field and inhomogeneous magnetic field. The apparatus is part of a torus, which has a winding on its surface to produce a magnetic field. Inside the chamber a homogeneous electric field is produced by a system of electrodes. The basic idea underlying the scheme is as follows. In order to slow down the charged particles the direction of the magnetic field is chosen so that the drift velocity in the inhomogeneous magnetic field (gradient drift) would be in the direction opposite to that of the electric field. In addition to the gradient drift, however, such a scheme also has electrical drift, $v = cE/B$) directed toward the outer wall of the apparatus. This explains the strong dependence of the conversion efficiency on the ratio R_0/R:

$$\eta = 1 - \frac{\varepsilon_\perp}{\varepsilon}\frac{R_0}{R} - \frac{\varepsilon_\parallel}{\varepsilon}\left(\frac{R_0}{R}\right)^2,$$

where R_0 and R, respectively, are the radius of beam injection and the radius of the outer wall of the apparatus, $\varepsilon_\perp$ and $\varepsilon_\parallel$ are the initial energies of the transverse and longitudinal components of motion (relative to the magnetic field lines).

A major disadvantage of this scheme is that in principle it is impossible to convert the energy of particles, practically all of whose kinetic energy is concentrated in the longitudinal component ($\varepsilon_\parallel / \varepsilon \approx 1$). The particle enters the end part of the recuperator without having managed to give up its energy to the field.

The proposed scheme (Fig. 1) differs from that A. V. Timofeev in that the end parts of the recuperator are regions of inhomogeneous electric field. This, on the one hand permits conversion of the energy of particles with any value of $\varepsilon_\parallel / \varepsilon$ (since the field in the end parts has a slowing-down effect on the particles) and, on the other hand, increases the efficiency of the recuperator (since in these regions no electrical drift exists in the presence of gradient drift).

We consider the principle of recuperation with this scheme. Without loss of generality in our considerations, instead of an inhomogeneous electric field in the end parts of the recuperator (equipotential lines are shown as solid lines in Fig. 2a) we can analyze the idealized case in which during motion the current is either in a region in which **E** is directed along the OZ axis (as in the Timofeev scheme) or in a region in which **E** has an azimuthal direction (i.e., slows down the particle).

The beam enters the recuperator through a channel (see Fig. 2a) and passes into a region in which the field **E** is directed vertically. The particles move along the curve AB. Then they enter a region in which **E** has only an azimuthal component. The particles describe the curve BCD. The process is then repeated. For comparison, the dot–dash curves in Fig. 2b shows the projection of the particle trajectory according to the Timofeev scheme.

Our scheme was investigated experimentally on an electron beam with a particle energy eU_0 = 20–40 eV and a ratio $\varepsilon_\parallel / \varepsilon$ = 0.9 of the longitudinal component to total energy. The apparatus constitutes a quarter-torus with a square cross section. The inner radius is 20 cm the outer radius is 40 cm, and the height is 20 cm.

Translated from Atomnaya Énergiya, Vol. 56, No. 5, pp. 291-293, May, 1984. Original article submitted June 27, 1983.

0038-531X/84/5605-0311$08.50 © 1984 Plenum Publishing Corporation

Declassified and Approved For Release 2013/09/14 : CIA-RDP10-02196R000300040005-3

Declassified and Approved For Release 2013/09/14 : CIA-RDP10-02196R000300040005-3

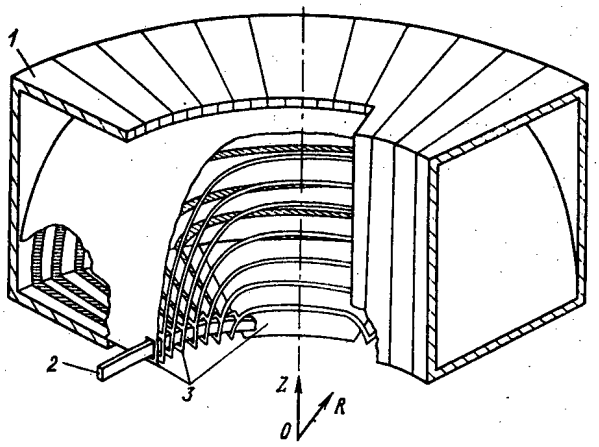

Fig. 1. External view of recuperator: 1) coil producing a magnetic field; 2) injection of charged-particle beam; 3) electrodes.

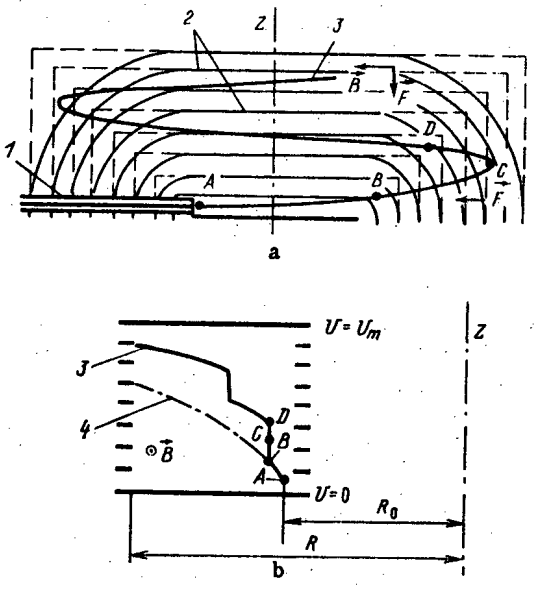

Fig. 2. Sections of recuperator ($\mathbf{F} = e\mathbf{E}$)): a) section by the surface R = const; b) the ZOR section; 1) injection of beam; 2) equipotential line; 3, 4) projections of particle trajectories in recuperator under study and in recuperator proposed by A. V. Timofeev, respectively.

The magnetic field B = 0.008-0.08 T (at the outer radius). The electric field is produced by a system of electrodes at the required potential.

With the assumption that the beam was monochromatic, we calculated the efficiency from the formula

$$\eta = \left(\sum_i I_i U_i\right) / \left(U_0 \sum_i I_i\right),$$

where U_i and I_i are the potential and current of the i-th electrode, and U_0 is the potential of the cathode, determining the electron energy. In a system of 14 electrodes (nine are shown in Figs. 1 and 2) with equal potentials $U_i = U_m i/13$ (U_m is the voltage of the power supply and i = 0, ..., 13).

Declassified and Approved For Release 2013/09/14 : CIA-RDP10-02196R000300040005-3

Declassified and Approved For Release 2013/09/14 : CIA-RDP10-02196R000300040005-3

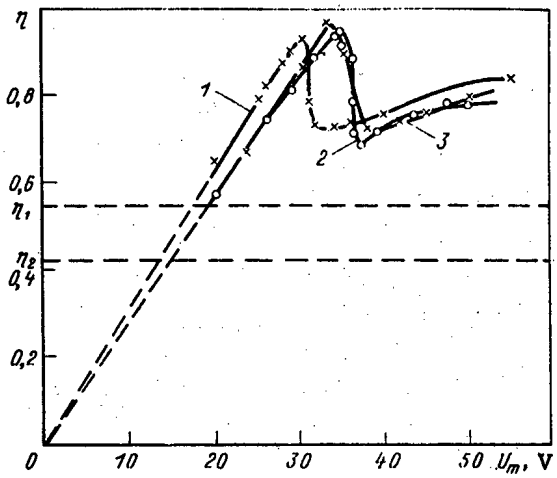

Fig. 3. Dependence of the recuperator efficiency on the decelerating potential ($\varepsilon_{\parallel}/\varepsilon \approx 0.9$, relative error $\Delta\eta/\eta = 0.08$) for $U_0 = 31$ V, $\varkappa = 0.75$ (1), $U_0 = 35$ V, $\varkappa = 0.68$ (2), $U_0 = 35$ V, $\varkappa = 0.75$ (3); $\eta_1 = 0.53$ and $\eta_2 = 0.44$ were calculated from the formula presented by A. V. Timofeev, for $\varkappa = 0.68$ and $\varkappa = 0.75$, respectively.

Figure 3 presents the results of measurement of the dependence of the efficiency on the retarding potential U_m for different values of the electron energy eU_0 and the ratio of the radius of beam injection to the outer radius, $\varkappa = R_0/R$. For $U_m < U_0$ all the electrons of the beam impinge on the last continuous electrode. Here we observe the usual ordinary direct proportional dependence of the efficiency on the retarding potential for systems of the type monochromatic beam—Faraday cylinder. The principle presented above is realized when $U_m > U_0$. The mechanism of the rise in efficiency with increasing U_m has not been ascertained as yet. For comparison Fig. 3 gives the values found for the efficiency from the formulas presented by Timofeev [1].

Thus, the following conclusions can be made. For the conversion of the energy of plasma fluxes containing particles of both signs with a small longitudinal velocity component it is expeditious to use the recuperator described by Timofeev. But for nonmonoenergetic beams of charged particles of the same sign with an arbitrary ratio $\varepsilon_{\parallel}/\varepsilon$, the recuperator presented in this paper is more efficient ($\eta \geqslant 0.7$ for $\varepsilon_{\parallel}/\varepsilon \approx 0.9$ and $R_0/R \approx 0.7$). In order to increase its efficiency, it is necessary to increase the size of the apparatus, i.e., decrease the ratio R_0/R.

The recuperator discussed here can be used in the neutral-particle injectors of thermonuclear machines, microwave devices (traveling-wave tubes, klystrons), electron-beam valves, etc.

LITERATURE CITED

1. A. V. Timofeev, Fiz. Plazmy, 4, No. 4, 826 (1978).

Declassified and Approved For Release 2013/09/14 : CIA-RDP10-02196R000300040005-3

Declassified and Approved For Release 2013/09/14 : CIA-RDP10-02196R000300040005-3

CALCULATION OF MODEL HIGH-LEVEL WASTES IN A HORIZONTAL APPARATUS

V. V. Kulichenko, V. F. Savel'ev,
V. A. Prokhodtsev, and A. A. Ryabova

UDC 621.039.7.14

In the processing of radioactive wastes by calcination [1], the wastes are dried and the salts are thermally decomposed, the final product consisting mainly of oxides. As the wastes contain many different compounds, a wide temperature range is used: first the nitrates of the rare-earth and other trivalent elements decompose, then the nitrates of the alkaline-earth metals, and finally at the highest temperatures and with the lowest rates the same applies to the alkali-metal nitrates. Calcination is considered as the first stage before vitrification, the production of ceramics, etc.

Various calcination methods have been devised based on equipment of sprayer type, fluidized beds, and of horizontal type with a rotor or rotating body [2-4]. A horizontal plant is much less sensitive to the waste composition than is a fluidized-bed or sprayer one, and the volume of the gas discharged is determined only by the vapor–gas mixture formed during the drying and calcination. However, the design is more complicated, since there are moving mechanisms in the rotor (worm conveyer) or body. Also, the calcination is conducted in a thin layer and heat must be supplied through the wall of the apparatus, which makes it difficult to design a horizontal plant of large throughput.

A horizontal calcinator of throughput 40 liter/h [3-4] has been operated for several years in France in a plant for vitrifying high-level wastes. The calcinator consists of a heated tube of diameter 27 cm and length 3.6 m rotating at 30 rpm, which is tilted at 1°47'. Within it there is a free rod to grind up the solid product. The liquid wastes contain mainly the nitrates of aluminum (up to 81 g/liter), sodium (19-23 g/liter), and iron (15-17 g/liter) together with other salts at much lower concentrations. The product from any apparatus must be as dry as possible and contain the minimum amount of nitrate (source of corrosive oxides of nitrogen) and should flow freely, in order to provide for transfer to the vitrification apparatus.

We have examined the calcination conditions in a horizontal plant operating with wastes having elevated sodium nitrate contents.

The drying and calcination were performed in a horizontal tubular apparatus containing a rotating worm conveyer to mix and transport the product through the working zone into the bunker (Fig. 1). The length of the working zone was 1400 mm, internal diameter 160 mm, gap between projections on the blades of the worm conveyer and the inner wall of the apparatus about 2.5 mm. The apparatus was heated by six external demountable heaters of power 2.5 kW each. The temperatures in the sections of the working zone were 250-800°C in accordance with the required conditions.

The nitrate solutions were supplied by a dispensing pump to the input, where they were dewatered, denitrated, and calcinated as they moved thorugh the working zone. The solid product in the form of powder or granules was transmitted by the worm conveyer to the bunker. The steam–gas mixture containing oxides of nitrogen passed successively through a filter (to remove aerosols), a cooling condenser (to collect condensate), and to a bubble tower containing alkaline solution to neutralize the oxides of nitrogen.

The final product was analyzed for nitrogen, water, total carbon, carbon in the form of carbonate, and iron, and some mechanical properties were determined. The specific surface was measured by thermal nitrogen desorption; the data curves were recorded with an OD-103 instrument by the standard method. Table 1 gives data on the calcination of model solutions of various compositions in the presence of molasses and without them at temperatures below 800°C with throughputs of 4.0-17 liter/h and time spent by the product in the apparatus of 2 and 4 min.

Translated from Atomnaya Énergiya, Vol. 56, No. 5, pp. 293-297, May, 1984. Original article submitted August 18, 1983.

 0038-531X/84/5605-0314$08.50 1984 Plenum Publishing Corporation

Declassified and Approved For Release 2013/09/14 : CIA-RDP10-02196R000300040005-3

Declassified and Approved For Release 2013/09/14 : CIA-RDP10-02196R000300040005-3

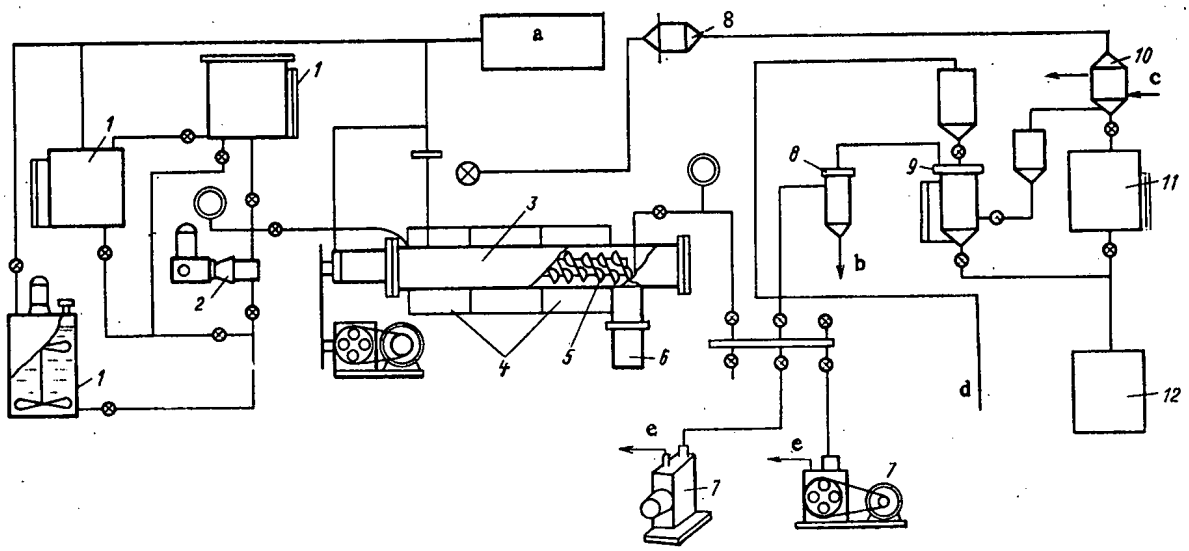

Fig. 1. Apparatus with calcinator of work-conveyer type: 1) tanks for preparing, storing, and handling solution; 2) dispensing pump; 3) calcinator proper; 4) removable electric heaters; 5) worm conveyer; 6) receiving bunker; 7) pumps; 8) filters; 9) bubble tower for removing oxides of nitrogen; 10) cooled condenser; 11) condensate receiving tank; 12) tank for neutralizing condensate and holding used alkali; a) extraction fan; b) to point 12; c) cooling; d) line supplying concentrated alkali solution; e) ventilation.

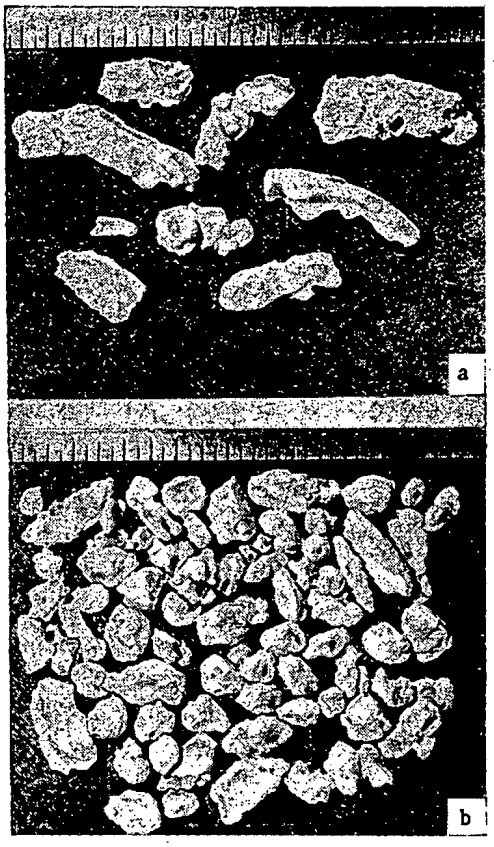

Fig. 2. Appearance of calcinate granules (runs 3-4): a) granules of maximum size (about 1%); b) granules of main fraction (about 85%).

Declassified and Approved For Release 2013/09/14 : CIA-RDP10-02196R000300040005-3

Declassified and Approved For Release 2013/09/14 : CIA-RDP10-02196R000300040005-3

TABLE 1. Calcination Data for Model Solutions and Characteristics of Calcinates

Run number	Composition of initial solution, g/liter			Temps. in working sections, °C			Conveyer speed,* rpm	Solution throughput, liter/h	Element contents in calcinate, mass %				Poured density, 10^{-2} g/cm³	Specific surface, m²/g
	$Al(NO_3)_3$	$NaNO_3$	molasses	1	2	3			NO_3^-	carbon total	carbon in CO_3^{2-}	H_2O in product		
1	300	–	–	265	440	520	18	5,2	25,0	–	–	4,98	27,3	0,63
2	170	–	100	280	500	470	18	4,8	2,0	11,0	–	6,41	10,6	3,66
3	141	122	–	220	415	560	18	4,1	60,0	–	–	–	615,0	0,18
4	141	122	–	260	450	560	18	4,3	59,4	–	–	–	720,0	–
5	141	122	–	250	460	590	18	4,5	61,6	–	–	–	780,0	–
6	300	30	11	270	430	440	18	4,0	25,0	1,0	0,1	2,9	37,0	0,48
7†	141	122	50	260	440	540	18	4,0	30,0	1,0	0,7	3,1	34,3	1,00
8†	141	122	50	270	460	560	18	4,0	34,0	0,6	0,2	1,86	54,0	1,37
9	141	122	120	260	600	620	18	4,0	20,0	–	–	–	38,6	–
10	141	122	120	280	530	620	18	6,0	27,7	–	–	–	34,8	–
11	141	122	120	275	500	630	18	8,4	28,2	–	–	–	42,4	–
12	141	122	120	255	530	640	18	10,0	29,5	3,5	2,1	–	42,0	1,17
13	141	122	120	260	570	640	22	4,0	22,0	3,5	3,5	–	29,0	–
14	141	122	120	280	520	590	18	4,0	13,0	4,5	4,4	1,6	52,5	1,49
15	141	122	120	290	550	590	18	4,0	13,0	2,8	2,7	–	43,1	–
16	141	122	120	320	760	770	18	4,0	7,5	4,6	4,9	–	21,4	–
17	141	122	200	340	760	750	18	4,0	1,1	5,4	5,3	–	34,1	–
18	175	260	164	240	600	610	18	4,0	49,3	–	–	1,0	39,2	–
19	175	260	164	250	600	610	18	4,0	54,2	3,6	3,3	10,6	30,0	–
20	175	260	164	250	620	620	9	4,0	49,2	3,7	2,8	5,3	34,4	0,58
21	141	122	120	260	650	590	9	4,0	50,6	–	–	–	43,5	–
22	141	122	120	255	520	570	9	7,0	41,8	3,3	2,9	–	33,2	–
23	141	122	120	265	540	650	9	11,0	41,4	–	–	9,5	19,7	–
24	141	122	120	270	470	610	9	15,0	47,0	3,9	2,4	11,0	22,3	1,60
25	141	122	120	260	550	620	9	17,0	40,0	3,1	3,3	–	32,0	–
26	141	122	120	620	740	700	18	4,0	32,1	–	–	–	48,3	–
27	141	122	120	720	800	760	18	4,0	26,8	3,3	3,1	–	61,2	0,38
28	141	122	200	740	780	750	18	4,0	12,8	4,3	4,2	–	32,1	–

*The conveyer speeds of 9 and 18 rpm correspond to calculated times spent by the product in the apparatus of 4 and 2 min;
†In runs 7 and 8, the initial solution contained 10 g/liter $Fe(NO_3)_3$, 1.0 g/liter $Cr(NO_3)_3$, 1.0 g/liter $Mn(NO_3)_2$, and 0.1 g/liter $Ni(NO_3)_2$.

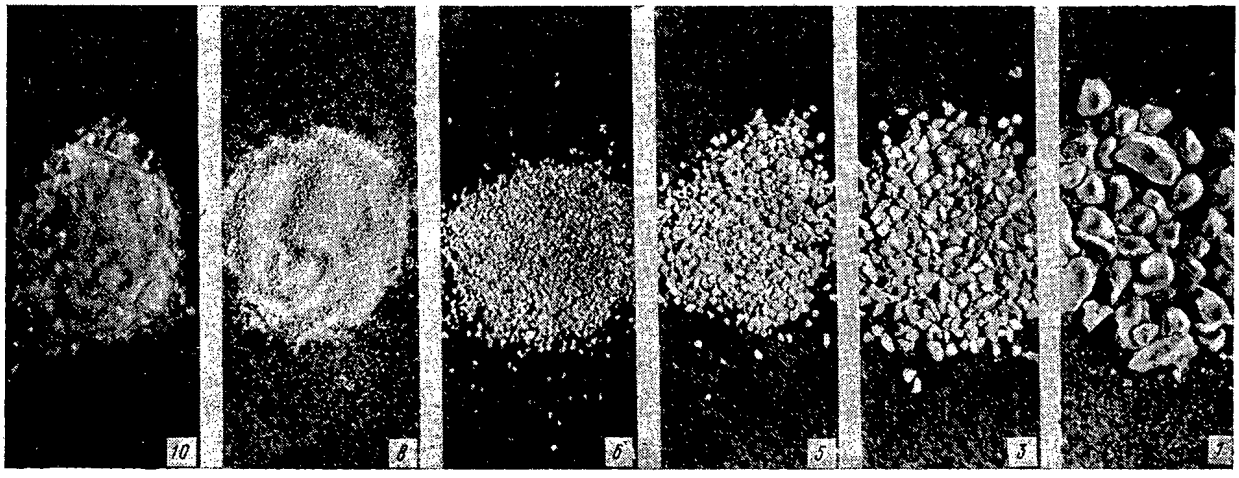

Fig. 3. Appearance of some calcinate fractions (run 14) immediately after unloading. The numbers are those of the fractions in Table 2.

The apparatus worked satisfactorily with and without molasses, which favor the denitration and swelling, and the worm conveyer provided complete unloading from the working zone into the bunker. In the absence of molasses (runs 3-5), the main body of the calcinate (about 85%) was granulated material (Fig. 2). The largest fraction to some extent resembled

Declassified and Approved For Release 2013/09/14 : CIA-RDP10-02196R000300040005-3

Declassified and Approved For Release 2013/09/14 : CIA-RDP10-02196R000300040005-3

TABLE 2. Fractional Compositions of Typical Calcinates, Mass%*

Run number	Number and size of fraction, mm										S_{sp} of 0.6-0.2 mm fraction, m^2/g
	№ 1; 2,5	№ 2; 2,5–1,6	№ 3; 1,6–1,0	№ 4; 1,0–0,6	№ 5; 0,6–0,4	№ 6; 0,4–0,3	№ 7; 0,3–0,2	№ 8; 0,2–0,16	№ 9; 0,16–0,1	№ 10; 0,1 (пыль)	
Run 14	21,0	18,1	4,3	5,3	4,1	2,3	5,0	2,2	7,7	29,6	1,49
Run 3	85,1	3,6	1,8	1,5	0,7	0,2	0,4	0,1	0,2	0,2	0,18
Run 20	6,8	8,5	8,8	12,8	11,4	5,5	11,8	5,3	10,5	19,8	0,58
Run 12	18,3	9,2	7,1	8,8	8,2	4,3	9,9	4,8	11,0	17,9	—

*The fractional analysis was performed after the calcinates had been stored for 2-9 months.

the shape of the depressions in the worm conveyer between the blades; the main fraction was represented by granules of size 10-35 mm (Fig. 2). When the initial solution contained molasses, the product was loose material varying in fractional composition (Table 2 and Fig. 3). Much of the product consisted of readily poured powder, which did not stick together on storage.

The nitrate contents in the calcinate (Table 1) were directly related to the amount of molasses added. For example, in runs 3-5 (without molasses) the nitrate content was highest (about 60 mass %). The addition of about 50 g/liter of molasses to a solution containing 141 g/liter of $Al(NO_3)_3$ and 122 g/liter of $NaNO_3$ reduced the nitrate content by about a factor two (30-35 mass % in runs 7 and 8). Increasing the molasses content to 120 g/liter provided the fullest denitration. Under otherwise equal conditions, the products from runs 9, 14, and 15 contained 13-20 mass % nitrate, because a redox reaction occurs between the molasses and the nitrate at elevated temperatures:

$$C_6H_{12}O_6 + 6NO_3^- \rightarrow 6CO_2 + 6NO + 6H_2O.$$

The degree of denitration increases with the molasses content, while the carbon (carbonate) content also increases. When the sodium nitrate concentration increases (from 122 to 260 g/liter) and the aluminum nitrate concentration also increases (from 141 to 175 g/liter), the degree of denitration decreases.

Table 1 also gives data on the effects of temperature. Raising the temperature in all three sections above 600°C (runs 26 and 27) reduced the degree of denitration appreciably. Increasing the temperature in the first section (to 620-720°C) led to partial decomposition of the molasses and reduced participation in the denitration. When the molasses concentration was increased to 200 g/liter with the same temperature (run 28), the nitrate content of the calcinate was reduced to 13 mass %. Reducing the temperature in the first section to 320-340°C and increasing the molasses concentration to 200 g/liter produced the minimal nitrate content of 1.1 mass % (run 17). The degree of denitration obtained with the worm conveyer rotating at 18 rpm was higher than that at 9 rpm, because of the more vigorous mixing at the heated wall during the transport. There was no appreciable change in the nitrate content in the product on increasing the throughput from 4 to 17 liter/h under otherwise equal conditions.

Data recordings on samples of the calcinate showed that at 125-130°C there were endothermic peaks for all the specimens related to evaporation of the water sorbed on the extensive surface of the calcinate. The specific surface S_{sp} in run 14 (with molasses) was about 1.5 m^2/g, while that in run 3 (without molasses) was 0.18 m^2/g, and correspondingly the endothermic peak was small. In run 3, for which calculations indicated that about 7% of the aluminum nitrate was undecomposed, there was an endothermic peak at about 195°C [5, 6], indicating final decomposition of this salt residue. The product from run 3 also had an endothermic peak at 290°C corresponding to melting in the $NaNO_3$. The $Al(NO_3)_3$ in the mixture reduced the melting point of $NaNO_3$ from 310 to 290°C. The endothermic peaks for the products from runs 14 and 3 at 660°C correspond to the decomposition of sodium nitrate [5, 6]. The molasses in calcinate 14 reduced the decomposition temperature for the $NaNO_3$ by 20°C (from

Declassified and Approved For Release 2013/09/14 : CIA-RDP10-02196R000300040005-3

Declassified and Approved For Release 2013/09/14 : CIA-RDP10-02196R000300040005-3

660 to 640°C). The specimen 14 also had two small exothermic peaks at 200 and 300°C, and analysis of this calcinate showed that it contained 3 mass % residual nitrogen and about 0.1 mass % free carbon. One assumes that the reaction of the residual carbon with the sodium nitrate continues at these temperatures, which is accompanied by the production of heat.

The calcinates in runs with molasses contained carbon in the form of carbonate at from 0.1 to 20 mass % (Table 1), and there was a strong alkaline reaction when the calcinate contacted water: $CO_3^{2-} + 2H_2O \rightleftarrows 2OH^- + H_2CO_3$, and there was an endothermic peak corresponding to carbonate decomposition at 840°C (run 27), which shows that the calcination produces carbonates. Physicochemical analysis showed that the following salts and oxides occur in the product when molasses are added: $NaNO_3$, $NaAlO_2$, Al_2O_3, Na_2CO_3.

These results enable one to evaluate the scope for using equipment of worm conveyer type for trating model solutions of high-level wastes containing elevated amounts of the nitrates of sodium (up to 260 g/liter) and aluminum (up to 175 g/liter) with or without the addition of molasses at temperatures below 650°C (800°C), and it may be noted that a horizontal apparatus enables one to perform the dewatering and denitration in a stable fashion and to produce a fairly dry product (1-6% water) that is porous (poured mass mass 10.6×10^{-2}–52.5×10^{-2} g/cm^3) that flows readily (natural piling angle 40-46°) and which does not stick together, this having a specific surface of 0.5-1.5 m^2/g; the material absorbs water but does not lose the capacity to flow on storage. A calcinator of horizontal type has been used with the conditions shown in Table 1 to process about 160 liter of model solutions, which produced over 22 kg of calcinate.

When the apparatus was overhauled and the worm conveyer was removed, it was found that there was very little sticking of the calcinate to the walls and conveyer. There were no visually obvious signs of corrosion on the shaft, the walls, and the conveyer blades. Chemical analysis indicated some entry of iron into the calcinate in the first six runs at levels from 0.76 to 1.37%, which was due to contamination by scale (remaining after welding) and erosion products in the form of small particles taken up by the calcinate from the unworked surfaces of the body and conveyer. The iron contents tended to fall subsequently from run to run (to about 0.1 mass % in run 9). These results and the data from examining the calcinator show that it is possible to use 1Kh18N10T stainless steel as the material.

Therefore, it has been shown to be possible in principle to use a horizontal calcinator to process wastes with elevated $NaNo_3$ contents (up to 260 g/liter) and to produce a fairly dry calcinate that does not stick together and which remains in a freely flowing and transportable state, in conjunction with minimal nitrate contents, where the subsequent vitrification will be accompanied by relatively small release of corrosive oxides of nitrogen. However, the subsequent vitrification of material containing carbonate will involve considerable gas release from the latter, so the next stage of research on the calcination involves binding the sodium as nonvolatile salts such as silicates by introducing fluxing additives such as quartz sand, datolite, etc.

LITERATURE CITED

1. Nuclear Power, Man, and the Environment [in Russian], Énergoizdat, Moscow (1981).
2. A. S. Nikoforov, V. V. Kulichenko, and M. I. Zhikharev, Rendering Liquid Power-Station Wastes and Chemical Products Harmless [in Russian], Énergoatomizdat, Moscow (1984).
3. A. Jouan et al., in: Management of Radioactive Wastes from the Nuclear Fuel Cycle, Vol. 1, IAEA, Vienna (1976), p. 259.
4. A. Redon et al., in: Nuclear Power and Its Fuel Cycle, Vol. 4, IAEA, Vienna (1977), p. 143.
5. Chemist's Handbook [in Russian], Vol. 2, Goskhimizdat, Moscow (1963).
6. C. Duval, Inorganic Thermogravimetric Analysis, Elsevier, Amsterdam–London–New York (1963).

Declassified and Approved For Release 2013/09/14 : CIA-RDP10-02196R000300040005-3

Declassified and Approved For Release 2013/09/14 : CIA-RDP10-02196R000300040005-3

CONCENTRATION RATIOS FOR RADIOGENIC LEAD AND URANIUM IN AUREOLES AROUND HYDROTHERMAL URANIUM MINERALIZATION

V. M. Ershov

UDC 550.84.092.1

Considerable importance attaches to the origin of radiogenic lead aureoles in hydrothermal uranium mineralization zones, since one can use anomalies in radiogenic lead concentrations as features of the mineralization on a scientific basis only when the nature of these aureoles around the mineralization has been elucidated. One of the main aspects is to establish the source of the radiogenic lead. Some researchers (for example, [1]) consider that the ore bodies are the sources. However, it has been pointed out [2] that there is no proper basis for this view on the origin of the radiogenic lead aureoles. Other workers take a different view (the radiogenic lead in the aureoles is due to the decay of uranium atoms in the geochemical aureoles), and the primary concentrations are recovered from the radiogenic lead [3, 4].

In research on the states of the uranium-lead system in unmetamorphosed uranium minerals, it has been found that the state can be perturbed not only as a result of supergenesis [3] but also during the final stages of hydrothermal mineralization [5]. Within large volumes of the ore body in a metamorphic deposit, the relations between the radiogenic lead and the uranium correspond to the age of the mineralization [2]. Therefore, one assumes that the radiogenic lead in the ores does not participate in producing the aureoles. However, this does not demonstrate that the radiogenic-lead aureoles in all hydrothermal deposits are derived from primary uranium geochemical aureoles. To demonstrate this, it is necessary to use a number of instances to show that the concentrations of the radiogenic lead isotopes Pb_{rad} are related to the uranium contents and the age of the aureole t:

$$Pb_{rad} = U\left\{K_1\left(1-\frac{1}{138}\right)[\exp(\lambda_8 t)-1] + \frac{K_2}{138}[\exp(\lambda_5 t)-1]\right\}, \quad (1)$$

where λ_8 and λ_5 are the decay constants of uranium and actinouranium correspondingly, while K is a coefficient that incorporates the changes in atomic mass. This formula shows that the dependence of the radiogenic lead concentration on the uranium content is linear for given t. This relationship was first established in a Precambrian mineralization aureole [2]. If this correlation could be demonstrated for aureoles in hydrothermal mineralization zones of various ages in various geological settings, it would enable one to establish a general relationship between uranium and lead around ores and to draw sound conclusions on the nature of the radiogenic lead aureoles at hydrothermal deposits.

The studies were made on aureoles on hydrothermal uranium mineralization zones differing in age of the mineralization and of the country rocks, as well as in type of mineralization and the subsequent changes, the extent of supergenesis, and the rock composition. The uranium and lead contents were determined in the main by x-ray spectral methods [6], while the lead isotope compositions were determined spectrally with an isotope-analysis system [7]. The relative errors in the ratios of the radiogenic lead to uranium were dependent in the main on the errors in determining the radiogenic lead concentrations and were usually 10-30%.

The data were used to derive linear-regression equations and correlation coefficients. Table 1 gives the slopes in these equations and the correlation coefficients, which indicate that the experimental and calculated slopes are quite similar and increase regularly with the age of the mineralization. The relative discrepancies between these slopes are less than 10% in most cases. The aureoles in two zones (Nos. 3 and 6) had relative deviations of 13 and 17%, while the aureole in the youngest zone (No. 1) gave 40% difference. Here the experimental values of the slopes differed substantially for the zones differing in age, while

Translated from Atomnaya Énergiya, Vol. 56, No. 5, pp. 298-300, May, 1984. Original article submitted March 15, 1983.

0038-531X/84/5605-0319$08.50 © 1984 Plenum Publishing Corporation

Declassified and Approved For Release 2013/09/14 : CIA-RDP10-02196R000300040005-3

Declassified and Approved For Release 2013/09/14 : CIA-RDP10-02196R000300040005-3

TABLE 1. Slopes of Linear Regression Equations for Radiogenic Lead and Uranium Contents in Aureoles

No.	Mineralization characteristics	Slopes		Pb_{rad}–U pair correlation coefficients
		Calc. from mineralization age	Found by expt.	
1	Uranium–Titanium mineralization in crushed zones in Precambrian migmatites and granites	0,0205	0,029	0,999
2	Uranium mineralization in a fault line in Precambrian sandstones, clay shales, and dolomites	0,041	0,039	0,711
3	Uranium mineralization in Cambrian carbonaceous–clay shales	0,053	0,046	0,832
4	Uranium mineralization in terrigenous sediments of Middle and Lower Paleozic age	0,053	0,050	0,988
5	Uranium–molvbdenum mineralization in Middle and Lower Paleozoic riolite porphyry	0,053	0,058	0,733
6	Uranium–molybdenum mineralization in Devonian volcanites and sediments	0,053	0,062	0,615
7	Uranium mineralization at tectonic contacts between granites and terigenous sediments	0,053	0,055	0,877
8	Uraninite mineralization in alkali metasomatites amongst Precambrian metamorphites	0,319	0,291	0,993

the positive pair correlation coefficients between radiogenic lead and uranium are such as to imply close or extremely close correlations. We therefore conclude that the aureoles contain mainly radiogenic lead derived from the decay of the uranium in the primary geochemical aureoles.

There are comparatively large deviations in the slopes and low values for the pair correlation coefficients in aureoles where the country rocks show extensive supergene alteration. The geochemical features of uranium in the supergenesis zone indicate that the correlation between radiogenic lead and uranium is here disrupted because of the extensive supergene alterations in the uranium–lead system in the aureoles. The following data confirm this. There are low and fairly uniform backgrounds of trace lead in the aureole rocks in most cases, and then the total lead Pb_t is linearly related to the concentration of radiogenic lead or uranium. In the latter case, the slope of the regression line should correspond to the age of the uranium mineralization, while the constant term corresponds to the background lead level. The total lead contents in % for the aureoles numbers 6 and 8 are described by

$$Pb_t = 0.0038 + 0.053U, \quad (2)$$

$$Pb_t = 0.0031 + 0.31U \quad (3)$$

Declassified and Approved For Release 2013/09/14 : CIA-RDP10-02196R000300040005-3

Declassified and Approved For Release 2013/09/14 : CIA-RDP10-02196R000300040005-3

with correlation coefficients of 0.5 and 0.99 correspondingly. The constant terms in these equations indicate the background lead levels quite satisfactorily for the aureole rocks, while the slopes hardly differ from the calculated values. There is a low correlation coefficient for No. 6 in the table, which evidently reflects not only disruptive relations between the radiogenic lead and uranium, where the correlation coefficient is 0.615, but also variations in the lead geochemical field in the aureole. Consequently, correlations between the total and radiogenic lead can serve to indicate alterations in the uranium–lead system due to supergene processes.

The following equations describe the relation between the total lead (in %) in the aureoles in these two mineralization zones and the contents of radiogenic lead:

$$Pb_t = 0.0037 + 1.058\ Pb_{rad} \quad (4)$$

$$Pb_t = 0.0038 + 1.06\ Pb_{rad} \quad (5)$$

The pair correlation coefficients are 0.893 and 0.997 correspondingly. The relative differences between the constant terms in these equations and those in (2) and (3) are 3 and 20%, which may be taken as satisfactory in estimating the background aureole lead concentrations from the two types of correlation. The slopes in (4) and (5) are almost one and indicate that the main source of lead in excess of the background in the aureoles is radiogenic. The correlation between the ordinary and radiogenic leads is closer than that between the uranium and radiogenic lead, so the uranium–lead system has been disturbed, with this occurring recently relative to the age of the mineralization. As endogenous processes in these regions essentially ceased in the Early Paleozoic period, and as the mineralization zones show extensive processes related to Mesozoic–Cenozoic crust formation, there is every reason for the disruption of the uranium to radiogenic lead relation being associated with supergenesis.

It has thus been established that radiogenic lead aureoles around hydrothermal uranium mineralization are formed by radiogenic lead isotopes accumulating from the decay of uranium in the primary geochemical aureoles. There is no basis to consider these aureoles as representing a space that has received radiogenic lead from the ore bodies. Consequently, the radiogenic lead aureoles represent a form of indication for uranium geochemical aureoles and have the same practical significance as the latter. There are advantages in using radiogenic lead aureoles in geochemical prospecting for uranium ores relative to uranium-measuring methods only in areas where the uranium aureoles are weak or diffuse, as occurs in weathering crusts. In small-case exploration, information on radiogenic lead contents in radiometric anomalies provides more reliable conclusions on the nature of the latter.

LITERATURE CITED

1. A. V. Tarkhanov and V. I. Zhukova, At. Énerg., 34, No. 6, 455 (1973).
2. V. M. Ershov, ibid., 40, No. 6, 485 (1976).
3. V. M. Ershov and E. S. Lobov, in: Nuclear Geophysics Researches [in Russian], Ural Science Center, Academy of Sciences of the USSR, Sverdlovsk (1975), p. 88.
4. A. G. Vetrov in: Radiometric and Geochemical Methods of Prospecting for Uranium Mineralization: Methods in Ore Geophysics [in Russian], Issue 11, Izd. VNII Geofizika, Leningrad (1976), p. 3.
5. V. V. Pavshukov et al., Geokhimiya, No. 4, 603 (1975).
6. A. V. Bakhtiyarov et al., Razvedka i Okhrana Nedr. No. 6, 23 (1969).
7. M. S. Kashtan, V. V. Bulatov, and I. S. Zykova, Geokhimiya, No. 5, 633 (1967).

Declassified and Approved For Release 2013/09/14 : CIA-RDP10-02196R000300040005-3

Declassified and Approved For Release 2013/09/14 : CIA-RDP10-02196R000300040005-3

EFFECT OF GAMMA-NEUTRON RADIATION FROM A NUCLEAR REACTOR ON THE ELECTRICAL STABILITY OF MICROLITE

N. S. Kostyukov, M. I. Muminov,
and V. M. Lanskov

UDC 620.22

Ceramic insulators of microlite (MK) can be used as bushings in nuclear reactors, and also in electronic, electrical, and automatic control systems [1-3]. The electrical stability is one of the most important characteristics of an insulator and it frequently limits the use of many dielectrics in zones of action of the intense ionizing radiation fluxes existing in a nuclear reactor. However, at the present time here is little published work on the investigation of the change of electrical stability of ceramic materials during irradiation with γ-neutron and γ-radiation fluxes. In connection with this, in physics and material behavior interest arises in a study of the effect of the radiation mentioned on the electrical stability of microlite.

A test of ceramic samples in γ-neutron fluxes was carried out in the reactor of the Institute of Nuclear Physics of the Academy of Sciences, Uzbek SSR, with a dry channel passing through the core and having an outlet in a hot box. The neutron flux density was equal to $1.2 \cdot 10^{13}$ neutrons/cm^2·sec with a cadmium ratio with respect to gold of 2.1 and an absorbed dose intensity of $4 \cdot 10^2$ Gy/sec. The investigations of the electrical stability after receiving a specified fluence in a ^{60}Co γ-field were conducted on the gamma-facility of the Institute of Nuclear Physics, Academy of Sciences of the Uzbek SSR, in a channel in which the exposed dose intensity of γ radiation amounted to 1.08 C/(kg·sec).

Samples in the form of thimbles, with a wall height of 50 mm, were used for the tests in the reactor. Small balls of ball bearings with a diameter of 6 mm were used as high-voltage electrodes. The high-voltage cable was the inner core in a polyethylene sheath of an RK-50 radiofrequency cable. The electrodes were contained in cylindrical insulators of epoxy resin, glued to the samples with epoxy glue.

The electrical stability of the microlite in the ^{60}Co γ-field, after setting up the specified neutron fluence, was determined by means of measurement cells assembled on a base of samples — disks with a diameter of 30 mm. For setting up the fluence, the disks were packed into stacks (3 pieces in each), which then were immersed in picene in order to exclude contact of the ceramic with water. These stacks were wrapped in copper foil and placed in standard block-containers used in the VVR-SM reactor. After completion of irradiation, the samples were retained in the hot box for a month in order to reduce the induced activity. As the exposed dose intensity of a single stack did not exceed $2.58 \cdot 10^{-4}$ C/(kg·sec), further treatment of the samples could be carried out inside the box. The foil was removed from the stack in the box, the picene was dissolved in benzene, and the samples were cleaned from residual picene films by wet polishing with silicon carbide powder. After washing in distilled water, the samples were dried at room temperature over a day. Then, one common electrode of copper foil was fastened to it and four electrode-beads. The electrodes were contained by insulators of epoxy resin, which were glued to the samples with VGO-1 hermetic glue. The thickness of the samples was measured with a micrometer with a moveable pivot. For the samples in the form of thimbles, the required value of the thickness was assumed to be the minimum value of the series of measurements at the site of the proposed breakdown, and for the plane samples — the average value of ten measurements at the point of application of the globular electrodes.

For the purpose of monitoring the density of the ceramic at the point to be tested according to the absorption coefficient, a collimated ^{90}Y + ^{90}Sr β-source with a diameter of up to 2 mm was used. The value of the density in this case was found from the expression

Translated from Atomnaya Énergiya, Vol. 56, No. 5, pp. 300-302, May, 1984. Original article submitted July 26, 1983.

 0038-531X/84/5605-0322$08.50 © 1984 Plenum Publishing Corporation

Declassified and Approved For Release 2013/09/14 : CIA-RDP10-02196R000300040005-3

Declassified and Approved For Release 2013/09/14 : CIA-RDP10-02196R000300040005-3

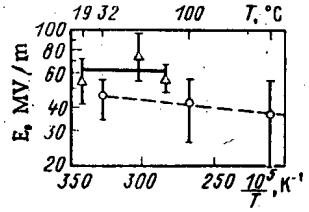

Fig. 1. Dependence of the electrical stability of microlite on the temperature during irradiation in a nuclear reactor (——) and without irradiation (- - -) for a frequency of the applied voltage f = 0; Δ, ○) experiment.

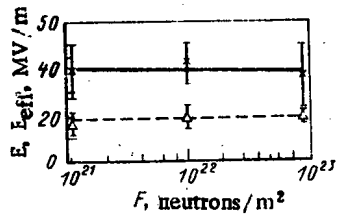

Fig. 2. Dependence of electrical stability of microlite in the case of a constant polarity voltage (—) and an alternating voltage of industrial frequency (- - -), one the neutron fluence: ×, Δ) experiment.

$$\rho = -\frac{\ln (I/I_0)}{\mu\delta},$$

where I_0 and I are the intensities of β-radiation before and after the sample, respectively; μ is the mass coefficient of attenuation of β radiation; δ is the sample thickness. The thickness of the samples tested was 0.3-0.5 mm.

The temperature was measured by a contact method with Chromel–Alumel thermocouples [4, 5]. A KSP-2 automatic potentiometer served as a secondary instrument. When determining the temperature at the instant of breakdown, a temperature–time characteristic curve was used, which was constructed on a basis of data recorded on the potentiometer film, obtained with three cell-simulators installed in the core of the working reactor. Using the characteristic curve obtained and measuring the time elapsed from the instant of introduction of the measurement cell into the zone of action of the γ-neutron radiation up to application of the test voltage, the temperature of the section being determined at the instant of sample breakdown was determined. Subsequently, in order to monitor individual measurement cells, a thermocouple was installed from the side of the earthed electrode. The accuracy of the temperature determination amounted to ±10%.

The test voltage of constant and alternating polarity was supplied from an AII-70 m apparatus, on which an electric motor was installed of the manual drive, which ensured a constant rate of voltage increase equal to 3 kV/sec. The voltage was measured with an S-96 kilovoltmeter. The instant of breakdown was recorded by the maximum position of the pointer on the instrument scale. If the breakdown voltage was like (according to estimate) to exceed 30 kV, then a resistance voltage divider was used.

The results of the investigation of the microlite, presented in Fig. 1, were obtained in conditions of the action of the γ-neutron radiation of the VVR-SM nuclear reactor with a uniformly increasing voltage of constant polarity and in conditions of normal heating. Before the application of the voltage, the samples were held in the core during a time from a few seconds to 20 min at a temperature of 19-79°C for the purpose of obtaining the required tem-

Declassified and Approved For Release 2013/09/14 : CIA-RDP10-02196R000300040005-3

Declassified and Approved For Release 2013/09/14 : CIA-RDP10-02196R000300040005-3

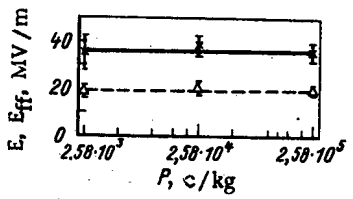

Fig. 3. Dependence of the electrical stability of microlite, obtained for a constant polarity voltage (——) and an alternating voltage of industrial frequency (- - -), on the γ-radiation dose P during testing of samples in a ^{60}Co source γ-field with an exposed dose intensity of 1.08 C/(kg·sec): ×, Δ) experiment.

perature. Each average experimental value of the electrical stability was derived from the breakdown results of six samples. The spread of the experimental values in this case amounted to 17-27% for a 90% reliability of the results.

The experimental dependence of the electrical stability E on the fluence of γ-neutron fluxes are shown in Fig. 2, obtained during tests of microlite after collection of the fluence in the ^{60}Co γ-radiation field with an exposed dose intensity of 1.08 C/(kg·sec) for voltage of constant polarity. The difference between the maximum and minimum values did not exceed 8.5%, and the spread of the values relative to the average values amounted to 10-21%, i.e., the electrical stability with the stated conditions of the test did not change.

Figure 2 also shows the dependence of the electrical stability E_{eff} on the neutron fluence, obtained by testing samples irradiated in the reactor in a ^{60}Co γ-radiation field for an alternating voltage of industrial frequency. The calculation of the average values was performed with the results of the breakdowns of 10 samples, for which the spread of the values was equal to 8-15% with a reliability of the results obtained of 90%. The difference between the maximum and minimum values did not exceed 11%, from which it follows that E_{eff} in the given conditions of the test also was unchanged.

The investigation of the dependence of the electrical stability of microlite on the γ-radiation dose (Fig. 3) was carried out for the purpose of explaining the effect of the γ-radiation dose as a factor leading to filling up levels, related with the presence of structural defects, with electrons, having developed as a result of disturbances in the zone of conductivity, and to explain the effect of this filling on the electrical stability of the ceramic.

The experiment consists of two stages: collection by the samples of the necessary dose of γ radiation and testing the samples to breakdown in a γ-radiation field. The temperature of the samples at the instant of application of the voltage was equal to 50°C. The spread of values relative to the average values amounted to 20-40% with a reliability of results obtained of 90%, and the difference between the maximum and minimum values was 20%. From the data presented, it follows that the electrical stability of microlite for a unipolar voltage does not vary in the range of exposed doses of $2.58 \cdot 10^3$-$2.58 \cdot 10^5$ C/kg for tests in the γ-radiation field of ^{60}Co [6, 7].

Figure 3 depicts the experimental dependence E_{ef} of microlite on the γ-radiation dose with a steady rise in the voltage of industrial frequency. The spread of values relative to the average values in the present case amounted to 18-30% and the difference between the maximum and minimum values did not exceed 13%. Thus in this way the effective values of the electrical stability remain invariable.

The characteristic curves shown in Fig. 1 show the absence of a reduction of electrical stability of microlite in conditions of continuous irradiation, although the electrical conductivity of the ceramic in the case of an absorbed dose intensity of 400 Gy/sec is increased by 2-3 orders of magnitude [8-10]. In accordance with this, it can be concluded that breakdown of this ceramic is now related with an electrothermal mechanism, but to a considerable degree is determined by electronic processes.

Declassified and Approved For Release 2013/09/14 : CIA-RDP10-02196R000300040005-3

Declassified and Approved For Release 2013/09/14 : CIA-RDP10-02196R000300040005-3

Starting from the characteristic curves shown in Fig. 2, which confirm that the buildup of defects in the microlite during irradiation with a fluence of up to 10^{23} neutrons/m^2, does not change the electrical stability, it can be supposed that the density of the radiation defects is still lower than the density of the technological defects present in ceramic materials. Moreover, as the test was conducted in a γ-field, it can be confirmed that there is no change of mechanism of electric breakdown. The data of Fig. 3 confirm that the filling of the defect levels, in which the appearance is shown of a brown coloration of the samples in the case of an absorbed dose of not less than $2.58 \cdot 10^5$ C/kg, does not change the value of the electrical stability and the electrical breakdown of microlite.

Based on what has been said, the following principal conclusions can be drawn:

breakdown of microlite in the range of temperatures investigated is due to electronic processes;

the γ-neutron radiation of the core of the operating VVR-SM reactor for a neutron flux density of $1.2 \cdot 10^{13}$ neutron/($cm^2 \cdot$sec) increases the average value of the electrical stability of microlite by 22-70% (see Fig. 1);

a neutron fluence of less than 10^{23} neutron/m^2 does not change the internal mechanism of electrical breakdown of microlite;

filling of defect levels with electrons, excited by γ radiation, does not affect the electrical stability of the material considered.

LITERATURE CITED

1. M. G. Mitel'man et al., Detectors for Intrareactor Measurements of Energy Release [in Russian], Atomizdat, Moscow (1977).
2. F. Clinard, J. Nucl. Mater., 85/86, 393 (1979).
3. A. B. Ochilov, Author's Abstract of Candidate's Disseration, Physico Mathematical Science [in Russian], Institute of Nuclear Physics, Academy of Sciences of the Uzbek SSR (1981).
4. Electrical Measurements [in Russian], Énergiya, Moscow (1972), p. 450.
5. A. S. Kruglov, P. V. Vyrodov, and M. I. Redchenko, At. Énerg., 42, No. 6, 504 (1977).
6. N. S. Kostyukov et al., in: Breakdown of Semiconductors and Dielectrics [in Russian], Part 1, Makhachkala, Publ. Dagestan State Univ. (1975), p. 183.
7. L. A. Buldakov et al., Radiation Safety in Nuclear Power Generation [in Russian], Atomizdat, Moscow (1981).
8. N. S. Kostyukov, F. Ya. Kharitonov, and N. P. Antonova, Radiation and Corrosion Resistance of Electroceramics [in Russian], Atomizdat, Moscow (1973), p. 194.
9. N. S. Kostyukov et al., Radiation Electromaterial Behavior [in Russian], Atomizdat, Moscow (1979), p. 155.
10. N. S. Kostyukov, V. V. Maslov, and M. I. Mumimov, Radiation Stability of Dielectrics [in Russian], Tashkent Branch, Academy of Sciences of the SSSR (1981), pp. 143, 176.

Declassified and Approved For Release 2013/09/14 : CIA-RDP10-02196R000300040005-3

Declassified and Approved For Release 2013/09/14 : CIA-RDP10-02196R000300040005-3

THE NEW GENERATION OF HIGHLY-CHARGED ION SOURCES

K. S. Golovanivskii

UDC 621.3.038.612

Introduction. Highly charged ion sources are major components in heavy-ion accelerators employing classical systems, and they ultimately determine design features such as the size, mass, cost, and facilities. Up to the 1970s, virtually the only type of ion source for heavy-ion accelerators was based on the Penning reflective discharge with oscillating electrons (PIG). Most accelerators were equipped with these sources, and the ongoing upgrading of them has meant that the intensities and charges of the beams they provide have attained the theoretical limits realted to the restricted plasma temperature, density, and lifetime.

PIG sources typically have the following plasma parameters: $n_e \approx 10^{13}$ cm^{-3}; $T_e \approx 20$ eV, and ion and electron lifetimes $\tau_i = \tau_e \approx 10$ μsec. The HILAC acceperator in Berkeley [1] has these plasma parameters provided by supplying a discharge with over 20 kW (dicharge current 15 A at an anode voltage of 1.5 kV). Discharge optimization, in particular the pulse supply of the working substance to the plasma [2], has resulted in the best beam parameters at present with the PIG source of the U-300 cyclotron in Dubnas (Table 1). The discharge consumes about 15 kW (el.) at 10-14 A. Table 1 shows that the percent content of ions in the beam decreases sharply as the degree of ionization Z increases. Éninger's estimates [3] indicate that the ratio of charge to mass for ions that can be extracted from a PIG source in satisfactory amounts is $\leqslant 0.3$ for light elements, $\leqslant 0.1$ for medium ones, and $\leqslant 0.5$ for heavy ones.

A considerable step forward was provided by the suggestion [4] of low-charge ion stripping at energies of the order of 1 MeV/nucleon on passage through thin foils. For example, a uranium ion under these conditions loses up to half of its electrons and acquires $Z/A \approx 0.2$. This method is extremely expensive and has serious disadvantages associated with the beam scattering during stripping and the brittleness of the very thin foil, which is easily damaged by the beam. An elementary ionization in the foil (as in a PIG plasma) is provided by electron–ion collision, whose effect is dependent on the relative velocity of the colliding particles. Therefore, it is completely unimportant which of the colliding particles acts as the target at rest. In a plasma, the ions are the target, while in a foil the electrons act as the target. There are differences only in the relative velocity of the colliding particle (electron) density. When the energy of an ion in a foil is 1 MeV/nucleon, the relative collision velocity is 1.4×10^9 cm/sec. To provide this electron velocity to bombard ions at rest, an energy of only 550 eV is required, which represents a hardly soluble problem for PIG plasma. The electron density and the ion stripping tim τ_i are determined by the number of ionizing collisions. The stripping time in a metal foil ($n_e \approx 5 \cdot 10^{22}$ cm^{-3}) of thickness 3 μm is equal to the time of flight $\tau_i \approx 0.2$ psec, and therefore the characteristic Lawson parameter is $n_e\tau_i \approx 1 \cdot 10^{10}$ sec·cm^{-3} for an electron kinetic energy of 550 eV in the coordinate system linked to the incident ions.

Therefore, the costly stripping method with foils can be replaced by the cheaper method of producing a plasma having $T_e \approx 0.5$ keV and $n_e\tau_i \approx 1 \cdot 10^{10}$ cm^{-3}. The specifications for the plasma parameters are much higher in controlled fusion: $T_e \approx T_i \approx 10$—$100$ keV and $n_e\tau_i \approx 5 \cdot 10^{14}$ sec· cm^{-3}. This means that the vast experience accumulated on controlled fusion can be extremely useful and possibly decisive for producing highly chargen ions. The only essential difference between the two cases is that the ion temperature in an ion-source plasma must be as low as possible in order to provide sufficiently low ion-beam emittance, whereas ion heating is one of the objects most difficult to attain in a fusion plasma.

To produce nuclei of heavy elements, the electron energy must be sufficient to empty the K shell. Also, the value of $n_e\tau_i$ should be higher than that given above, which is typical of stripping half the electrons from the uranium. Evidently, an ideal source capable of producing uranium nuclei would be a plasma containing cold ions and having an electron tempera-

Translated from Atomnaya Énergiya, Vol. 56, No. 5, pp. 303-310, May, 1984. Original article submitted August 1, 1983; revision submitted January 2, 1984.

0038-531X/84/5605-0326$08.50 © 1984 Plenum Publishing Corporation

Declassified and Approved For Release 2013/09/14 : CIA-RDP10-02196R000300040005-3

Declassified and Approved For Release 2013/09/14 : CIA-RDP10-02196R000300040005-3

ture $T_e \approx 200$ keV together with a retention parameter $\approx 1 \cdot 10^{12}$ sec$\cdot$ cm^{-3}, which from the viewpoint of fusion research is a difficult but soluble problem at the current stage. Lower plasma parameters are required for less extreme purposes such as producing neon-type heavy ions, helium-type ions from middle elements, and bare nuclei from light ones. In that case, it is probable that the optimum parameters are $T_e \approx 5-50$ keV and $\approx 10^9-10^{11}$ sec$\cdot$ cm^{-3}.

The first of the new generation of sources of highly charged ions was the electron-beam source invented by Donets in Dubna in 1967 [5] and now usually called the EBIS (Electron Beam Ion Source). Sone time later, papers appeared from Geller's group in Grenoble [6, 7] on the use of a fusion mirror trap containing a magnetic well and having plasma heating by electron cyclotron resonance, together with the proposals of Peacock and Pease [8] from Culham to use laser microtarget heating, the proposal from Tonon in Lima [9], and that from Bykovskii's group in Moscow [10] to produce highly charged ions from a laser plasma produced by a focussed beam from a solid specimen. In the same period, there was the suggestion from Trivelpiece's group [11] in Maryland to produce ions by adiabatic plasma compression in a mirror magnetic trap, as well as the suggestion that a toroidal magnetic trap containing a potential well for the ions made by Daughkerty et al. [12] in the Avco Everett laboratory. In 1969, Stix [13] from Rehovoth suggested producing a negatively charged stationary plasma with electron cyclotron resonance heating in a mirror magnetic trap, which would provide for a rapid in $n_e\tau_i$ as the ion charge increased. However, it is complicated to produce a charged plasma of sufficient density, and it was some while before this idea was realized in a somewhat modified form [14, 15].

Not all of these proposals ended in actual sources. At present, there are three main lines of advance in this area: EBIS, lasers, and ECR, which have either already led to working sources or are expected to do so in the near future. The present review deals with the state of the art in these three lines.* The main attention is devoted to the major aspects of each and to elucidating the potential and discussing the best results so far obtained. We do not describe identical or slightly different sources made in different laboratories and concentrate attention mainly on the best specimen in each family.

EBIS. The EBIS concept is that ions are retained for a long time within a dense electron beam of energy optimum for multiple ionization. Current electronic technology enables one to produce electron beams of the required energy (tens of keV) at current densities of about 1 kA$\cdot$ cm^{-2} without particular difficulty, which corresponds to an electron density of $n_e \approx 10^{11}$ cm^{-3}. Therefore, to attain $n_e\tau_i \approx 10^{10} - 10^{12}$ sec$\cdot$cm^{-3}, we require an ion retention time of $\tau_i \approx 0{,}1 - 10$ c. sec. The ions are retained in directions perpendicular to the beam axis automatically by the electrostatic field of the electron space charge (at least until the beam is neutralized by ions of the working substance and residual gas). To eliminate rapid neutralization, one should introduce only small batches of the working substance and provide a sufficiently high vacuum. Special measures are needed to provide longitudinal retention, which have to produce potential barriers near the ends of the beam for the stripping time τ_i.

Figure 1 shows the scheme for the KRION source (cryogenic ionizer), which is the best device of the EBIS type [16-19]. Only the key elements in the source are shown together with the longitudinal distributions of the magnetic field and electrostatic potential. The magnetic field H is homogeneous along the entire beam length, and its function amounts to transverse electron retention in order to keep the current density constant. The profile of the longitudinal electrostatic field is controlled by programmed potentials φ on the electrically insulated sections of the drift tube (total number 25). The potentials applied to the sections are switched by a special automatic device [20], which produces three different longitudinal profiles at set instants, which are denoted by A, B, and C in Fig. 1. First one produces profile A, in which the beam is cleared of trapped parasitic ions. Then a batch of the working substance is supplied in the region of section 3 and profile B is applied, which constitutes a potential well for positively charged particles. When a sufficient number of ions of low charge has accumulated in this well, profile C is switched in, which shuts off access to the well from new ions from the injector. Profile C is maintained during the set ionization time τ_i; then A is again applied and the highly charged ions are ejected along the axis to the extraction system. Complete stripping for argon requires τ_i = 2 sec under the conditions of the KRION-2 source, whose technical parameters are as follows:

*There are regular specialized international seminars on EBIS and ECR sources.

Declassified and Approved For Release 2013/09/14 : CIA-RDP10-02196R000300040005-3

Declassified and Approved For Release 2013/09/14 : CIA-RDP10-02196R000300040005-3

TABLE 1. Ion Currents of Various Charge States in the PIG Source for the U-300 Cyclotron, mA

Gas	Z												
	3	4	5	6	7	8	9	10	11	12	13	14	15
Argon	20	13	5,9	2,7	0,8	0,2	—	—	—	—	—	—	—
Krypton	24	15	8,4	8,0	7,3	4,3	1,7	0,5	0,1	—	—	—	—
Xenon	24	24	12	10	9,3	8,0	5,8	4,0	3,6	1,1	0,4	0,2	0,05

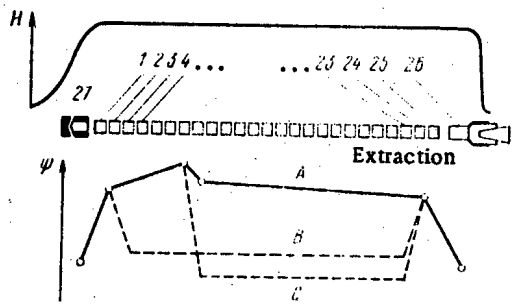

Fig. 1. Scheme for the KRION source: 1-25) drift-tube sections; 26) electrical collector; 27) electrical gun.

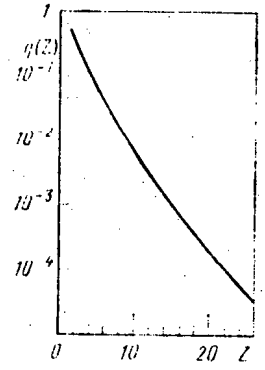

Fig. 2. Empirical dependence of proportion of ions with charge Z on total number of ions in laser source [29].

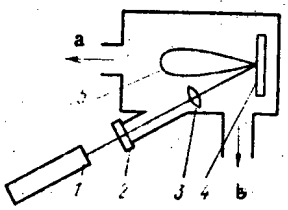

Fig. 3. A simple scheme for a laser source of highly charged ions HCI: 1) laser; 2) window; 3) lens; 4) target; 5) plasma; a) HCI; b) pump.

Declassified and Approved For Release 2013/09/14 : CIA-RDP10-02196R000300040005-3

Declassified and Approved For Release 2013/09/14 : CIA-RDP10-02196R000300040005-3

TABLE 2. Fluxes Γ_Z of Ions in Charge State Z in MINIMAFIOS

Nitrogen		Oxygen		Argon		Krypton		Molybdenum		Tungsten		Neon	
Z	Γ_Z	Z	Γ_Z	Z	Γ_Z	Z	Γ_Z	Z	Γ_Z	Z	Γ_Z	Z	Γ_Z
7	$2\cdot10^{11}$	8	$1\cdot10^{11}$	13	$4\cdot10^{9}$	19	$3\cdot10^{9}$	20	$1\cdot10^{11}$	29	$2\cdot10^{11}$	10	$1\cdot10^{9}$

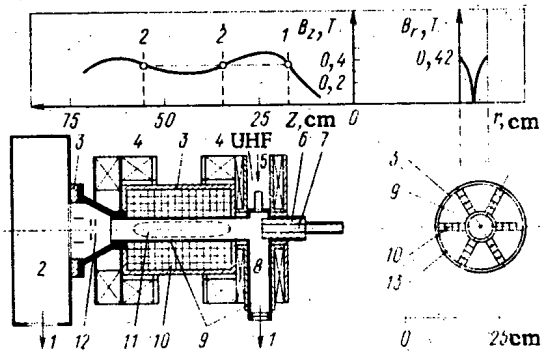

Fig. 4. The MINIMAFIOS scheme [3]: 1) pump; 2) high-vacuum region; 3) insulator; 4) magnetic coils; 5) window for UHF power; 6) insulating tube for ejection and preliminary ionization; 7) first resonance zone; 8) j_1 region; 9) multimode cavity; 10) hexapole $SmCo_5$ magnet; 11) ECR heating region; 12) extraction system; 13) radiation shield; B_z longitudinal magnetic field; B_r radial magnetic field between poles.

Beam length, cm	140
Vacuum, mm Hg*	10^{-12}
Beam current density, $A\cdot cm^{-2}$	600
Beam energy, keV	22
τ_i, sec	10
$n_e\tau_i$, $sec\cdot cm^{-3}$	6×10^{12}

The best result at present is the production of 2×10^6 helium-type ions from xenon in a pulse (2×10^5 ions/sec). The nuclei of light elements are stripped in substantially larger numbers. For example, one can produce 2×10^9 carbon nuclei per pulse.

So far, the main efforts have been devoted to attaining the maximum degree of ionization, and the problem appears to have been solved. An unsolved problem remains the low intensity of the EBIS beam. The following are the most optimistic forecasts for this [19, 21]:

	Ions/sec
U^{92+}	$2\cdot10^{10}$
Xe^{54+}	$5\cdot10^{11}$
Ar^{18+}	$4\cdot10^{12}$
Ne^{10+}	$3\cdot10^{13}$

A bunch of higher intensity of highly charged beams from EBIS involves raising the energy efficiency. Essentially, the energy deposited in the electron beam is used directly for ionization with very low efficiency because the electrons spend only a short time in the stripping region (0.01-0.02 μsec in the KRION-2). The efficiency can be characterized from τ_e/τ_i, which in the best EBIS models is 10^{-9} (the optimum value clearly is $\tau_e/\tau_i = 1$). The value of τ_e/τ_i means that only a small proportion of the beam energy is used in stripping, wich means that there is an exceptionally high energy price for a single ion. For example, in the KRION-2 the production of one Xe^{52+} ion consumes about 0.3 J. At that level, the

1 mm Hg = 133.322 Pa.

Declassified and Approved For Release 2013/09/14 : CIA-RDP10-02196R000300040005-3

Declassified and Approved For Release 2013/09/14 : CIA-RDP10-02196R000300040005-3

TABLE 3. Values of $n_e\tau_{iZ}$ for the HELIOS-12A Plasma

Z	$n_e\tau_{iZ}$, sec·cm^{-3}	Z	$n_e\tau_{iZ}$, sec·cm^{-3}	Z	$n_e\tau_{iZ}$, sec·cm^{-3}
2	$2\cdot10^{7}$	5	$2\cdot10^{9}$	8	$2\cdot10^{11}$
3	$1\cdot10^{8}$	6	$1\cdot10^{10}$	9	$8\cdot10^{11}$
4	$5\cdot10^{8}$	7	$4\cdot10^{10}$	10	$4\cdot10^{12}$

production of the forecast yield of Xe^{52+} ions of 1×10^{12} per second for future EBIS [19] will require an impossibly high beam power (about 3×10^{5} MW). Production of that number of xenon nuclei would indoubtedly require even more power. To increase the efficiency, one organizes energy circulation in the EBIS by recuperating and reusing the beam energy [22]. This is a complicated electrical engineering problem when the circulating power is very high, since even with quite high recuperation coefficients the dissipated proportion of the circulating energy would represent very large absolute values. One way of cheapening the ions is to use ionic supercompression, which was observed by Arianer's group at Orsay [23]. This effect leads one to hope to raise the current density by 2-3 orders of magnitude, which greatly reduce τ_i and correspondingly increase τ_e/τ_i. Here however there is a fundamental problem of providing stability in the system with high energy density under highly nonequilibrium conditions represented by the superdense electron beam filled with ions.

This indicates that EBIS is a sensitive and extremely complicated physics instrument that has opened up new scope for fundamental research in nuclear physics [24] and also for injecting highly charged ions (as far as stripped nuclei) into pulsed accelartors with low repetition frequencies (synchrotrons). It would become acceptable to use this source as an injector for a continuous-running accelerator if a solution could be found providing radical improvement in the energy efficiency.*

Laser. When a laser beam with a power density Φ of over 10^{8} W·cm^{-2} falls on a solid target, the energy and the radiation pulse are transferred in a short time to a small amount of material, which produces a hot dense plasma moving in a particular direction. Highly charged ions in this plasma have been detected spectroscopically [25-27], which led to suggestions [9, 10] that a laser plasma of this type could be used as a highly charged ions source.

The physical characteristics of such a plasma are determined by the energy transfer, which can be represented schematically as follows. In the initial stage, a cold plasma is forme at the surface whose density attains the critical value ($n_{ec}=10^{21}/\lambda^{2}$ cm^{-3}, where λ is the wavelength in μm). This plasma is an intermediate body that transmits the laser energy to the solid target. The rapid plasma heating produces a shock wave, which propagates in the target, heats it, and accelerates the atoms in the propagation direction, i.e., into the target. The local compression causes the target atoms to be ejected into the vacuum, where they pass through the hot plasma and are ionized. Therefore, the final result is a jet of ions directed into the vacuum, some of which are highly charged.

A theoretical analysis of this model was performed in [28], where the following expressions were derived for the electron temperature and parameter $n_e\tau_i$:

$$T_e=1.25\cdot10^{-6}(A/Z)^{1/3}(\lambda^{2}\Phi)^{2/3}; \quad (1)$$

$$n_e\tau_i=10^{8}(A/Z)\,T_e^{3/2}. \quad (2)$$

Here τ_i is the ion time of flight through the hot plasma in sec, T_e is electron temperature in eV, Φ is the flux density in V·cm^{-2}, λ is the wavelength in μm, and $n_e\tau_i$ is the Lawson parameter in sec·cm^{-3}. The formulas show that $T_e\sim\lambda^{4/3}$ and $n_e\tau_i\sim\lambda^{2}$, so long-wave lasers are the best, such as a CO_2 laser ($\lambda=10.6$ μm). At flux densities of about 10^{10} W·cm^{-2}, which are readily attained with such lasers, it follows from (1) and (2) that the plasma has $T_e\approx150$ eV, $n_e\tau_i\approx5\cdot10^{11}$

*See the recent review by Donets concerned with EBIS (ÉChAYa, 13, 941 (1982)).

Declassified and Approved For Release 2013/09/14 : CIA-RDP10-02196R000300040005-3

Declassified and Approved For Release 2013/09/14 : CIA-RDP10-02196R000300040005-3

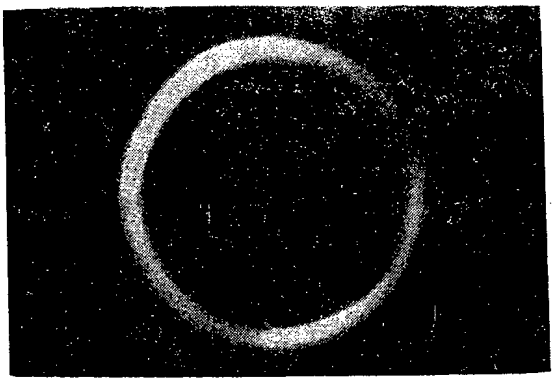

Fig. 5. Hot-electron ring ($T_e = 4$ keV) of diameter 2 cm recorded in x rays.

$sec \cdot cm^{-3}$, and high efficiency, since $\tau_e/\tau_i > 1$. The total number of ions formed in a pulse is given [29] by

$$N_i \approx \frac{10^{2/4}}{A^{1/3}Z^{2/3}} (\Phi/\lambda^4)^{1/3} S t_l, \tag{3}$$

where S is the area irradiated by the laser in cm^2 at t_1 is the irradiation time in sec. For example, with $\Phi \approx 10^{10}$ $W \cdot cm^{-2}$, $S = 1$ mm^2, and $t_1 = 50$ nsec we get $N_i \approx 10^{15}$ ions/pulse for iron. The number of highly charged ions N_{iZ} is some fraction η of N_i:

$$N_{iZ} = \eta(Z) N_i, \tag{4}$$

where η (Z) < 1 is the function of Z shown in Fig. 2 [29]. In the present case, of the 10^{15} ions produced in a pulse one expects a yield of 10^{11} ions of Fe^{20+}. Therefore, the physical conditions in a laser plasma are extremely favorable to generating highly charged ions. Therefore, the physical conditions in a laser plasma are extremely favorable to generating highly charged ions.

A laser source is attractive also because of the exceptional simplicity. The design essentially consists of a laser, the optical system, and the target in a vacuum chamber. Figure 3 shows a very simple scheme for a laser source. At fluxes of 10^9 -10^{10} $W \cdot cm^{-2}$ and a wavelength of 10.6 μm, the source provides stable yields of ions such as C^{6+}, Al^{11+}, Pb^{16+}, W^{15+}, V^{14+}, Co^{20+}, Fe^{20+} [31]. The processes accelerate the ions perpendicular to the target, and these separate the ions differing in charge not only in coordinate space but also in momentum space. The highly charged ions are produced as a cone of angle $\leqslant 30°$, and this angle decreases as the charge increases. The energies of the highly charged ions are distributed over the range 5-50 keV.

A disavantage of the laser method is that the electron temperature is comparatively low (30-60 eV) [32], and this is inadequate even at high $n_e\tau_i$ to provide extensive stripping for heavy elements. Nevertheless, a source of this type produces light nuclei in amounts sufficient for injection to pulse accelerators designed for relativistic energies [33]. For element of medium mass, the source can give 10^{10} sec^{-1} ions with $Z/A \approx 0.3$, in a solid angle of 10^{-4} sr, whereas heavy ions can be produced at 10^9 sec^{-1} with $Z/A \approx 0.05$, 10^{10} sec^{-1} with $Z/A \approx 0.03$, and 5×10^{10} sec^{-1} with $Z/A \approx 0.01$ at a pulse repetition frequency of 1 Hz [32].

Another substantial disadvantage of a laser source is that the target must be moved to prevent the beam from falling on the same point many times. The essential pulsed mode of operation makes a laser source not very convenient for injecting heavy ions into a cyclotron, although such experiments have been performed [31]. However, the total number of ions produced in a pulse is very large (about 10^{15}), which makes this source promising for heavy-ion fusion research [32], and also for providing ions for relativistic electron rings in collective accelerators.

ECR. At present there are two essentially different families of ECR sources: the MAFIOS sources (Machine à Faire Ions Strippés) and the (HELIOS ones Hot Electron Laver Ion Source). For brevity, we call the first family ECR-M and the second ECR-H.

ECR-M. Geller's group in Grenoble proposed and developed the ECR-M sources, in which a plasma trap containing a magnetic well is used, in which the electron component of the plasma

Declassified and Approved For Release 2013/09/14 : CIA-RDP10-02196R000300040005-3

Declassified and Approved For Release 2013/09/14 : CIA-RDP10-02196R000300040005-3

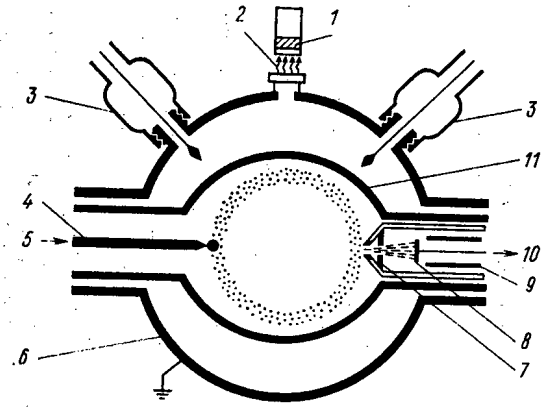

Fig. 6. Scheme for the HELIOS-12A source [43]: 1) NaI(Tl) detector; 2) x rays; 3) microwave feeder; 4) 10 kV pusher; 5) gas inlet; 6) TE_{111} cavity; 7) collector; 8) target; 9) liner; 10) pump; 11) pyrex chamber.

is heated by UHF fields in electron cyclotron resonance. The most powerful device of this family is SUPERMAFIOS-B [34-37], which was based on a fusion trap containing a system of six Ioffe rods producing a hexapole transverse lagnetic field superimposed on a field of simple mirror configuration. The plasma has the maximal diamagnetism of $n_e T_e = 3 \cdot 10^{15}$ eV·cm^{-3}, which with $T_e \approx 10$ keV gives $n_e \approx 3 \cdot 10^{11}$ cm^{-3} with $\tau_e = \tau_i \approx 30$ msec for the particle lifetime. Therefore, the SUPERMAFIOS-B plasma attains $n_e \tau_i \approx 1 \cdot 10^{10}$ с·см$^{-3}$ with $T_e \approx 10$ keV.

The efforts of the Grenoble group directed to optimizing and miniaturizing the ECR-M have led to a final form termed MINIMAFIOS [30]. Figure 4 shows the scheme for the commercial model (the cost of one of these is about 600,000 dollars). Five coils produce a longitudinal magnetic field of simple mirror configuration, whose profile is shown in Figure 4. The transverse magnetic field providing the minimum-B configuration is provided by a current-free hexapole lens consisting of six plates of samarium–cobalt permanent magnets placed within the coils. Figure 4 also shows the radical magnetic-induction distribution. Along the axis of the magnetic system there is a cylindrical section made of stainless steel (diameter 7 cm and length 30 cm) for a multimode cavity, whose second section takes the form of a parallelipiped and is used to supply the UHF power ($\omega/2\pi = 10$ GHz, $P^{\sim} = 2.5$ kW) along a circular waveguide through a vacuum-tight beryllium oxide window, which is provided with cryogenic pumping (1000 liter·sec^{-1}), with a facility for injecting a cold plasma from an insulating tube, where the primary ionization is provided in the working gas supplied at a pressure of about 10^{-3} mm Hg. The condition for electron cyclotron resonance is met within the insulating tube in region 3 where there is a sharp fall in pressure (10^{-3}–10^{-5}mm Hg), and also in region 11. The residual-gas pressure measured in region j_1 is about 10^{-6} mm Hg when the source is working, but it is much less (possibly by two orders of magnitude) within the hot plasma because the neutral atoms are burned out by ionization in times shorter than the time of flight through the plasma [38]. Therefore, the effects of charge transfer on the charge composition of the ionic omponent are slight. Table 2 gives the optimized values of parameters such as the pressure, microwave power, and injection system obtained in 1982 in the steady state [8].

The MINIMAFIOS source consumes about 80 kW (el.), but not more than 2 kW is deposited in the plasma. The efficiency can be estimated from the total power consumed, which gives that the energy price of a light nucleus is about 3×10^{-7} J/ion. Mo^{20+} and W^{29+} have about the same price, whereas Ne^{10+}, Ar^{13+}, and Kr^{19+} are about 100 times cheaper. Nevertheless, the efficiency in the ECR-M sources is quite high because of the optimal value of τ_e/τ_i, which is one. At present, ECR-M sources analoguous to that described above such as the ECREVETTE [39] and HISKA [40] are used in external light-nucleus injection into cyclotrons at Louvain la Neuve and Karlsruhe respectively. In the first case, the source provides 2×10^8 sec^{-1} of C^{6+} and 2×10^7 sec^{-1} of O^{8+}, while in the second case the target has provided 2×10^8 sec^{-1} of energy 26 MeV/nucleon.

ECR-H. The sources in this family were suggested and began to be examined about 10 years later than the ECR-M ones, after it had been observed that there was a specific radial ambipolar potential distribution in the UHF discharge excited in a single-mode cavity with electron cyclotron resonance in a mirror magnetic trap, which took the form of a potential

Declassified and Approved For Release 2013/09/14 : CIA-RDP10-02196R000300040005-3

Declassified and Approved For Release 2013/09/14 : CIA-RDP10-02196R000300040005-3

well* instead of the usual potential hump found in a gas discharge [41].

A magnetic trap is used in the ECR-M and ECR-H sources, in which the electron component is heated by electron cyclotron resonance. A key element in the ECR-H sources is the ring layer of hot electrons encompassing the central densest part of the plasma. This layer is formed automatically via the upper hybrid resonance in the heating of the plasma enclosed in the insulating chamber within the single-mode cavity excited in a right-hand rotating mode. The axially symmetrical local plasma heating leads to a rise in the potential of the peripheral parts relative to the colder central part, i.e., to the formation of an electrostatic well for the ions in a cross section of the plasma with respect to the static magnetic field. The magnetic mirrors reflect the hot electrons moving in the transverse direction towards the center of the trap, which increases the potential at the ends of the plasma relative to the center. These factors produce a time-stationary three-dimensional potential well for positive ions. Figure 5 shows the annular layer of hot electrons from the x rays photographed along the axis of the magneric field [14] at a UHF power less than 20 W.

The three-dimensional electrostatic well provides the conditions necessary for separating and retaining the highly charged ions, whose lifetimes increase exponentially with the charge in the presence of good thermal contact between the differently charged populations. Therefore, the ECR-H sources can produce highly charged ions not because the retention time for the plasma is long (as in the ECR-M) but because the retention times are long only for the highly charged ions. Under these conditions, $n_e\tau_i$ ceases to be single-valued, since τ_i is a function of Z:

$$\tau_{iZ}/\tau_{i1} = \exp[\beta(Z-1)], \tag{5}$$

where τ_{i1} is the singly charged ion lifetime, τ_{iZ} is the lifetime of an ion in charge state Z, $\beta = e\varphi/kT_i$; φ is the depth of the potential well for singly charged ions, and T_i is the temperature of the ions of all charges in thermal equilibrium.

The following parameters are typical of the plasma in the HELIOS-12A source [43]: $n_e = 5\cdot10^{10}$ см$^{-3}$; $\beta = 1.5$; $\tau_{i1} = 100$ μsec, i.e., $n_e\tau_{i1} = 5\cdot10^6$ sec × cm^{-3}. Table 3 gives values of $n_e\tau_{iZ}$ for Z = 2-10, which shows how rapidly $n_e\tau_{iZ}$, increases with Z, so that the retention parameter becomes comparable with that for the ECR-M even at Z = 6, in spite of the relatively small value of $n_e\tau_{i_1}$, while the former exceeds the latter considerably for larger Z and attains values characteristic of EBIS.

The HELIOS-12A [43] is shown in Fig. 6. The cylindrical single-mode cavity is placed between the poles of a permanent magnet (the lines of force are perpendicular to the plane of the figure), and it is excited in the TE_{111} mode from a magnetron ($\omega/2\pi = 2375$ MHz, $P \approx 150$ W) by two coaxial feeders separated by 90° in azimuth, whose phases are also displaced by 90°. Within the cavity is a pyrex vacuum chamber, which is supplied with the working gas. At a pressure of about 5×10^{-5} mm Hg, a discharge is excited in electron cyclotron resonance in the magnetic field of mirror configuration set up by the poles of the permanent magnet. Figure 6 schematically shows the hot-electron ring (T_e = 4 keV) automatically formed when the magnetic-field configuration and strength are appropriate. The plasma contains a graphite electrode (pusher), to which is applied a positive potential of 10 kV relative to the grounded cavity. The plasma as a whole then acquires a potential equal to that of the pusher, which provides for extracting the ions in the direction of the grounded target.

The ECR-H sources have exceptionally high efficiency, since the UHF supply is only 100-200 W. Under these conditions, the HELIOS-12A source has given 4×10^{11} sec^{-1} of Ne^{6+}, $6\cdot10^{10}$ sec^{-1} of Ne^{8+} and 5×10^9 sec^{-1} of Ne^{10+}. The values for argon are 1×10^{12} sec^{-1} of Ar^{8+} and 8×10^{10} sec^{-1} of Ar^{11+}. The energy price of one neon nucleus is low at 3×10^{-8} J/ion, while one Ar^{8+} ion requires 1.5×10^{10} J/ion. The other advantages of the ECR-H include small dimensions and simple design together with the absence of heavy damage to components during operation, the absence of any need to maintain the source or any outer part at a high voltage in order to extract the ions, and the availability of continous operation.

The main disadvantage of this type of source is that it is impossible to produce metallic ions because the pyrex chamber rapidly becomes coated with metal, which prevents the UHF en-

*Shortly afterwards, the same effect was observed in the NBT fusion system [42], where the physical situation is analogous.

Declassified and Approved For Release 2013/09/14 : CIA-RDP10-02196R000300040005-3

Declassified and Approved For Release 2013/09/14 : CIA-RDP10-02196R000300040005-3

ergy reaching the plasma. Studies are being made on the scope for using an evacuated cavity without an insulating chamber together with preliminary ionization of solid-state substances (including metals) by means of laser radiation.

Conclusions. During the last 10-15 years, there has been a vigorous search for new ways of generating highly charged ions. Of the many suggestions, the most promising appear to be EBIS, laser sources, and ECR. The latter has two parallel branches: ECR-M and ECR-H. Researches on all three lines have already been completed or are being completed by the construction of working sources capable of producing light nuclei (C^{6+}, N^{7+}, O^{8+}, Ne^{10+}) at rates of 10^9 -10^{12} per second.

Nuclei from elements in the middle of the periodic table are at present produced only by EBIS sources, but the rates are low (10^5 -10^7 per second) and the energy price is extremely high. The feature is a central problem in this approach.

A laser source provides a large number of heavy ions with moderate charges ($Z \leqslant 10$) in the form of periodic short pulses, which may be of interest to fusion research.

The ECR sources are promising for continuous-running ion accelerators because they can produce reasonably strong beams in continous mode [46, 47] (10^{10} -10^{13} sec^{-1}) of medium and heavy ions having $Z/A = 0.2 - 0.3$. These sources may be improved without obvious essential difficulties by raising the electron temperature to hundreds of keV and increasing the striping times to some seconds with $\tau_e/\tau_i = 1$. The basis for such developments can be provided by results on the production of relativistic plasma by means of electron cyclotron resonance together with stable retention in a magnetic trap for an adequate time [44, 45].

LITERATURE CITED

1. A. Ghiorso et al., IEEE Trans. Nucl. Sci., 13, 280 (1966).
2. A. S. Pasyuk and V. B. Kutner, in: Proceedings of the All-Union Conference on Medium and Low Energy Accelerators [in Russian], Naukova Dumka, Kiev (1983), p. 229.
3. J. Eninger, Nucl. Instrum. Method., 97, 19 (1971).
4. E. Hubbard et al., Rev. Sci. Instrum., 32, 621 (1961).
5. E. D. Donets, Inventor's Certificate No. 248860, Byull. Izobret., No. 24, 65 (1969).
6. R. Geller, Appl. Phys. Lett., 16, 401 (1970).
7. J. Consolino et al., in: First Int. Conf. on Ion Sources, Proc. INSTN, Saclay (1969), p. 537.
8. N. Peacock and R. Pease, J. Phys. D, 2, 1705 (1969).
9. G. Tonon, C. R. Acad. Sci. (Paris), 262, 706 (1966).
10. Yu. A. Bykovskii et al., Inventor's Certificate No. 324938, Byull. Izobret., No. 7, 227 (1974).
11. A. Trivelpiece et al., Phys. Rev. Lett., 21, 1436 (1968).
12. J. Daugkerty et al., ibid., 20, 369.
13. T. Stix, ibid., 23, 1093 (1969).
14. V. Dugar-Zhabon et al., Phys. Scr., 18, 506 (1978).
15. V. Dugar-Zhabon et al., ibid., 25, 639 (1982).
16. E. D. Donets and A. I. Pikin, Zh. Tekh. Fiz., 45, 2373 (1975).
17. E. Donets, IEEE Trans. Nucl. Sci., 23, 897 (1976).
18. E. D. Donets and V. P. Ovsyannikov, Preprint JINR, R7-80-515, Dubna (1980).
19. E. Donets, Phys. Scr., 26, 11 (1983).
20. E. D. Donets and A. I. Pikin, Inventor's Certificate No. 741766, Byull. Izobret., No. 29, 290 (1981).
21. R. Becker, Worshop on ECR Ion Sources, GSI-81 (1981), p. 165.
22. V. G. Abdul'manov et al., in: Proceedings of the Seventh All-Union Conference on Charged-Particle Accelerators [in Russian], JINR, Dubna (1981), p. 75.
23. J. Arianer and R. Geller, Ann. Rev. Nucl. Part. Sci., 31, 19 (1981).
24. E. D. Donets and V. P. Ovsyannikov, Zh. Eksp. Teor. Fiz., 80, No. 3, 916 (1981).
25. W. Linlor, Appl. Phys. Lett., 3, 11 (1963).
26. N. Isenor, ibid., 4, 8 (1964).
27. N. G. Basov et al., Pis'ma Zh. Eksp. Teor. Fiz., No. 6, 9 (1967).
28. J. Bobin and G. Tonon, Bull. Inf. Sci. Technol. (Paris). 160, 23 (1971).
29. J. Tonon, IEEE Trans. Nucl. Sci., 19, 172 (1972).
30. R. Geller and B. Jacquot, Nucl. Instrum. Method., 184, 293 (1981).

Declassified and Approved For Release 2013/09/14 : CIA-RDP10-02196R000300040005-3

Declassified and Approved For Release 2013/09/14 : CIA-RDP10-02196R000300040005-3

31. Yu. A. Bykovskii et al., in: Proceedings of the Seventh All-Union Conference on Charged-Particle Accelerators [in Russian], JINR, Dubna (1981), p. 95.
32. L. Z. Barabash et al., Preprint ITEF-126, Moscow (1981).
33. A. M. Baldin et al., Kvantovaya. Élektron., 4, 1547 (1977).
34. R. Geller, in: Proc. 13th Int. Conf. Phen. Ion Gases, Invited Lectures, Berlin (1977), p. 103.
35. P. Briand et al., Nucl. Instrum. Method., 131, 407 (1975).
36. P. Briand et al., Paper P. 3.77, G. S. I., Darmstadt (1977), p. 42.
37. R. Geller, IEEE Trans. Nucl. Sci., 2, 2120 (1979).
38. S. Dousson et al., in: Proc. 2nd Int. Conf. Low Energy Ion Beams (LEIB-2) (1980).
39. Y. Jongen et al., in: Proc. 4th Int. Workshop on ECR Ion Sources, CENG Press (1982), p. 3.1.
40. V. Bechtold et al., ibid., p. 6.1.
41. V. Dugar-Zhabon et al., in: Proc. 8th Eur. Conf. on Contributions to Fusion and Plasma Physics, Prague (1977), p. 102.
42. T. Shoji et al., Amm. Rev. IPP. Nagoya Univ. (1979), p. 84.
43. V. Dugar-Zhabon et al., in: Fifth ECR Ion Source Workshop, Louvain-la-Neuve (1983), p. 3.
44. N. Luchmann and A. Trivelpiece, Phys. Fluids, 21, 2038 (1978).
45. V. Andreev and K. Golovanisvsky, Phys. Lett., December (1983), p. 123.
46. R. Geller, Rev. Phys. Appl., 15, 995 (1980).
47. R. Bourg et al., in: Proc. 4th Int. Workshop on ECR Ion Sources, CENG Press (1982), p. 5.1.

Declassified and Approved For Release 2013/09/14 : CIA-RDP10-02196R000300040005-3

Declassified and Approved For Release 2013/09/14 : CIA-RDP10-02196R000300040005-3

SMALL-SCALE SYSTEM FOR THE FORMATION OF A FIELD OF IRRADIATION WITH ACCELERATED ELECTRONS

O. A. Gusev, S. P. Dmitriev, A. S. Ivanov, V. P. Ovchinnikov, M. P. Svin'in, and M. T. Fedotov

UDC 621.384.6

High-voltage electron accelerators are used extensively today in some industrial radiation-chemical processes [1]. With an irradiation-field size of 1.5-2 m, however, it is often difficult to fit the accelerators into standard industrial premises in view of the fact that, with the customary method of forming the irradiation field by scanning the beam through an angle of ± 30°, the height of the accelerator reaches 5-6 m above the surface of the object to be irradiated. A possible way of solving this problem is to use single-gap accelerators with an extended cathode [2] or to design electron-beam-scanning systems with deflection through angles greater than 30°. The application of single-gap accelerators is limited by the maximum voltage across the vacuum gap, viz., no more than 200-250 keV at the present time. In systems with scanning through large angles, in order to reduce the electron energy losses the beam extractor must provide for a correction to the electron trajectory so as to ensure that the electrons impinge on the foil at nearly 90° [3].

In this paper we consider a method of correcting the electron trajectory by means of a constant-field beam-deflection electromagnet, installed directly in front of the extraction window. Implementation of this method of correction for a strip beam was considered in [4] and for an axisymmetric beam with small-angle scanning, in [5].

For a strip beam with parallel trajectories (Fig. 1) the correcting electromangent turns into a converter of the beam width, which varies in accordance with the relation

$$L = l/\cos\alpha, \tag{1}$$

where l and L are the initial and final beam width and α is the slope angle of the beam relative to the vertical axis. A strip beam can be obtained from an extended cathode of length l (see Fig. 1a) or can be formed by means of axisymmetric scanning with double deflection [6].

In order to increase the height of the scanning chamber, it is desirable to choose the angle within the limits 75-85° and the correcting magnet ensures that the electrons enter the foil of the exit window at angles of nearly 90°. For an axisymmetric beam with angular scanning (see Fig. 1b), in order to reduce the vertical size of the facility the accelerator is placed horizontally and the beam is scanned within the limits of 5-20° to one side of the horizontal axis over the entrance plane of the correcting magnet. With this method of correction the angles of entrance into the foil differ from 90° by roughly half the scanning angle. This deviation can, in principle, be eliminated by setting up an appropiate magnetic field distribution in the gap or varying the height of the poles along the length of the magnet.

For a uniform distribution of the electron current over the length of the exit window the form of the current in the coils of the scanning electromagnet should differ from sawtooth since the velocity with which the beam moves over the object ceases to be constant when the scanning angle changes linearly in time; the reason is that the velocity is dependent on the scanning angle

$$v = -\frac{d\varphi}{dt}\frac{h}{\sin^2\varphi}, \tag{2}$$

where v is the velocity of the beam over the entrance plane of the magnet, h is the distance from the axis of the radiator to the entrance plane of the magnet, and φ and t are variable values of the angle and time.

Translated from Atomnay Énergiya, Vol. 56, No. 5, pp. 311-312, May, 1984. Original article submitted January 31, 1983.

 0038-531X/84/5605-0336$08.50 © 1984 Plenum Publishing Corporation

Declassified and Approved For Release 2013/09/14 : CIA-RDP10-02196R000300040005-3

Declassified and Approved For Release 2013/09/14 : CIA-RDP10-02196R000300040005-3

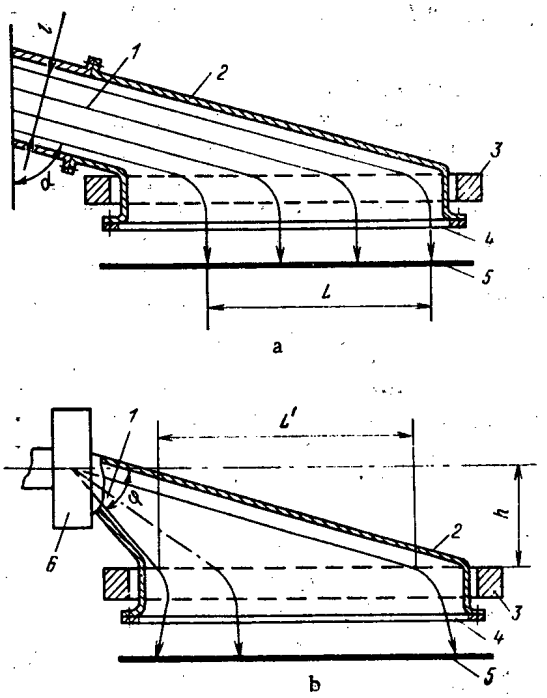

Fig. 1. Small-scale system for the formation of an irradiation field with a strip beam (a) and an axisymmetric beam b). 1) electron beam; 2) scanning chamber; 3) correcting electromagnet; 4) exit window; 5) irradiated object; 6) scanning electromagnet.

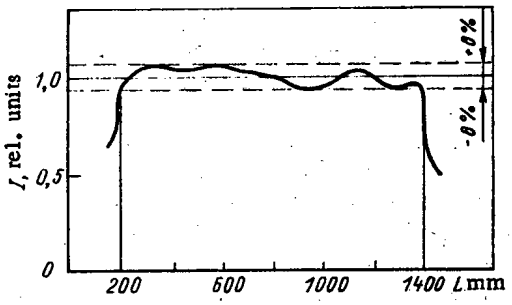

Fig. 2. Distribution of the linear current density along the exit window.

On integrating Eq. (2) for v = const and taking account of the dependence of the deflection angle in the scanning electromagnet on the magnetic field H(t), we get the law governing the variation of the scanning current I(t)

$$I(t) = \frac{\sqrt{2WE_0 + W^2}}{300b} \sin\left(\operatorname{arccot}\frac{L'}{h}t\right), \qquad (3)$$

where W is the electron energy, E_0 is the electron rest mass, b is the height of the poles of the scanning electromagnet, f is the sweeping frequency, and L' is the sweep length on the entrance plane of the magnet.

To verify the principle advanced here, we devised a mock-up of a system of irradiation-field formation with an exit window 1500 mm long and 80 mm wide, the height of the scanning chamber in this case being 600 mm. The law of current variation in the coils of the scanning magnet for the longitudinal sweep was realized with the aid of a generator of triangular voltage with subsequent approximation of the form of the current [7]. The mock-up was used to study systems of irradiation-field formation both with a strip beam, obtained from an axi symmetric beam, and with an axisymmetric beam, scanning through an angle of 5-20° to one side of the horizontal axis. The latter formation system is smaller in size and a lower power

Declassified and Approved For Release 2013/09/14 : CIA-RDP10-02196R000300040005-3

Declassified and Approved For Release 2013/09/14 : CIA-RDP10-02196R000300040005-3

supply for the scanning magnets while having practically identical characteristics of the expanded beam.

The uniformity of the distribution of the linear current density was determined at a distance of 60 mm from the foil of the exit window by a technique expounded in [8]. The measuring error of the linear current density, in the assessment of the authors of the technique, is ± 3%. The distribution of the linear current density for an axisymmetric beam scanning through an angle of 5-20° to one side of the horizontal axis at an electron energy of 300 keV and a beam power of 18 kW, is presented in Fig. 2. The uniformity of the distribution of the linear current density in this case ± 8% at a length of 1200 mm; this can be explained by the real shape of the current in the coils of the scanning magnet for longitudinal sweep not corresponding exactly to the required law of current variation in them. The angles at which the electrons enter the foil, measured with the aid of a small-aperture diaphragm, lie in the range 7 ± 0.5° from the normal to the plane of the exit window, which is close to half the scanning angle. Investigations of the mock-up confirmed the feasibility of the principle advanced here and the possibility of a commercial facility being built with a small-scale system of irradiation-field formation [9].

LITERATURE CITED

1. V. A. Glukhikh, in: Proceedings of Third All-Union Conference on the Application of Charged-Particle Accelerators in the National Economy [in Russian], A. D. Efremov Scientific-Research Institute of Electrophysical Apparatus, Leningrad (1979), Vol. I, p. 3.
2. S. Nablo and E. Tripp, Radiat. Phys. Chem., 9, 325 (1977).
3. US Patent No. 3748612 (1973).
4. S. P. Dmitriev, A. S. Ivanov, and M. P. Svin'in, International Application No. PCT/SU 80/00065. Device for Irradiation of Objects with Electrons [in Russian], Published October 29 (1981), No. WO/081/03104.
5. O. A. Gusev et al., International Application No. PCT/SU 81/00016. Device for Irradiation of Objects with Electrons [in Russian], Published September 2 (1982), No. WD 82/02990.
6. S. P. Dmitriev et al., Inventor's Certificate No. 708944, Byull. Izobret., No. 39, 324 (1980).
7. D. S. Val'tman, V. P. Ovchinnikov, and Yu. B. Rusak, in: Proceedings of Fourth All-Union Conference on the Application of Charged-Particle Accelerators in the National Economy [in Russian] Vol. II, A. D. Efremov Scientific-Research Institute of Electrophysical Apparatus, Leningrad (1982), p. 94.
8. M. I. Afanas'ev and I. V. Druzgal' skii, Proceedings of Third All-Union Conference on the Application of Charge-Particle Accelerators in the National Economy [in Russian], Vol. III, A. D. Efremov Scientific-Research Institute of Electrophysical Apparatus, Leningrad (1979), p. 244.
9. B. I. Al'bertinskii et al., Proceedings of Fourth All-Union Conference on the Application of Charge-Particle Accelerators in the National Economy [in Russian], Vol. I, A. D. Efremov Scientific-Research Institute of Electrophysical Apparatus, Leningrad (1982), p. 46.

Declassified and Approved For Release 2013/09/14 : CIA-RDP10-02196R000300040005-3

Declassified and Approved For Release 2013/09/14 : CIA-RDP10-02196R000300040005-3

DENSITY AND SURFACE TENSION OF MOLTEN MIXTURES OF URANIUM TETRAFLUORIDE WITH LITHIUM AND SODIUM FLUORIDES

A. A. Klimenkov, N. N. Kurbatov, S. P. Raspopin, and Yu. F. Chervinskii

UDC 532.14'61:54.161-143

Molten mixtures of uranium tetrafluoride with alkali-metal (Li and Na) fluorides may by of use in nuclear power [1], and it is therefore of interest to examine the physicochemical properties of these mixtures.

The density ρ and surface tension σ of molten binary mixtures were measured over the complete concentration range by means of the maximum pressure in a gas bubble, which provided stable and reproducible results. The salts were used in vitrocarbon crucibles. Nickel was used as the capillary material, which is resistant to fluorides. The working gas was purified argon.

We determined the density on the basis of the correction for the displacement of the melt by the capillary [2]. The surface tension was calculated from the Cantor–Shroedinger formula [3]. Much attention was given to the preparation of the initial anhydrous salts. The uranium tetrafluoride was made by a wet method involving precipitation from aqueous solution with excess hydrofluoric acid followed by drying and firing [4]. The anhydrous lithium and sodium fluorides were made by drying the corresponding chemically pure fluorides initially

TABLE 1. Density and Surface Tension for Molten LiF–UF_4 and NaF–UF_4 Mixtures

Content, mol. %	$\rho=a-b\cdot T$, g/cm³			$\sigma=A-B\cdot T$, mJ/m²			Temp. range, °K
	a	b	$S\cdot10^3$	A	B	S	
				LiF—UF_4			
0	2,3854	0,5141	0,5	335,9	0,0932	0,5	1130—1250
10	3,8676	0,7043	8	334,6	0,1004	0,8	1070—1265
15	4,4689	0,8471	8	336,0	0,1044	0,7	1060—1260
20	4,8880	0,9081	6	336,7	0,1068	0,9	975—1270
25	5,4160	1,0660	7	337,2	0,1092	0,6	950—1250
30	5,9114	1,2304	3	337,1	0,1109	0,9	947—1265
40	6,3032	1,1438	10	337,6	0,1149	0,8	972—1260
45	6,6081	1,1892	11	339,6	0,1183	0,7	977—1267
50	6,6951	1,1240	8	341,1	0,1201	0,8	1033—1260
55	6,8991	1,1038	6	344,1	0,1227	1,0	1117—1279
60	7,2132	1,2180	9	358,2	0,1334	1,0	1120—1271
70	7,7622	1,4122	1	368,4	0,1416	1,3	1220—1320
80	7,7033	1,1741	1	372,2	0,1442	1,2	1242—1330
100	7,8620	1,0179	9	408,2	0,1716	1,7	1316—1360
				NaF—UF_4			
0	2,6436	0,5498	2	288,4	0,0833	0,6	1270—1334
7	3,7134	0,8932	3	303,1	0,0954	0,3	1250—1300
10	4,0183	0,9630	1	301,6	0,0056	0,3	1219—1278
15	4,5063	1,0533	2	316,3	0,1093	0,2	1095—1270
25	5,0355	1,0463	6	313,9	0,1082	0,9	974—1268
30	5,3791	1,1010	7	318,9	0,1114	0,8	994—1253
35	5,6120	1,0851	9	320,8	0,1126	0,6	1002—1268
40	6,0762	1,2253	8	321,7	0,1130	0,6	1020—1271
50	6,7713	1,4234	8	322,5	0,1135	1,0	1053—1270
60	7,3041	1,4821	6	340,5	0,1272	1,0	1068—1275
70	7,3864	1,2742	7	348,6	0,1307	1,1	1162—1312
80	7,5116	1,1363	3	377,3	0,1523	0,8	1271—1334

Translated from Atomnaya Énergiya, Vol. 56, No. 5, pp. 312-313, May, 1984. Original article submitted July 4, 1983.

0038-531X/84/5605-0339$08.50 © 1984 Plenum Publishing Corporation

Declassified and Approved For Release 2013/09/14 : CIA-RDP10-02196R000300040005-3

Declassified and Approved For Release 2013/09/14 : CIA-RDP10-02196R000300040005-3

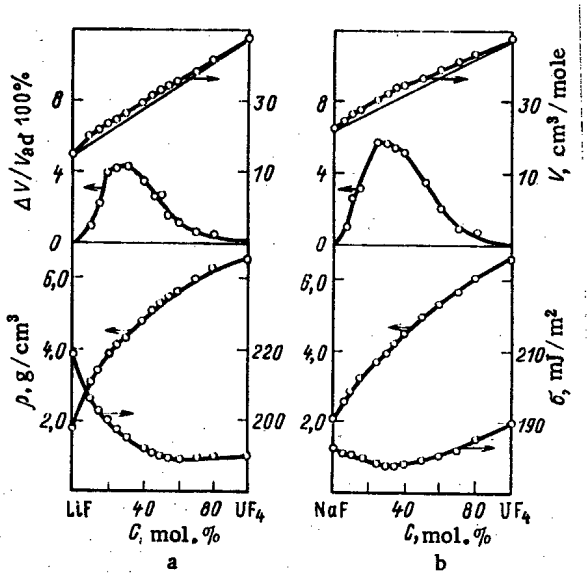

Fig. 1. Physicochemical parameters of melts in the systems $LiF—UF_4$ (a) and $NaF—UF_4$ (b) at 1270°K.

in air and the under vacuum with gradual heating to the melting point, followed by slow crystallization in argon. The melting points were determined by differential thermal analysis and agreed within ±2° with the most reliable published values [5].

The measurements were processed by least squares. The temperature dependence of the density and surface tension was closely described by linear equations in all cases. The values found for the densities of the lithium, sodium, and uranium flourides agreed well with published values [5]. There was not more than 2% deviation of the measured surface tension for lithium and sodium fluorides from the published data of [6], while the discrepancies for uranium tetrafluoride were not more than 5%.

Table 1 gives the density and surface-tension data in the form of the coefficients for the linear equations, together with the standard deviations S of the experimental values from those calculated from the equations as well as the temperature ranges used in the measurements. The available data on the density for individual compositions in the $LiF—UF_4$ and $NaF - UF_4$ [7] agree satisfactorily with out values.

Figure 1 shows the concentration dependence for the density and surface tension in these systems at 1270°K. The density increases monotonically with the uranium tetrafluoride content. In the lithium—fluoride system ,the surface tension falls as the uranium tetrafluoride content increases. In the $NaF—UF_4$ system, sodium fluoride reduces the surface tension of the uranium tetrafluoride.

The density data were used to calculated the molar volumes V and relative deviations from the additive values $\Delta V/V_{ad}$ at 1270°K. There are positive deviations from additivity in the molar volumes (Fig. 1), which indicate interaction between the components. The molar-volume isotherms are identical in trend for the two systems because the structural changes are of the same type. The mixing of lithium or sodium fluoride with uranium tetrafluoride is accompanied by the formation of complex groupings based on the uranium cation, as is evident from the concentration dependence of the relative deviation in molar volume from additivity. The maximum deviations occur at 20-30 mole % uranium tetrafluoride, evidently because stable UF_7^{3-} anionic complexes are formed in this concentration range, as is confirmed by spectral studies [8].

There is an increase in the excess molar volume on going from the lithium fluoride system to the sodium fluoride one, which indicates an increased interaction within the complex groups and weakening of the counter-polarizing action of the cations in the outer coordination sphere.

Declassified and Approved For Release 2013/09/14 : CIA-RDP10-02196R000300040005-3

Declassified and Approved For Release 2013/09/14 : CIA-RDP10-02196R000300040005-3

LITERATURE CITED

1. V. L. Blinkin and V. N. Novikov, Liquid-Salt Nuclear Reactors [in Russian], Atomizdat, Moscow (1978).
2. B. V. Linchevskii, Techniques in Metallurgical Experiments [in Russian], Metallurgizdat, Moscow (1967).
3. V. K. Semenchenko, Surface Phenomena in Metals and Alloys [in Russian], Fizmatgiz, Moscow (1957).
4. J. J. Katz and E. Rabinowitch, Chemistry of Uranium, Peter Smith.
5. Handbook on Fused Salts [in Russian], Vol. 1, Khimiya, Leningrad (1971).
6. Handbook on Fused Salts [in Russian], Vol. 2, Khimiya, Leningrad (1972).
7. G. Janz et al., J. Phys, Chem. Ref. Data, 3, No. 1, 1 (1974).
8. L. Toth, J. Phys, Chem., 75, No. 5, 631 (1971).

INFLUENCE OF GRAIN SIZE AND DOPING WITH BORON ON THE BEHAVIOR OF HELIUM IN STAINLESS STEEL 16-15

A. G. Zaluzhnyi, M. V. Cherednichenko-Alchevskii, O. M. Storozhuk and A. G. Zholnin

UDC 621.039.53:539.219.3

In investigating the influence of cold deformation on the behavior of helium in OKh16-N15M3B steel [1], several stages of gas liberation were established; this allowed the corresponding intrinsic mechanisms of helium liberation to be proposed and the activation energies corresponding to these processes to be estimated. In the present work, the investigation of the behavior of helium is continued, and an attempt is made to study the influence of grain size and doping with boron on the kinetics of helium liberation with linear heating and also after isochronous annealing, since it is known [2, 3] that reduction in grain size and doping with boron (to 10^{-2} mass %) significantly reduces the tendency of the steel to high-temperature radiational buckling.

To this end, the kinetics of helium liberation from samples of OKh16N15M3B steel preliminary treatment to produce grain sizes of 3-5, 30-50, and 100-200 μm and also from steel samples of grain size 30-50 μm containing 0.007 mass % boron was determined. The experimental samples were uniformly (over the thickness) saturated with helium to a concentration of $2 \cdot 10^{-3}$ at. %, as a result of α-particle bombardment in a cyclotron. The preparation of the samples and the experimental method were described earlier in [1, 4, 5].

Spectra of the rate of gas liberation obtained in the course of linear heating ar a rate of 7 K/min of samples of OKh16N15M3B steel with different grain sizes and a boride-steel sample (0.007 mass % B) are shown in Fig. 1, together with curves of the relative helium yield after isochronous annealing for 0.5 h.

Gas liberation from the experimental samples occurs in several stages, interpreted earlier [1]; peak A is associated with diffusion by the interstitial mechanism, peak B with migration of helium atoms along dislocational tubes, peak C with escape of helium accompanying the growth of the dislocation loop; and peak D with diffusion of helium atoms by a vacancy mechanism. Gas liberation at temperatures above 1200°K is attributed to migration of helium complexes to the sample surface. It may be noted that the spectra of the rate of gas liberation from samples of OKh16N15M3B with different grain sizes are identical; only a small shift of the diffusional peak D toward lower temperatures for samples with small (3-5 μm) grains is observed. However, the amount of helium (Fig. 1e) liberated from a sample with small grains is approximately ten times lower in all temperature ranges than for samples with moderate (30-50 μm) and large (100-200 μm) grains.

The significant distinguishing feature of gas liberation from a sample of boron-doped steel (Fig. 1d) is the almost complete absence of the stage associated with diffusion of

Translated from Atomnaya Énergiya, Vol. 56, No. 5, p. 314, May, 1984. Original article submitted May 30, 1983.

0038-531X/84/5605-0341$08.50 © 1984 Plenum Publishing Corporation

Declassified and Approved For Release 2013/09/14 : CIA-RDP10-02196R000300040005-3

Declassified and Approved For Release 2013/09/14 : CIA-RDP10-02196R000300040005-3

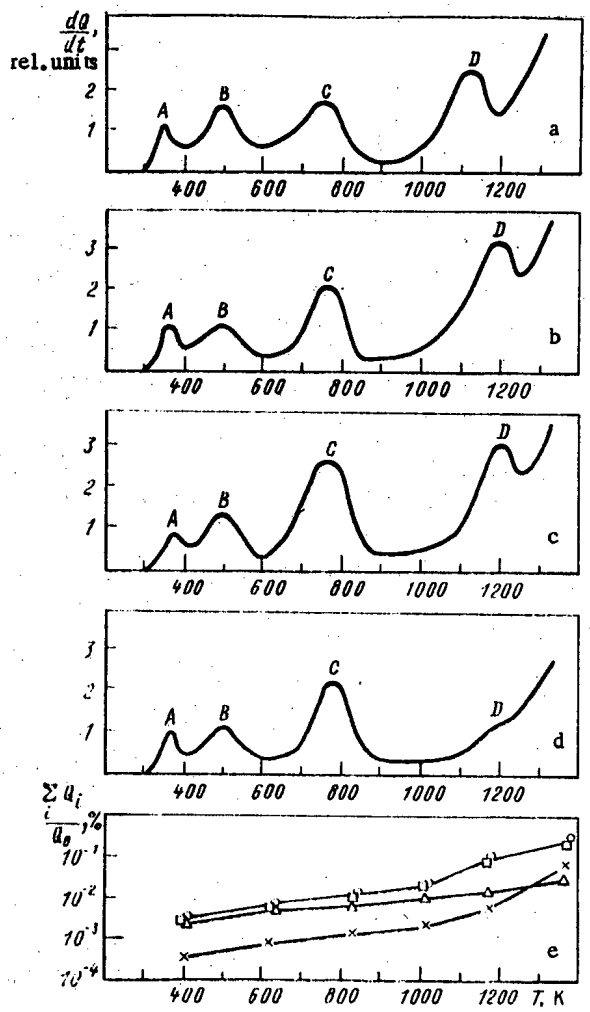

Fig. 1. Temperature dependence of the rate of helium liberation from samples of OKh16N15M3B (a-c) and OKh16N15M3BR (d) bombarded with α particles in a cyclotron, with grain sizes of 3-5 (a). 30-50 (b, d), and 100-200 μm (c); e) relative helium yield in the experimental volume of the apparatus: ○, □, ×) OKh16N15M3B, grain size 100-200, 30-50, and 3-5 μm, respectively; Δ) OKh16N15M3BR steel, grain size 30-50 μm.

helium atoms by the vacancy mechanism (peak D). Note also that the amount of helium liberated from this sample at temperatures above 770°K is considerably less than for analogous boron-free samples (Fig. 1e).

These features of helium liberation from samples with different grain sizes and samples doped with boron have not yet been subjected to exhaustive explanation. However, it may be assumed that the grain boundaries are of great importance here, since they are unsaturated traps for helium atoms; in connection with this, gas liberation occurs only from a thin surface layer of the samples. Boron doping leads to considerable reduction in gas liberation int the temperature range corresponding to diffusion of helium atoms by a vacancy mechanism (850-1250°K).

LITERATURE CITED

1. A. G. Zaluzhnyi, M. V. Cherednichenko-Alchevskii, and O. M. Storozhuk, At. Énerg., 56, No. 5 (1984) (this issue).
2. D. Kramer et al., J. Iron Steel Inst. 207, No. 3, 1141 (1969).

Declassified and Approved For Release 2013/09/14 : CIA-RDP10-02196R000300040005-3

Declassified and Approved For Release 2013/09/14 : CIA-RDP10-02196R000300040005-3

3. T. Williams and K. Gott, J. Nucl. Mater., 95, 265 (1980).
4. A. G. Zaluzhnyi et al., At. Énerg., 52, No. 6, 418 (1982).
5. D. M. Skorov, et al., At. Énerg., 40, No. 5, 387 (1976).

CONSIDERATION OF THE DECAY OF ^{238}Pu WHEN DETERMINING THE ISOTOPIC COMPOSITION OF URANIUM FUEL OF A HYBRID THERMONUCLEAR REACTOR

S. V. Marin and G. E. Shatalov

UDC 621.039.516.22

In this paper we consider the effect of the natural radioactive decay of ^{238}Pu and ^{235}Np on the content of ^{232}U, ^{234}U, and ^{235}U in depleted uranium fuel placed in the blanket of a thermonuclear reactor with an energetic neutron field. When taking account of this process in the numerical scheme of nuclear transformations of the isotopes of the original charge, it is necessary to pay attention to two circumstances. The first consists in the fact that with consideration of the natural radioactive decay of ^{238}Pu and ^{235}Np, closed chains are formed in the scheme of nuclear transformations, by which the makeup of ^{234}U and ^{235}U is affected. The makeup effect will be appreciable with a low content of ^{235}U in the fuel. The second circumstance is related with the fact that as a result of makeup, the ^{232}U content in the irradiated fuel can be increased.

The formation of ^{234}U in the initial charge of depleted uranium takes place mainly as a result of the nuclear transformations

$$^{235}\mathrm{U}\,(n, 2n)^{234}\mathrm{U}; \tag{1}$$

$$^{235}\mathrm{U}\,(n, \gamma)^{236}\mathrm{U}\,(n, 3n)^{234}\mathrm{U}; \tag{2}$$

$$^{235}\mathrm{U}\,(n, \gamma)^{236}\mathrm{U}\,(n, 2n)^{235}\mathrm{U}\,(n, 2n)^{234}\mathrm{U} \tag{3}$$

and the natural radioactive decay of ^{238}Pu (half-life 87.75 years)

$$^{238}\mathrm{Pu} \xrightarrow{\alpha} {}^{234}\mathrm{U}. \tag{4}$$

^{235}U makeup is affected as a consequence of the radiation capture of a neutron by the ^{234}U nucleus and in the process of the natural radioactive decay of ^{235}Np, formed during irradiation of the uranium fuel.

"Undesirable" from the point of view of ensuring radiation safety when working with irradiated fuel is ^{232}U, formed from ^{234}U through the following chains:

$$^{234}\mathrm{U}\,(n, 3n)^{232}\mathrm{U} \xrightarrow{\alpha} \ldots \tag{5}$$

$$^{234}\mathrm{U}\,(n, 2n)^{233}\mathrm{U}\,(n, 2n)^{232}\mathrm{U} \xrightarrow{\alpha} \ldots \tag{6}$$

$$^{234}\mathrm{U} \xrightarrow{\alpha} {}^{230}\mathrm{Th}\,(n, \gamma)^{231}\mathrm{Th} \xrightarrow{\beta^-} {}^{231}\mathrm{Pa}\,(n, \gamma)\,{}^{232}\mathrm{Pa} \xrightarrow{\beta^-} {}^{232}\mathrm{U} \xrightarrow{\alpha} \ldots \tag{7}$$

When analyzing these nuclear transformations, it should be borne in mind that ^{234}U to the amount of ∿0.0057% is contained in natural uranium, and therefore for a correct determination of the ^{232}U content, it is necessary to know the prehistory of the original nuclear fuel.

Numerical investigations of the change of the isotopic composition of depleted uranium fuel, irradiated in the blanket of a hybrid thermonuclear reactor, were conducted for a model of a hybrid thermonuclear reactor-Tokamak [1] using the BURNFL program [2]. When solving the equations of the change of isotopic composition describing the nuclear transformations of the nuclides of the original charge in the neutron field (Fig. 1), the authors of the present

Translated from Atomnaya Énergiya, Vol. 56, No. 5, pp. 315-316, May, 1984. Original article submitted August 18, 1983.

0038-531X/84/5605-0343$08.50 © 1984 Plenum Publishing Corporation

Declassified and Approved For Release 2013/09/14 : CIA-RDP10-02196R000300040005-3

Declassified and Approved For Release 2013/09/14 : CIA-RDP10-02196R000300040005-3

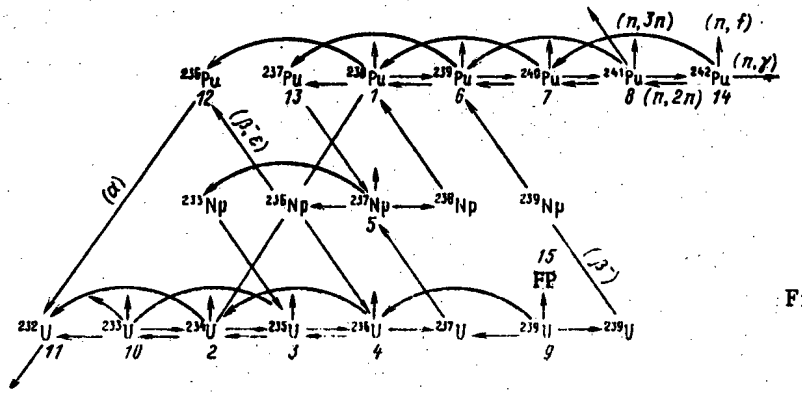

Fig. 1. Nuclear transformation scheme.

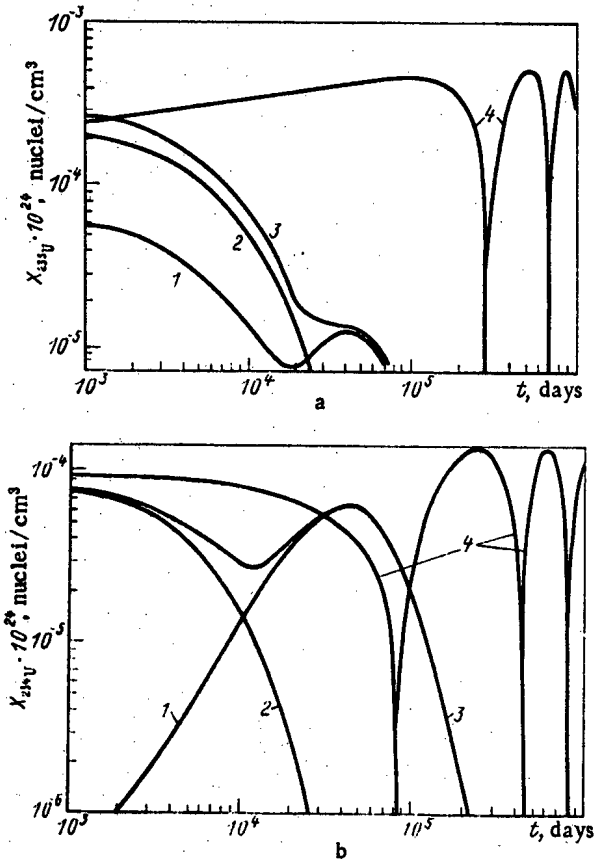

Fig. 2. Dependence of X_{235U} (a) and X_{234U} (b) on time: 1) X_{235U} and X_{234U}; 2) $F_{235U}(t)$ and $F_{234U}(t)$; 3) $\sum_{j=1}^{J} c_j \exp(\lambda_j t)$; 4) $\sum_{l=1}^{L} [a_l \cos(\lambda_l^{Im} t) + b_l \sin(\lambda_l^{Im} t)]$.

paper arrived at a conclusion concerning the expediency of the analytic solution of the system of ordinary differential equations (ODE). Numerical methods of integration of the system of ODE leave hidden that explicit combination of functions by which the solution is described. Moreover, consideration of small effects in the numerical integration imposes a number of demands on the choice of method, the integration step and other parameters. The solution of the system of ODE for the scheme of nuclear transformations (see Fig. 1) has the following form for each component:

$$X_i = \sum_{j=1}^{J} c_j \exp(\lambda_j t) X_{0j} + \sum_{l=1}^{L} \exp(\lambda_l^R t) [a_l \cos(\lambda_l^{Im} t) + b_l \sin(\lambda_l^{Im} t)] X_{0l}, \quad (8)$$

where X_i is the i-the component of the vector of isotope concentrations; λ_j, real eigenvalues of the matrix of the nuclear transformations (see Fig. 1) λ_j^R and λ_l^{Im}, real and imaginary parts

Declassified and Approved For Release 2013/09/14 : CIA-RDP10-02196R000300040005-3

Declassified and Approved For Release 2013/09/14 : CIA-RDP10-02196R000300040005-3

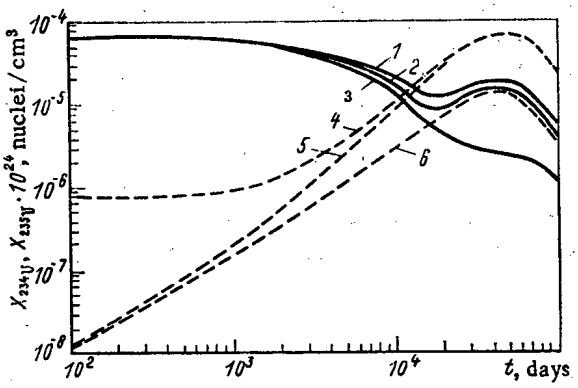

Fig. 3. Dependence of X_{234U} and X_{235U} on time, initial content of X^0_{235U} and consideration of the chain with decay of ^{238}Pu: 1) content of ^{238}U with consideration of the decay of ^{238}Pu and ^{235}Np, $X^0_{234U} = 0$; 2) content of ^{235}U with consideration of the decay of ^{238}Pu, $X^0_{234U} \neq 0$; 3) content of ^{235}U without consideration of the decay of ^{238}Pu, $X^0_{234U} = 4{,}5$) content of ^{234}U with consideration of the decay of ^{238}Pu, $X^0_{234U} \neq 0$ and $X^0_{234U} = 0$, respectively; 6) content of ^{234}U with consideration of the decay of ^{238}Pu, $X^0_{234U} = 0$.

of the complex eigen values of the matrix of nuclear transformations; (J + L), number of isotopes in the nuclear transformations scheme (L is the number of isotopes forming closed isotopes forming closed chains; J, number of isotopes not involved in the closed chains); $c_j a_\zeta$ and b_ζ numerical coefficients. The appearance in the solution of the system of ODE of a superposition of functions of the form

$$F_l(t) = \exp\{\lambda_l^R t\}\{a_l \cos(\lambda_l^{\mathrm{Im}} t) + b_l \sin(\lambda_l^{\mathrm{Im}} t)\} \qquad (9)$$

indicates the presence of oscillations. The physical nature of the oscillations is associated with the sequence of nuclear transformations in which the closed chains are formed, consisting of not less than three isotopes.

Calculations of the isotopic composition of the depleted uranium fuel were performed on a BÉSM-6 computer, using double accuracy arithmetic. Normal accuracy does not provide correctness of the calculations by formula (8) in the case of similar eigen values.

The results of the calculations are shown in Figs. 2 and 3. The oscillating part of the solution of $F_\zeta(t)$ is given in Fig. 2 for ^{234}U and ^{235}U in the time range up to 10^6 days. The period of the function $F_\zeta(t)$ is large and exceeds the actual irradiation time of the fuel. Moreover, the presence of an exponential factor smoothes out the oscillating part of the solution. An increase of the neutron loading on the primary wall of the reactor from 1 to 50 MW/m^2 corresponds to a compression of the actual time scale. With increase of the neutron loading on the primary wall of the reactor, the oscillating part of the solution in the time interval up to $(1\text{-}2)\cdot 10^3$ days appears more weakly than at low neutron loading values, as the relation between the values of the radioactive decay constants and the velocity of the nuclear reactions increases. The oscillating behavior of the ^{235}U content in the fuel being irradiated is expressed in the region far remote from the actual fuel irradiation time.

More significant is the analysis of the content of ^{234}U with consideration of the decay of ^{238}Pu. As mentioned above, the content of this isotope in the fuel affects the rate of formation of ^{232}U. With increase of the ^{234}U content, the contribution of chains (5-7) increases in the formation of ^{232}U. This is manifested particularly clearly in the spatial region of the blanket with a high-energy neutron field in the vicinity of the primary wall of the reactor.

Figure 3 shows how the ^{234}U and ^{235}U content depends on the irradiation time for the scheme of nuclear transformations, with and without consideration in the calculation of the

Declassified and Approved For Release 2013/09/14 : CIA-RDP10-02196R000300040005-3

Declassified and Approved For Release 2013/09/14 : CIA-RDP10-02196R000300040005-3

natural radioactive decay of ^{238}Pu. Both cases are considered for two types of initial charge. The first charge contains ^{235}U and ^{238}U. In the second charge, the initial content of $^{234}U(X^0_{234U})$ is taken into account to an amount proportional to the ^{235}U content in natural uranium. During irradiation of the fuel over 10^3 d, as a result of the decay of ^{238}Pu and the nuclear reaction $^{235}U(n, 2n)^{234}U$, $\sim(2\text{-}10^{-7})10^{24}$ nuclei/cm^3 of ^{234}U is formed. With a ^{234}U content in the charge of $1.2\cdot10^{-2}$ of the amount of ^{235}U at the instant of fuel discharge, the content of ^{234}U increases to approximately $(1.0\text{-}10^{-6})\cdot10^{24}$ nuclei/cm^3. The formation of ^{234}U is due to approximately 80% to the occurrence of the nuclear reaction (1) and to approximately 20% to the natural radioactive decay of ^{238}Pu. The content of ^{234}Pu in the spent fuel in the hybrid thermonuclear reactor being investigated, does not exceed its content in natural uranium.

In the spatial region of the blanket in the vicinity of the primary wall of the reactor, for a charge without ^{234}U at the initial instant of time and without taking account of natural radioactive decay in the computational scheme of nuclear transformations, the content of ^{232}U in the spent fuel amounts to $\sim13.5\cdot10^{-5}$ kg ^{232}U/ton of fuel. The presence of ^{234}U in the initial charge increases the content of ^{232}U up to approximately $17.0\cdot10^{-5}$ kg ^{232}U/ton of fuel. Taking account of the natural radioactive decay of ^{238}Pu in the computational scheme of nuclear transformations leads to a further increase of the ^{232}U content in the spent fuel up to approximately $17.2\cdot10^{-5}$ kg ^{232}U/ton of fuel. On the basis of [3], devoted to the analysis of the indeterminacy of the calculation of the velocity of the nuclear reactions, as a consequence of the inaccuracy of the nuclear data and the results of a calculation of the sensitivity coefficients for the principal nuclear reactions by which the formation of ^{232}U in the fuel of a fast reactor [4] is affected, the indeterminacy of the ^{232}U content is estimated as $\sim$100%. In order to determine the feasibility of the repeated use of the uranium from the spent fuel of a hybrid thermonuclear reactor, we point out that the ratio of the ^{232}U concentration to the concentration of ^{235}U must not exceed $1.1\cdot10^{-7}$ according to the limitations operative in the USA on the content of ^{232}U in uranium oxide being reprocessed into hexafluoride [5].

The practical consequence of the present paper is the conclusion about the admissibility of the calculation of the change of isotopic composition of fuel, without taking account in the scheme of nuclear transformations of the natural radioactive decay of ^{238}Pu and ^{235}Np.

LITARATURE CITED

1. S. V. Marin and G. E. Shatalov, At. Énerg., 52, No. 5, 301 (1982).
2. S. V. Marin, Preprint IAÉ-3111 [in Russian], Moscow (1979).
3. E. Cheng and D. Mathews, The Influence of Nuclear Data Uncertainties on Thorium-Fission Hybrid Blanket Nucleonic Performance, GA-A15594 (1979).
4. Yu. G. Bobkov et al. in: Neutron Physics [in Russian], TsNIIatominform, Moscow, Pt. 3 (1980), p. 234.
5. L. V. Matveev and É. M. Tsenter, At. Tekh. Rubezhom, No. 4, 10 (1980).

Declassified and Approved For Release 2013/09/14 : CIA-RDP10-02196R000300040005-3

Declassified and Approved For Release 2013/09/14 : CIA-RDP10-02196R000300040005-3

STATIC INSTABILITY OF ONCE-THROUGH STEAM GENERATORS WITH CONVECTIVE HEATING

I. I. Belyakov, M. A. Kvetnyi,
D. A. Loginov, and S. I. Mochan

UDC 621.18:039:532.5

The hydrodynamic stability of once-through steam generators (SG), in particular SG in nuclear power plants (NPP), is one of the most important conditions ensuring their reliable operation. The operation of a SG under unstable conditions can damage the heating surface as a result of overheating or temperature fluctuations, and lead to a decrease of the heat reception.

At present it is customary to distinguish two types of hydrodynamic instability of the flow of the medium in a steam generator tube: dynamic (oscillating) and static (aperiodic). Dynamic instability, which results from the effect of inertial forces and feedback, generally develops at low mass velocity of the medium in the tubes, and manifests itself in the form of periodic oscillations of the flow rate with an amplitude which is constant or increasing with time. The main method of preventing an oscillating instability is to ensure a sufficiently high mass velocity of the medium, and to install throttling devices, preferably at the tube entrance. A considerable number of experimental and theoretical studies in recent years have been devoted to this form of instability, and many methods have been proposed for estimating the conditions for the onset of oscillations, including the mathematical modeling of the process. Therefore, we do not consider this form of instability in the present article.

Static instability is a relative concept. It reflects the connection of a dynamical process with the controlling factor —a singularity in the relation between the pressure drop in a steam-generating tube and the flow rate of the medium in it:

$$\Delta p = f(G). \tag{1}$$

Each value of Δp_i is determined under steady operating conditions of the SG for a flow rate G_i of the medium being heated. The presence of a statically unstable regime is characterized mathematically by the derivative $d(\Delta p)/dG$ becoming nearly zero or negative. This form of instability generally manifests itself by aperiodic pulsations of the flow rate in the tube. If several channels are connected in parallel, under unstable conditions there may be either quasistationary operation of tubes with different flow rates, or aperiodic fluctuations of the flow rate in individual tubes. In the first case an oscillating instability may arise for a low flow rate.

The problem of static instability was first treated in papers of Petrov [1, 2] and Ledinegg [3] as applied to operating conditions of steam-generating tubes of once-through steam boilers. In these papers the heat flux through separate parts of the heating surface (preheater, evaporator) was assumed constant along the length of the part, and independent of the flow rate of the medium in the tube. Under these conditions the conclusions and computational recommendations of the authors of these papers are applicable, as is the method proposed in [2] for plotting the hydraulic characteristic of a steam-generating tube, i.e., the dependence of the pressure drop in the tube on the flow rate of the working medium (1). However, for a SG with convective heating, particularly for a relatively small temperature difference between the heating medium and the medium being heated (e.g., in a SG in a NPP with water-moderated–water-cooled reactors, or with a liquid metal coolant), the procedures indicated for plotting hydraulic characteristics are inapplicable. This occurs because the heat reception of the parts and the distribution of the heat flux along the length of a tube depend strongly on the temperature and the flow rate of the medium in it. The present article is devoted to a study of the hydraulic characteristics of steam-generator tubes, taking account of this dependence.

Translated from Atomnaya Énergiya, Vol. 56, No. 5, pp. 317-319, May, 1984. Original article submitted August 25, 1983.

0038-531X/84/5605-0347$08.50 © 1984 Plenum Publishing Corporation

Declassified and Approved For Release 2013/09/14 : CIA-RDP10-02196R000300040005-3

Declassified and Approved For Release 2013/09/14 : CIA-RDP10-02196R000300040005-3

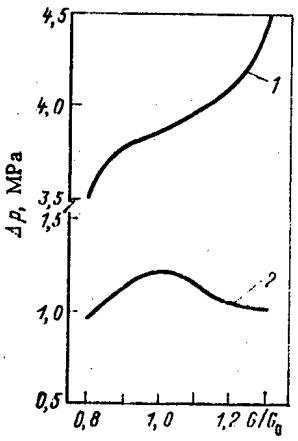

Fig. 1

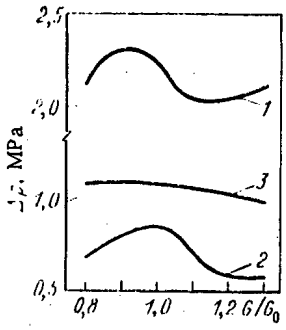

Fig. 2

Fig. 1. THC of SG at 1) 100%, and 2) 50% power.

Fig. 2. THC of a SB with tight spiral coils at 1) 100% and 2) 50% power; 3) calculated as recommended in [2].

In contrast with the term "hydraulic characteristic" (HC) which is used in calculating the heating surface with radiation heating, in convective heating it is more accurate to introduce the concpet of the thermal/hydraulic characteristic (THC). It is plotted by calculating Eq. (1) from the distribution of the heat flux along a tube corresponding to the flow rate and varying with the varying flow rate of the medium being heated in the tube. The THC can be studied by introducing new analytical relations for the dependence of the pressure drop on the determing factors, or by performing a numerical study of a mathematical model of thermal/hydraulic processes in a once-through SG. Since computer programs are available for calculating once-through SG, the second method is simpler.

In analyzing the static stability of a SG, or a module consisting of several channels connected in parallel, the following limiting conditions resulting in different THC must be considered:

a) the flow rate of the medium being heated varies the same way in all the tubes of the module; for several modules (and a nonunique THC) this leads to intermodular maldistribution. In this case for each values of the flow rate of the heat medium the heating medium has its own temperature distribution along a heating tube, differing from conditions for the nominal flow rate;

b) the flow rate of the heated medium varies only in individual tubes of the module as a result of intramodular maldistribution. The temperature distribution of the heating medium along a tube with a maldistribution remains practically unchanged when the flow rate of the medium being heated is changed.

In accordance with this the THC must be calculated under the following conditions. Under intermodular maldistribution (case a) for all values of the flow rate of the heated medium the temperatures of both heat-transfer media at the SG inlet are fixed, and the temperature at the SG outlet is determined by a verifying calculation. For intramodular maldistribution (case b), for all values of the flow rate of the heated medium a constant temperature distribution of the heating medium is assumed along the heating surface corresponding to the calculation of a module with a nominal flow rate of the medium in the tube for the given load. Since actually possible regimes correspond only to those points of the THC for which the pressure drops are the same as under the nominal regime, it does not matter whether the pressure of the medium being heated is fixed at the SG inlet or outlet. For a series connected module with inlet and outlet elements, it is necessary to include these elements in the calculation of the THC. In general the THC must be calculated by taking account of possible maldistributions over both heat-transfer media. The increase in the fraction of the leveling component of the pressure drop in most cases contributes to a decrease of the difference between the HC and the THC. Therefore, it is particularly necessary to use the THC in analyzing the static stability for a SG with a relatively small leving component.

Declassified and Approved For Release 2013/09/14 : CIA-RDP10-02196R000300040005-3

Declassified and Approved For Release 2013/09/14 : CIA-RDP10-02196R000300040005-3

Lately helical heating surfaces (coils) are being more widely used in various heat exchangers and once-through SG. They have considerable structural and technological advantages. They are compact, structurally stable, and they eliminate the necessity for a large number of spacing baffles. They can compensate for the difference of the thermal expansions of the coils and housing by the high values of the heat-transfer coefficients, and can ensure a given level of the mass velocity of the medium, etc. Such surfaces have been used, in particular, in a number of once-through SG developed and being developed abroad and in the USSR with a liquid metal coolant for NPP with fast reactors. One of the main virtues of helical coils is their small height (several times shorter than the length of the tube). At the same time this feature leads to a hydrodynamic resistance of the tube which is considerably higher than the leveling head in the tube, particularly for high flow rates of the heated material which are desirable for reliability. The static stability of a SG in this case must be verified by using the THC.

In the present article we present results of computational studies of THC based on a program of thermal/hydraulic calculations of a once-through SG with a heating surface of helical coils heated by liquid sodium. The THC was plotted from calculated pressure drops during steady operation of the SG for different flow rates of the heated medium through the module (through the SG): $G = 0.8G_0 - 1.3G_0$, where G_0 is the nominal flow rate corresponding to the specified power. The calculations were performed for operation at 50% and 100% power. Figure 1 shows the THC of a SG of the Super-Phenix (French) NPP plotted was assumed that: the sodium temperature at the SG inlet was 525°C, and the temperature of the feed water was 235°C. The absolute roughness of the tubes was 0.01 mm. According to data in [6], the absolute roughness of the tubes was ∿0.017 mm, which is close to the value assumed, and practically does not affect the result obtained. The average diameter of the winding of the coil was D = 1.9 m. Figure 2 shows the THC of a SG with a heating surface of tight helical coils with D ≈ 0.1 m [7, 8]. The ratio of the length of the SG tube to the height of the module $l/H = 3$, and the mass velocity of the medium in the tube was ∿2000 kg/m² sec. In addition, Fig. 2 shows for comparison the HC of this SG calculated as recommended in [2]. For nonuniform heating along the tube we used the formula

$$\Delta p = 6376\lambda \frac{G^2 l}{d^5}\left\{\frac{v'+v_0}{2}\frac{i'-i_0}{n(i''-i')}+\frac{v''+v'}{2}+0{,}5\left[\frac{0{,}01(i_0+Q/10^5G-4{,}7)}{p}+v''\right]\left[\frac{Q}{10^5G}-(i''-i_0)\right]\times\right.$$
$$\left.\times\frac{1}{m(i''-i')}\right\}\frac{1}{1+\frac{i'-i_0}{n(i''-i')}+\left[\frac{Q}{10^5G}-(i''-i_0)\right]\frac{1}{m(i''-i')}}, \qquad (2)$$

derived in the same way as formula 1-89 in [2] with corresponding notation under the conditions $q_{ec} = nq_{ev}$, $q_s = mq_{ev}$, where q_{ec}, q_{ev}, and q_s are, respectively, the average heat fluxes to the economizer, the evaporator, and the superheater. It follows from (2) that the total heat reception Q of the tube and the values of the coefficients m and n remain unchanged at values corresponding to nominal conditions with a change in the flow rate G of the material being heated, which is not actually the case. For a rather long steam superheater part and a low final thermal head, the calculation of the average specific volume of the steam by the equation used may lead to an appreciable error. In the term which determines the pressure drop across the evaporator part the inhomogeneity of two-phase flow in the tube is not taken into account. These features also determine the qualitative and quantitative difference between the relation obtained and the THC. It should be noted that, unlike a SG with radiation heating, in convective heat transfer the coefficients n and m are smaller than unity, and the effect of parts of the heating of the medium on the HC as a function of the form of heating may be very different.

Calculations show that the instability (multivaluedness) of the THC manifests itself at the power for which long operation of the power plant is envisaged. Obtaining a stable unique THC with the necessary margin may require a complex of structural measures: for example, an arrangement of throttling devices, "breathing" collectors in the region of transition to superheated steam, the use of tubes of different diameters in different heat-transfer regions etc. An attempt to ensure the stability of the THC under all operating conditions of the SG, in particular at power below 25% and at startup power (∿10-15%) may necessitate assuming special solutions of the hydraulic circuit of the steam generating loop. However, the advisability of such a requirement is not obvious. Taking account of the short time (small number of cycles), the plant operates at power below 25% of nominal, and the appreciable excess heat-transfer surface at these loads, which even in the presence of pulsations of the flow rate of the medium being heated ensures the required parameters of the super-

Declassified and Approved For Release 2013/09/14 : CIA-RDP10-02196R000300040005-3

Declassified and Approved For Release 2013/09/14 : CIA-RDP10-02196R000300040005-3

heated steam at the SG outlet, it is evidently possible to tolerate the use of a SG with an unstable THC at loads below 25% of nominal. The final solution of this problem requires further research to obtain data on the actual dynamical characteristics of processes in steam-generating channels connected in parallel when operating in the region where the THC is multivalued. The question of whether aperiodic pulsations necessarily appear in a module with channels connected in parallel remains open. As was stated above, it is possible that with certain combinations of operating parameters a regime may be established without fluctuations and with different flow rates of the medium being heated in individual tubes.

Thus, it has been shown that convective heating conditions are less favorable from the point of view of ensuring static stability of a SG. In certain cases this form of instability becomes determining. The study of the THC of a once-through SG is quite complicated, and cannot be performed by the simplified relations in [2]. In view of the modern trend to build compact heat exchangers and various forms of heat-transfer surfaces, the analysis of their THC must be considered a necessary step in their design. In addition, it is necessary to develop reliable recommendations for estimating the static stability for the selected SG parameters at the earliest stages of design.

LITERATURE CITED

1. P. A. Petrov, Sov. Kotloturbostr., No. 10-11, 381 (1939).
2. P. A. Petrov, Hydrodynamics of a Once-Through Boiler [in Russian], Gosénergoizdat, Moscow (1960).
3. M. Ledinegg, Die Wärme, 61, 891 (1938).
4. E. A. Kremenevskaya, Nuclear Power Plants with Fast Reactors. Itogi Nauki i Tekhniki, Ser. At. Energ., Vol. 2, VINITI, Moscow (1983).
5. Super-Phenix steam generators: Design and Construction, Rev. Gen. Nucl. No. 4 (1981), p. 384.
6. I. Sykora et al., in: Experience in the Development and Operation of Steam Generators for Fast Reactors. Papers of a Seminar of CMEA Member Countries [in Russian], Dimitrovgrad (1982), p. 41.
7. L. N. Artemov, ibid. p. 11.
8. S. I. Mochan et al., Inventor's Certificate No. 819490, Byull. Izobret., No. 13, 156 (1981).

Declassified and Approved For Release 2013/09/14 : CIA-RDP10-02196R000300040005-3

Declassified and Approved For Release 2013/09/14 : CIA-RDP10-02196R000300040005-3

CRYOGENIC LOOP FOR γ-RAY SOURCES

I. I. Buzukashvili
and G. S. Karumidze

UDC 621.039.516

Circulating gaseous helium is ordinarily used to cool irradiated speciments to a cryogenic temperature. This method makes it possible to attain temperatures of 10-15°K, but it requires the application of expensive cryogenic machines and complicated communication systems [1].

Meanwhile, many radiation investigations are carried out at a temperature of 80°K. For such investigations a simple cryogenic loop with natural circulation of the cryogenic agent, developed at the Physics Institute of the Academy of Sciences of the Georgian SSR, has been installed in the indium-gallium circuit of the IRT-2M [2]. The design of this loop differs from those described in [3, 4]. Instead of spectrally pure argon, which eliminates the danger of explosion due to the accumulation of azides [5], the cryogenic agent used in this case is chemically pure argon which is cooled with commercially pure nitrogen outside the radiation field.

The cryogenic loop (Fig. 1) consists of a working channel 1, a reservoir 2, a jacket 3, a packing gland 4, a rod 5 with a specimen 6, valves 7, a manometer 8, and a manovacuumeter 9. The temperaute of the specimen during the irradiation is monitored with a thermocouple.

During operation of the loop the working channel is first pumped down to a pressure of 1.3 Pa. Liquid nitrogen from the tank is fed into the reservoir 2 until a pressure of 0.2 MPa is reached in it, after which the working channel is fed argon from the gas holder; the argon is cooled, condenses, and flows downward. The pressure of 0.2 MPa maintained in the

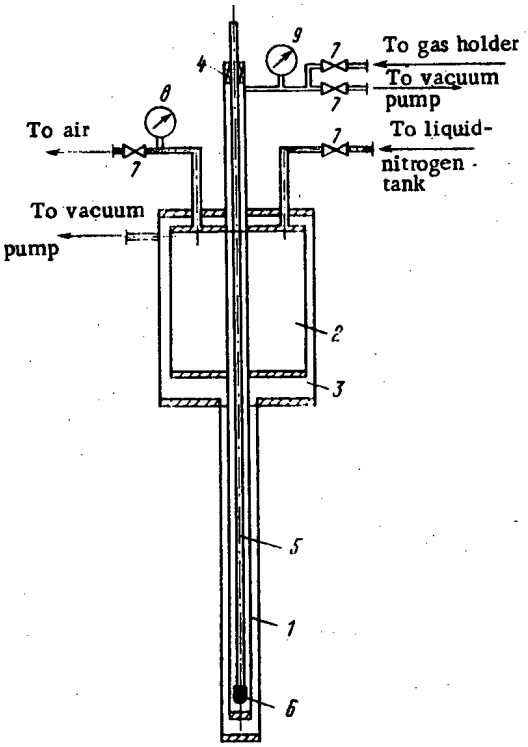

Fig. 1. Cryogenic loop of the thermosiphon type.

Translated from Atomnaya Énergiya, Vol. 56, No. 5, p. 319, May, 1984. Original article submitted September 21, 1983.

0038-531X/84/5605-0351$08.50 © 1984 Plenum Publishing Corporation

Declassified and Approved For Release 2013/09/14 : CIA-RDP10-02196R000300040005-3

Declassified and Approved For Release 2013/09/14 : CIA-RDP10-02196R000300040005-3

reservoir ensures an argon evaporation temperature of ∿85°K, which eliminates the possibility of the argon solidifying in the cooling zone. The argon condensed in the lower part of the channel evaporates, cooling the specimen, and rises to the zone of the reservoir, where is recondenses. In order to prevent heating during start-up of the loop the specimen is introduced into the irradiation zone after the working regime has been established. When the loop warms up the argon returns to the gas holder.

The cryogenic loop described here provided stable cooling of specimen-simulators with a heat release of up to 50 W to a tempeature of 85-100°K. Such a loop can also be used in the neutron loops of nuclear reactors, provided that radiation safety is observed by removing the radioactive argon formed as a result of the $^{40}Ar(n, \gamma)^{41}Ar$ reaction.

The authors express their thanks to V. A. Chernomordin, N. N. Datunaishvili, and R. B. Lyudvigov for their collaboration in tests with the loop.

LITERATURE CITED

1. L. A. Badachkoriya et al., "Low-Temperature Loops in the IRT-2000 Reactor," Proceedings of Fourth Working Meeting on the Physics and Engineering of Research Reactors [in Russian], Budapest (1965).
2. R. B. Lyudvigov, in: Abstracts of Symposium on Radiation Chemistry [in Russian], Tbilisi (1978), p. 220.
3. L. Bochjrol et al., Les installations cryogeniques our irradiations des reacteurs melusine et siloe, CEA-R-2514 (1964).
4. T. Bleuitt, Low-Temperature Irradiation Studies, Solid State Division, ORNL, Oak Ridge (1956).
5. Handbook of Physicotechnical Principles of Cryogenics [in Russian], Énergiya, Moscow (1973).

Declassified and Approved For Release 2013/09/14 : CIA-RDP10-02196R000300040005-3

Declassified and Approved For Release 2013/09/14 : CIA-RDP10-02196R000300040005-3

INFLUENCE OF NEUTRON SPECTRUM ON FORMATION OF ^{233}U FROM ^{232}Th

A. S. Gerasimov, G. V. Kiselev, and A. P. Rudik

UDC 621.039.8.002:621.039.554

As is well known, thorium fuel cycles are very promising in the nuclear power industry. A detailed discussion of the problems involved and a review of the published data are given in the monograph [1]. We emphasize only the specific nature of the process of the formation of ^{233}U from ^{232}Th, which is due to the presence of intermediate ^{233}Pa, whose decay after reactor shut-down leads to increased reactivity.

The aim of this paper is to determine the dependence of the concentration of ^{233}U formed from ^{232}Th and the number of neutrons from ^{232}Th burn-up that are expended in the process, and the absolute value of the flux density and the neutron energy spectrum. In essence, this paper is a continuation of [2] in which the formation of some actinides in nuclear reactors was considered. The procedure employed was discussed in detail in [2].

The scheme of the formation of ^{233}U from ^{232}Th is presented in Fig. 1. Above the horizontal arrows are the cross sections for the absorption of neutrons at an energy of 0.0253 eV while beneath these arrows are the resonance integrals from a energy of 0.5 eV [3] (1 b = 10^{-28} m^2). For ^{233}U we give the total thermal cross section and resonance integral of absorption, including fission and radiative capture. The partial values are, respectively, σ_f = 531.1 b, I_f = 764 b, σ_γ = 47.7 b, and I_γ = 140 b. The value of the ^{233}Pa half-life was taken from the handbook [4]. The scheme in Fig. 1 has been simplified and it does not take into further transformations of ^{234}U. This is justified by the fact that ^{235}U follows after ^{234}U, which results in roughly a zero expenditure of neutrons in the processes of ^{234}U transformation. Moreover, the formation of ^{232}U is considered. This is due mainly to the fact that the calculation of the ^{232}U formation requires detailed knowledge of the reactor design,* and the aim of this paper is to obtain sufficiently broad results that depend only on the neutron spectrum and the blocking of resonance absorption in ^{232}Th. The problems of ^{232}U formation are discussed in detail in [5] while some problems of the influence of the neutron spectrum on the ^{232}U formation are considered in [6].

Figure 1 presents the value I_1 of the ^{232}Th resonance integral for the case of infinite dilution.† Under real conditions resonance absorption in ^{232}Th is blocked. The calculations were thus carried out for three values I_1 = 11, 50, and 85 b, corresponding to strong and weak blocking, or the absence of blocking. The number of fast neutrons per ^{233}U fission is ν = 2.492 [3]. We considered two values of the effective thermal neutron flux density Φ = $5 \cdot 10^{13}$ and 10^{14} neutrons/cm^2·sec, and for each value of Φ we considered three values of the

*For this reason we did not consider the fission of ^{232}Th by fast neutrons, which justified the smallness of the ^{232}Th fission cross section.

†A slightly higher value, I_1 = 95 b, is given in [1].

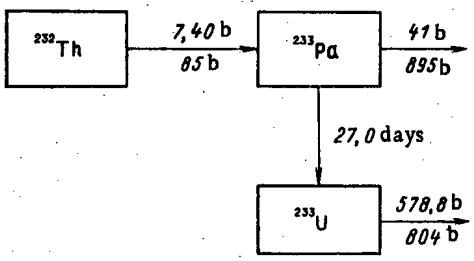

Fig. 1. Scheme of formation of ^{233}U from ^{232}Th.

Translated from Atomnaya Énergiya, Vol. 56, No. 5, pp. 320-322, May, 1984. Original article submitted October 3, 1983.

0038-531X/84/5605-0353$08.50 © 1984 Plenum Publishing Corporation

Declassified and Approved For Release 2013/09/14 : CIA-RDP10-02196R000300040005-3

Declassified and Approved For Release 2013/09/14 : CIA-RDP10-02196R000300040005-3

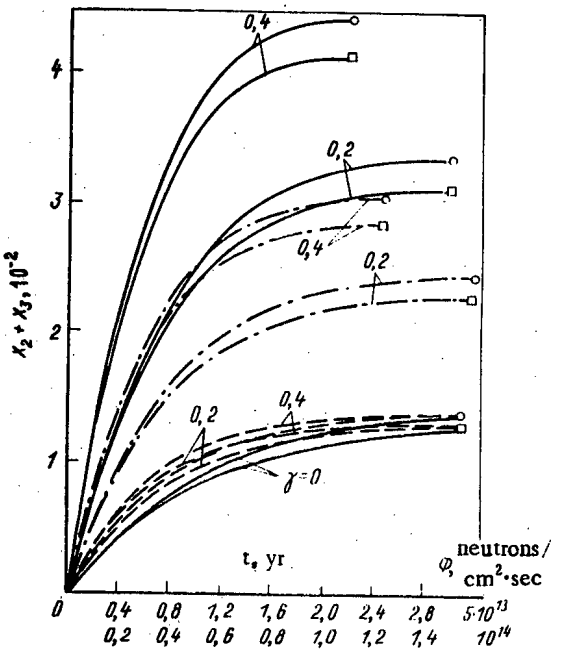

Fig. 2. Dependence of the total concentration of ^{233}Pa and ^{233}U on the irradiation time. Here and in subsequent figures $\Phi = 5 \cdot 10^{13}$ (□) and 10^{14} (○) neutrons/cm^2·sec. Blocking: I_1 = 85 (——), 50 (—·—), and 11 b (- - -).

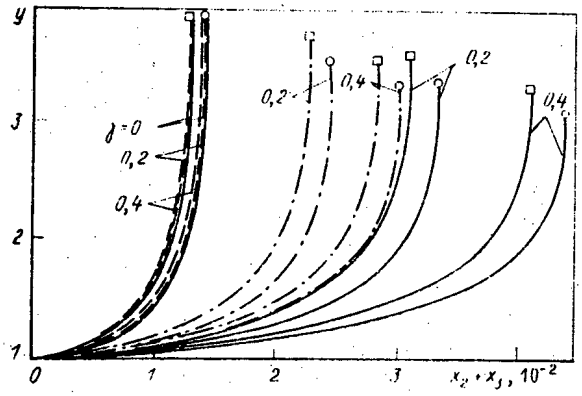

Fig. 3. Consumption of ^{232}Th for the production of one nucleus of a mixture of ^{233}Pa and ^{233}U.

effective denseness of the neutron spectra, γ = 0, 0.2 ,and 0.4. The range of γ values indicates that the calculated results presented apply to thermal reactors.

^{233}U Concentration. The nuclide concentrations are denoted as $x_1(t)$ for ^{232}Th, $x_2(t)$ for ^{233}Pa, and $x_3(t)$ for ^{233}U, normalized to one nucleus of the original ^{232}Th, so that $x_1(0) = 1$. The amount of ^{233}U produced is determined by the sum $x_2 + x_3$ at the time of unloading since in the short time after completion of the irradiation all of the remaining ^{233}Pa is transformed into ^{233}U. Figure 2 shows how $x_2 + x_3$ depends on irradiation time t. A flat maximum can be detected: In half the time taken to reach the maximum 90% $(x_2 + x_3)_{max}$ is accumulated. From Fig. 2 we see that the influence of the neutron flux density on $(x_2 + x_3)_{max}$ is weak: In the passage from $\Phi = 5 \cdot 10^{13}$ neutrons/cm^2·sec to 10^{14} the value of the maximum increases by 7-8%. This growth is explained by the fact that when the neutron flux density increases the rate of transformation of ^{232}Th into ^{233}Pa also increases in proportion, while the rate of transformation of ^{233}Pa into ^{233}U depends on the β decay and not on Φ. Thus, for a high Φ the fraction of ^{233}Pa in accumulated mixture of ^{233}Pa and ^{233}U is larger and the ^{233}U has a correspondingly smaller effect. Since ^{233}Pa is a relatively short-lived isotope ($T_{1/2}$ = 27.0 days), however, these effects prove to be weak.

Declassified and Approved For Release 2013/09/14 : CIA-RDP10-02196R000300040005-3

Declassified and Approved For Release 2013/09/14 : CIA-RDP10-02196R000300040005-3

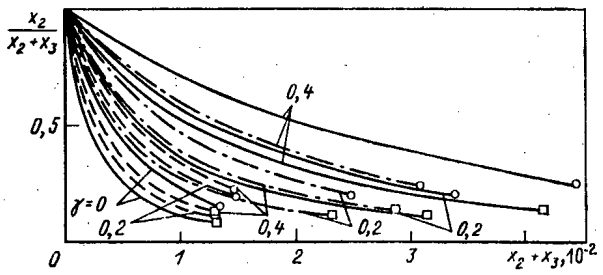

Fig. 4. Content of ^{233}Pa in accumulated mixture of ^{233}Pa and ^{233}U.

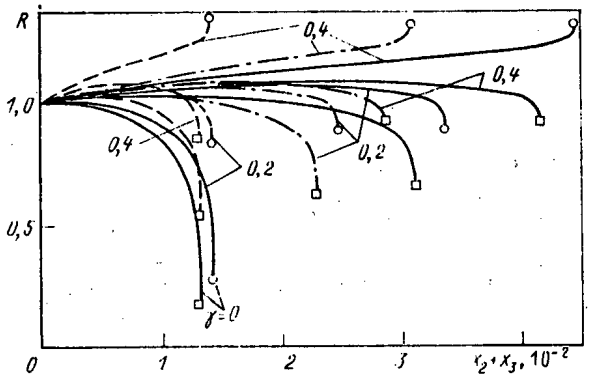

Fig. 5. Consumption of neutrons for the production of one nucleus of the mixture of ^{233}Pa and ^{233}U.

In practice the curves $x_2(t) + x_3(t)$ corresponding to different values of Φ (for the same spectrum denseness γ and identical blocking of the ^{232}Th resonance integral) coincide to within the time renormilization, which is proportional to the ratio of flux densities.

The effect of the denseness of the neutron spectrum on the formation of ^{233}Pa and ^{233}U is determined by the blocking of the ^{232}Th resonance integral. When the blocking is relatively weak the value of γ has a very strong effect on $(x_2 + x_3)_{max}$, since the contribution of resonance neutrons to the rate of transformation of ^{232}Th into ^{233}Pa is significant. When the blocking is strong the role of resonance neutrons in the formation of ^{233}Pa diminishes and the maximum $x_2 + x_3$ depends only weakly on γ.

Consumption of ^{232}Th. Figure 3 shows the consumption of ^{232}Th nuclei per nucleus of the mixture ^{233}Pa and ^{233}U, $y = [x_1(0) - x_1(t)]/[x_2(t) + x_3(t)]$. The flux density has a weak effect on the ^{232}Th consumption, which can be atrributed to the causes mentioned above. The influence of the denseness of the spectrum depends on the blocking of the ^{232}Th resonance integral: When the blocking is strong y depends weakly on γ while with weak blocking y decreases as γ grows; weakening of the blocking also leads to a decrease in y.

Content of ^{233}Pa. Figure 4 gives the ratio $x_2/(x_2 + x_3)$ as a function of $x_2 + x_3$. As $x_2 + x_3 \to 0$, i.e., as $t \to 0$, the mixture contains only ^{233}Pa which has not yet managed to be transformed into ^{233}U. Next, ^{233}Pa fairly rapidly reaches saturation and its relative fraction decreases. The ^{233}Pa content is lowest form small Φ and γ and strong blocking since in this case the relative decay rate of ^{233}Pa is high (when the rate of transformation of ^{232}Th into ^{233}Pa is very low the latter could be disregarded altogether as decaying instantaneously). As Φ and γ increases or the blocking is weakened the ^{233}Pa content grows. This law is explained by the fact that in this case the rate of transformation of ^{232}Th into ^{233}Pa increases ans the ^{233}Pa decay rate does not change. When $\Phi = 10^{14}$ neutrons/cm^2•sec and $\gamma = 0.4$ at the maximum $x_2 + x_3$ the ^{233}Pa fraction is $\sim$25%.

Neutron consumption R. For processes of the formation of nuclides, part of which may undergo fission, the neutron consumption is the number of neutrons expended on the formation of one nucleus of the desired nuclide, taking into account the neutrons produced in the fission of the nuclides under consideration. With this treatment R is more general than the

Declassified and Approved For Release 2013/09/14 : CIA-RDP10-02196R000300040005-3

Declassified and Approved For Release 2013/09/14 : CIA-RDP10-02196R000300040005-3

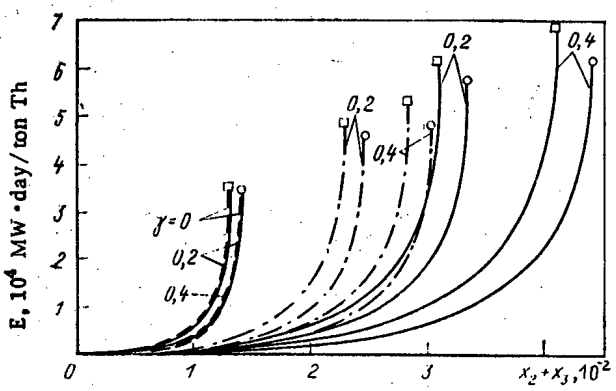

Fig. 6. Energy release in ^{233}Th.

conversion ratio usually required because concrete data about the reactor design must be known in order to determine the latter. For the relation between R and the conversion ratio it is necessary to know how many nuclei of the fissionable nuclide in the fuel (not entering into the nuclide transformation chain under consideration) are involved in the formation of one neutron external to the given process. If, e.g., one fissionable nuclide in the fuel is required for the production of one neutron when $R < 1$ expanded production of the fissionable material will be observed.

The dependence of R on $x_2 + x_3$ is given in Fig. 5. As $x_2 + x_3 \to 0$, i.e., as $t \to 0$, $R = 1$ (one neutron is absorbed in ^{232}Th, transforming it into ^{233}Pa which does not manage to decay or burn up) and $(dR/dt) > 0$. As $x_2 + x_3$ increases the value of R grows insignificantly and the decreases for all the regimes considered, except $\Phi = 10^{14}$ neutrons/cm^2·sec and $\gamma = 0.4$, its value being $R < 1$ at the maximum of $x_2 + x_3$ (this is attributed to the contribution of neutrons formed in the fission of ^{233}U). The value of R increase substantially with the growth of Φ and γ and the weakening of the blocking since in this case the ^{233}Pa content rises and the ^{233}U fraction decreases correspondingly and together with it, the contribution of ^{233}U fission neutrons. This effect manifests itself most clearly in the regime with $\Phi = 10^{14}$ neutrons/cm^2·sec and $\gamma = 0.4$: The number of ^{233}U fission neutrons is insufficient to compensate the external neutrons absorbed and $R > 1$ for all values of $x_2 + x_3$ (we note that in this case R increases as the blocking is intensified).

Energy Release E. During the fission of the ^{233}U formed energy is released in the ^{232}Th charged. In Fig. 6 we give the dependence of E on $x_2 + x_3$ per ton of the initial ^{232}Th. The energy released in one ^{232}Th fission event was assumed to be 191 MeV [7]. For a fixed $x_2 + x_3$ the energy release E decreases as Φ and γ increase and the blocking becomes weaker; this is explained by the lowering of the fraction of ^{233}U in the mixture of ^{233}Pa and ^{233}U. Clearly, the energy release is proportional to the number of neutrons produced during the fission of ^{233}U.

Conclusion. The results of the calculations are of interest from two points of view: First, the main physical characteristics of the ^{232}Th → ^{233}U process are presented as a function of the flux density and the energy spectrum of thethermal neutrons, making it possible to evaluate the efficiency of one reactor design or other; second, the decrease in the ^{232}Th consumption and the increase in the neutral consumption R as γ grows give reason to hope that the problem of economic optimization for the ^{232}Th → ^{233}U process will have a nontrivial solution.

LITERATURE CITED

1. V. M. Murogov, M. F. Troyanov, and A. N. Shmelev, Use of Thorium in Nuclear Reactors [in Russian], Énergoatomizdat, Moscow (1983).
2. A. S. Gerasimov, A. K. Kruglov, and A. P. Rudik, At. Énerg., 51, No. 4, 237 (1981).

Declassified and Approved For Release 2013/09/14 : CIA-RDP10-02196R000300040005-3

Declassified and Approved For Release 2013/09/14 : CIA-RDP10-02196R000300040005-3

3. S. Mughabhab and D. Garber, Neutron Cross Sections, BNL-325, 3rd ed. (1973), Vol. 1.
4. G. N. Gusev and P. P. Dmitriev, Radioative Chains (Handbook) [in Russian], Atomizdat, Moscow (1978).
5. L. V. Matveev and É. M. Tsenter, At. Tekh. Rubezhom, No. 4, 10 (1980).
6. T. S. Zaritskaya et al., At. Énerg., 48, No. 2, 67 (1980).
7. I. V. Gordeev, D. A. Kardashev, and A. V. Malyshev, Nuclear-Physical Constants [in Russian], Gosatomizdat, Moscow (1963).

SPECTRAL-ANGULAR DISTRIBUTION OF γ RADIATION BEHIND AN INSTRUMENTATION UNIT

P. A. Barsov, V. M. Sakharov, and V. G. Semenov

UDC 621.039.538.7

The weight fraction of the various equipment and devices is appreciable on transporting apparatuses with nuclear reactors; therefore taking correct account of the shielding properties of these items is rather important. The possibility of using an effective attenuation coefficient to estimate the shielding properties of the equipment, which has been modeled in such a way that a binomial distribution of the units of material was realized, has been verified experimentally in [1, 2]. It has been shown that the dose is attenuated exponentially along the axis of a wide radiation beam with an effective coefficient determined by the binomial law.

The possibility of using an effective attenuation coefficient in calculations by the Monte Carlo method of the differential characteristics of γ radiation behind actual equipment units is discussed in this paper. With this goal we have performed experiments and calculations in the identical geometry.

In the experiments monoenergetic γ radiation of a point isotropic ^{137}Cs source with a photon energy E_γ = 662 keV was directed at a rectangular equipment unit with a geometrical thickness at the irradiation site of Z = 53 cm and an average density of $\bar{\rho}$ = 0.43 g/cm^3. We used a scintillation spectrometer with a CsI(Tl) crystal 16 mm in diameter and 40 mm in height placed in a conical collimator as the γ-radiation detector. The isotropy of the detector is no better than ±5% within the limits of the collimation angle. The distance between the equipment unit and the detector was selected so that all the γ radiation emergent from the unit in the direction of the detector was recorded. Measurements were made for angles of 0, 30, 60, and 90° to the inner normal relative to the irradiated surface. The error of the instrumental spectra was ∿30% in the region of $E_\gamma \approx$ 130-250 keV and 15-20% for higher values of the energy. It did not prove possible to make measurements for E_γ < 130 keV due to the high background.

The calculations were performed by the Monte Carlo method using the BSERAD program [3], whose geometrical section simulated the geometry of the source, detector, and equipment unit made out of aluminum. The effective attenuation coefficient of the unscattered γ radiation used to determine the mean free path of a photon by simulating the trajectory was found using the formula [4]:

Translated from Atomnaya Énergiya, Vol. 56, No. 5, pp. 322-323, May, 1984. Original article submitted October 12, 1983.

0038-531X/84/5605-0357$08.50 © 1984 Plenum Publishing Corporation

Declassified and Approved For Release 2013/09/14 : CIA-RDP10-02196R000300040005-3

Declassified and Approved For Release 2013/09/14 : CIA-RDP10-02196R000300040005-3

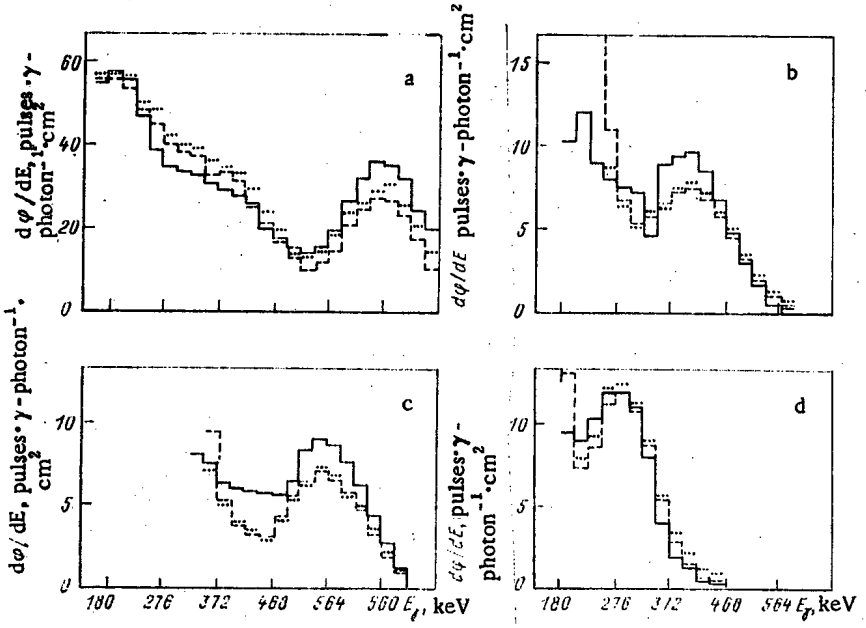

Fig. 1. Calculated and experimental instrumental spectra of the γ radiation behind an equipment unit at angles to the beam axis of (a) θ = 0, (b) 60, (c) 30, and (d) 90° with a photon energy of 662 keV: ——) experiment; - - - -) calculation for the quipment unit; .....) calculation for a layer of aluminum 7.2 cm thick with a density of 2.7 g/cm³.

$$\mu_{eff}(E_\gamma) = -\frac{\ln \int_0^Z e^{-\mu(E_\gamma)x} f(x, z)\,dx}{Z}. \qquad (1)$$

The distribution function of the material thickness f(x, Z) was obtained experimentally by the method of γ transillumination of the unit in different directions [5]. We used the sensitivity matrix determined experimentally as the sensitivity function of the detector in the calculations. The error of the spectra calculated for the indicated angles does not exceed 15% over the entire energy range.

The calculated and experimental instrumental spectra normalized per photon emitted from the source in the direction of the equipment unit are similar in shape for all detection angles (see Fig. 1). A certain systematic understating of the computational results in comparison with the experimental results in the region of the single-scattering peak is evidently associated with the use of an attenuation coefficient for aluminum, whereas the unit being investigated contains an appreciable amount of lighter elements (hydrogen, carbon, oxygen). The total mass attenuation coefficient for these elements is smaller than for aluminum, which leads to the indicated difference of 20-30%.

The dependence of the γ-radiation intensity on the recording angle is of an exponential nature. The value of the characteristic angle θ = 47° turned out to be close to its value for a homogeneous layer of aluminum and a point isotropic ^{137}Cs source [6]. This fact served as the reason for doing similar experiments and calculations for a homogeneous layer of aluminum with ρ_{Al} = 2.7 g/cm³ and Z = 7.2 cm, which corresponds to an optical thickness of the equipment unit, which is defined as the product of the effective attenuation coefficient by the geometrical thickness of the unit in the direction of the incident beam of γ-photons. The thickness of the layer, which is calculated as $\rho Z/\rho_{Al}$, is equal to 8.4 cm.

The experiments and calculations for a layer of aluminum 7.2 cm thick have shown that the spectral-angular distributions behind the layer and behind the equipment unit are practically identical. At the same time the calculations for a layer of aluminum 8.4 cm thick give results which are understated by a factor of 1.5 in comparison with those given for the equipment unit over the entire energy range.

Declassified and Approved For Release 2013/09/14 : CIA-RDP10-02196R000300040005-3

Declassified and Approved For Release 2013/09/14 : CIA-RDP10-02196R000300040005-3

The calculations performed for an optical thickness of the unit of $\mu x = 4$ have shown that the use of a homogeneous layer with thickness $\mu_{eff}x$ leads to an understating by a factor of 1.5 of the flux of γ-photons in the region $E_\gamma > 400$ keV and to some softening of the spectrum in contrast to the direct calculations, in which the distance between successive interactions is determined with the use of μ_{eff}.

The investigations carried out have led to the conclusion that the passage of γ radiation in equipment with a thickness $Z < 30$ g/cm^2 ($\mu x \leqslant 2$) can be calculated as in a homogeneous material with the use of the usual interaction constants, determining the optical thickness of the layer with the help of the effective attenuation coefficient. For equipment of greater thickness it is necessary to use the effective attenuation coefficient. The latter assertion requires further experimental verification however.

LITERATURE CITED

1. V. V. Bolyatko et al. in: Problems of Dosimetry and Shielding from Radiation [in Russian], No. 8, Atomizdat, Moscow (1968), p. 80.
2. P. A. Barsov et al., in: Abstracts of Lectures at the 2nd All-Union Scientific Conference on Shielding from Ionizing Radiations of Nuclear Engineering Facilities [in Russian], Atomizdat, Moscow (1978), p. 40.
3. P. A. Barsov et al., in: Radiation Safety of Nuclear Power Plants [in Russian], No. 26, Moscow (1979), p. 75.
4. A. V. Kolomenskii et al. At. Énerg., 44, No. 6, 517 (1978).
5. V. V. Bodin et al., in: Abstracts of Lectures at the 2nd All-Union Scientifiec Conference on Shielding from Ionizing Radiations of Nuclear Engineering Facilities [in Russian], Atomizdat, Moscow (1978), p. 103.
6. Yu. A. Kazanskii et al., Physical Investigations of Reactor Shielding [in Russian], Atomizdat, Moscow (1966).

Declassified and Approved For Release 2013/09/14 : CIA-RDP10-02196R000300040005-3

Declassified and Approved For Release 2013/09/14 : CIA-RDP10-02196R000300040005-3

MEASUREMENT TECHNIQUES
Izmeritel'naya Tekhnika
Vol. 27, 1984 (12 issues) $520

MECHANICS OF COMPOSITE MATERIALS
Mekhanika Kompozitnykh Materialov
Vol. 20, 1984 (6 issues) $430

METAL SCIENCE AND HEAT TREATMENT
Metallovedenie i Termicheskaya Obrabotka Metallov
Vol. 26, 1984 (12 issues) $540

METALLURGIST
Metallurg
Vol. 28, 1984 (12 issues) $555

PROBLEMS OF INFORMATION TRANSMISSION
Problemy Peredachi Informatsii
Vol. 20, 1984 (4 issues) $420

PROGRAMMING AND COMPUTER SOFTWARE
Programmirovanie
Vol. 10, 1984 (6 issues) $175

PROTECTION OF METALS
Zashchita Metallov
Vol. 20, 1984 (6 issues) $480

RADIOPHYSICS AND QUANTUM ELECTRONICS
Izvestiya Vysshikh Uchebnykh Zavedenii, Radiofizika
Vol. 27, 1984 (12 issues) $520

REFRACTORIES
Ogneupory
Vol. 25, 1984 (12 issues) $480

SIBERIAN MATHEMATICAL JOURNAL
Sibirskii Matematicheskii Zhurnal
Vol. 25, 1984 (6 issues) $625

SOIL MECHANICS AND FOUNDATION ENGINEERING
Osnovaniya, Fundamenty i Mekhanika Gruntov
Vol. 21, 1984 (6 issues) $500

SOLAR SYSTEM RESEARCH
Astronomicheskii Vestnik
Vol. 18, 1984 (6 issues) $365

SOVIET APPLIED MECHANICS
Prikladnaya Mekhanika
Vol. 20, 1984 (12 issues) $520

SOVIET ATOMIC ENERGY
Atomnaya Énergiya
Vols. 56-57, 1984 (12 issues) $560

SOVIET JOURNAL OF GLASS PHYSICS AND CHEMISTRY
Fizika i Khimiya Stekla
Vol. 10, 1984 (6 issues) $235

SOVIET JOURNAL OF NONDESTRUCTIVE TESTING
Defektoskopiya
Vol. 20, 1984 (12 issues) $615

SOVIET MATERIALS SCIENCE
Fiziko-khimicheskaya Mekhanika Materialov
Vol. 20, 1984 (6 issues) $445

SOVIET MICROELECTRONICS
Mikroèlektronika
Vol. 13, 1984 (6 issues) $255

SOVIET MINING SCIENCE
Fiziko-tekhnicheskie Problemy Razrabotki Poleznykh Iskopaemykh
Vol. 20, 1984 (6 issues) $540

SOVIET PHYSICS JOURNAL
Izvestiya Vysshikh Uchebnykh Zavedenii, Fizika
Vol. 27, 1984 (12 issues) $520

SOVIET POWDER METALLURGY AND METAL CERAMICS
Poroshkovaya Metallurgiya
Vol. 23, 1984 (12 issues) $555

STRENGTH OF MATERIALS
Problemy Prochnosti
Vol. 16, 1984 (12 issues) $625

THEORETICAL AND MATHEMATICAL PHYSICS
Teoreticheskaya i Matematicheskaya Fizika
Vol. 58-61, 1984 (12 issues) $500

UKRAINIAN MATHEMATICAL JOURNAL
Ukrainskii Matematicheskii Zhurnal
Vol. 36, 1984 (6 issues) $500

Send for Your Free Examination Copy

Plenum Publishing Corporation, 233 Spring St., New York, N.Y. 10013
In United Kingdom: 88/90 Middlesex St., London E1 7EZ, England
Prices slightly higher outside the U.S. Prices subject to change without notice.

Declassified and Approved For Release 2013/09/14 : CIA-RDP10-02196R000300040005-3

Declassified and Approved For Release 2013/09/14 : CIA-RDP10-02196R000300040005-3

RUSSIAN JOURNALS IN THE PHYSICAL AND MATHEMATICAL SCIENCES

AVAILABLE IN ENGLISH TRANSLATION

ALGEBRA AND LOGIC
Algebra i Logika
Vol. 23, 1984 (6 issues) $360

ASTROPHYSICS
Astrofizika
Vol. 20, 1984 (4 issues) $420

AUTOMATION AND REMOTE CONTROL
Avtomatika i Telemekhanika
Vol. 45, 1984 (24 issues) $625

COMBUSTION, EXPLOSION, AND SHOCK WAVES
Fizika Goreniya i Vzryva
Vol. 20, 1984 (6 issues) $445

COSMIC RESEARCH
Kosmicheskie Issledovaniya
Vol. 22, 1984 (6 issues) $545

CYBERNETICS
Kibernetika
Vol. 20, 1984 (6 issues) $445

DIFFERENTIAL EQUATIONS
Differentsial'nye Uravneniya
Vol. 20, 1984 (12 issues) $505

DOKLADY BIOPHYSICS
Doklady Akademii Nauk SSSR
Vols. 274-279, 1984 (2 issues) $145

FLUID DYNAMICS
Izvestiya Akademii Nauk SSSR, Mekhanika Zhidkosti i Gaza
Vol. 19, 1984 (6 issues) $500

FUNCTIONAL ANALYSIS AND ITS APPLICATIONS
Funktsional'nyi Analiz i Ego Prilozheniya
Vol. 18, 1984 (4 issues) $410

GLASS AND CERAMICS
Steklo i Keramika
Vol. 41, 1984 (6 issues) $590

HIGH TEMPERATURE
Teplofizika Vysokikh Temperatur
Vol. 22, 1984 (6 issues) $520

HYDROTECHNICAL CONSTRUCTION
Gidrotekhnicheskoe Stroitel'stvo
Vol. 18, 1984 (12 issues) $385

INDUSTRIAL LABORATORY
Zavodskaya Laboratoriya
Vol. 50, 1984 (12 issues) $520

INSTRUMENTS AND EXPERIMENTAL TECHNIQUES
Pribory i Tekhnika Eksperimenta
Vol. 27, 1984 (12 issues) $590

JOURNAL OF APPLIED MECHANICS AND TECHNICAL PHYSICS
Zhurnal Prikladnoi Mekhaniki i Tekhnicheskoi Fiziki
Vol. 25, 1984 (6 issues) $540

JOURNAL OF APPLIED SPECTROSCOPY
Zhurnal Prikladnoi Spektroskopii
Vols. 40-41, 1984 (12 issues) $540

JOURNAL OF ENGINEERING PHYSICS
Inzhenerno-fizicheskii Zhurnal
Vols. 46-47, 1984 (12 issues) $540

JOURNAL OF SOVIET LASER RESEARCH
A translation of articles based on the best Soviet research in the field of lasers
Vol. 5, 1984 (6 issues) $180

JOURNAL OF SOVIET MATHEMATICS
A translation of Itogi Nauki i Tekhniki and *Zapiski Nauchnykh Seminarov Leningradskogo Otdeleniya Matematicheskogo Instituta im. V. A. Steklova AN SSSR*
Vols. 24-27, 1984 (24 issues) $1035

LITHOLOGY AND MINERAL RESOURCES
Litologiya i Poleznye Iskopaemye
Vol. 19, 1984 (6 issues) $540

LITHUANIAN MATHEMATICAL JOURNAL
Litovskii Matematicheskii Sbornik
Vol. 24, 1984 (4 issues) $255

MAGNETOHYDRO[redacted]
[redacted] issues) $520

PEEL H[redacted]5

continued on inside back cover

Declassified and Approved For Release 2013/09/14 : CIA-RDP10-02196R000300040005-3